NOTE TO USERS

Dynamic Modeling and Capacity Control of Multiple Chiller Systems

Yang Guan

A thesis in
Department of Building, Civil and Environmental Engineering

Presented in Partial Fulfillment of the Requirements
For the Degree of Master of Applied Science at
Concordia University
Montreal, Quebec, Canada

May 2005

Your file Votre référence
ISBN: 0-494-10218-7
Our file Notre référence
ISBN: 0-494-10218-7

ABSTRACT

Dynamic Modeling and Capacity Control of Multiple Chiller Systems

Yang Guan

Multiple chiller systems are widely utilized for space cooling in industrial and commercial buildings. Good chiller control methods could offer benefits to users for more energy savings. Matching the anticipated cooling load and achieving higher coefficient of performance (COP) are the main objectives of multiple chiller capacity control strategies. With this as a main motivation, a dynamic model of compressor refrigeration chiller (CRC) and design of a closed loop PI controller for single CRC and multiple CRC systems are presented in this thesis.

The dynamic model of vapor compressor refrigeration system includes thermostat expansion valve, evaporator, compressor, compressor motor, and condenser. The model equations were solved and open loop simulations were made to evaluate the time response characteristics of each component and whole chiller system under varying cooling load. A PI controller was designed and output responses of supply water temperatures, refrigerant mass flow rate and compressor motor rotor speed were studied. An optimization methodology to compute optimal chilled water temperature setpoints is proposed and simulation results showing the implementation of optimal setpoints are presented.

A control strategy for operating multiple chiller systems which yields maximum COP is developed. To evaluate the developed multiple chiller capacity control strategy, two chillers 5 ton and 10 ton capacity were considered. The simulation results show that (1) the PI controller can maintain chilled water temperature close to the setpoint temperature under variable load conditions; (2). By varying the compressor motor rotor speed, the chiller capacity can be modulated; (3). To achieve maximum COP, it is beneficial to operate both chillers at lower capacities than to operate one chiller alone at higher capacity.

ACKNOWLEDGMENTS

I would like to take this opportunity to express my sincere gratitude to my supervisor, Dr. M.Zaheer-uddin for his invaluable guidance, beneficial suggestions and financial support during the research.

I also would like to dedicate this thesis to my mother, Yuwen Ma, my wife Huijuan Yu, and my lovely daughter Emily Guan.

My thanks are also extended to all staff in department of BCEE for their help, as well as my colleagues, especially to Lianzhong Li.

I also express my faithful thanks to Siemens Building Technology (China) operation manager, Mr. Wei Feng, who led me to the way of HVAC control.

TABLE OF CONTENTS

LIST OF FIGURES

LIST OF TABLES

NOMENCLATURE

A_{ci} = heat transfer area of the condenser tube inside (m^2)

A_{co} = heat transfer area of the condenser tube outside (m^2)

A_{cot} = area of the condenser outside tubes (m^2)

A_{eic} = cross section area of inner tube (m^2)

A_{ei} = heat transfer area of the evaporator tube inside (m^2)

A_{eo} = heat transfer area of the evaporator tube outside (m^2)

A_{eoc} = cross section area between inner tube and outside tube (m^2)

A_{eot} = area of the evaporator outside tubes (m^2)

A_{es} = cross section area of the evaporator tubes (m^2)

A_v = expansion valve area (m^2)

C_{ct} = specific heat of the condenser tubes (KJ/kg°C)

$C_{c(e)w}$ = specific heat of condenser or evaporator water (KJ/kg°C)

C_{esh} = specific heat of superheated refrigerant vapor (KJ/kg °C)

C_{et} = specific heat of the evaporator tubes (KJ/kg°C)

COP = Coefficient of Performance (unitless)

C_p = specific heat of water (KJ/kg°C)

C_v = orifice coefficient (unitless)

D = inside tube diameter (m)

D_{ei} = diameter of evaporator inner tube (m)

D_{eo} = diameter of evaporator outer tube (m)

$e(t)$ = error

f = viscous friction coefficient (Nm/Ωs)

Fre = frequency (Hz)

G = mass velocity of water (Kg/s)

G_v = vapor mass velocity (m/s)

H_1 = enthalpy of the superheat vapor (KJ/kg)

H_2 = refrigerant enthalpy in compressor discharge port (KJ/kg)

H_3 = enthalpy of entering the expansion valve (KJ/kg)

H_4 = enthalpy of entering the evaporator (KJ/kg)

H_{ci} = enthalpy of liquid refrigerant entering condenser (KJ/kg)

H_{clv} = enthalpy of liquid and gas refrigerant in condenser (KJ/kg)

H_{co} = enthalpy of gas refrigerant leaving condenser (KJ/kg)

H_{ei} = enthalpy of liquid refrigerant entering evaporator (KJ/kg)

H_{elv} = enthalpy of liquid and gas refrigerant in evaporator (KJ/kg)

H_{eo} = enthalpy of gas refrigerant leaving evaporator (KJ/kg)

H_{cv} = enthalpy of saturated vapor refrigerant in condenser (KJ/kg)

H_{cl} = enthalpy of saturated liquid refrigerant in condenser (KJ/kg)

H_{ev} = enthalpy of saturated vapor refrigerant in evaporator (KJ/kg)

h_{ci} =heat transfer coefficient between the refrigeration and the condenser wall (KJ/sm^2°C)

h_{co} = heat transfer coefficient between the condenser water and the condenser wall (KJ/sm^2°C)

h_{cot} = heat transfer coefficient between the water and the condenser outside wall (KJ/sm^2°C)

h_{ei} =heat transfer coefficient between the refrigeration and the evaporator tube wall (KJ/sm^2°C)

h_{ei} = refrigerant side heat transfer coefficient of evaporation (KJ/s m^2°C)

h_{eo} = heat transfer coefficient between the chilled water and the evaporator tube wall (KJ/sm^2°C)

h_{eot} = heat transfer coefficient between the water and the evaporator outside wall (KJ/sm^2°C)

h_{esh} = the equivalent heat transfer coefficient between tube wall and refrigerant in superheat section (KJ/s m^2 K)

h_{fg} = latent heat (KJ/kg mol)

i_{sa} = single phase A current (A)

i_{sb} = single phase B current (A)

i_{sc} = single phase C current (A)

J = rotor moment of inertia (Kg m m)

k = thermal conductivity of water (W/m°C)

k_l = liquid thermal conduct (W/m°C)

K_p = proportional gain

l_e = length of the evaporator tubes two phase sections (m)

L_e = length of evaporator (m)

l_c = length of the condenser two phase section (m)

L_c = length of condenser (m)

Lr = rotor self inductance (H)

Ls = stator self inductance (H)

$\dot{m}$ = mass flow rate of multiple chiller total supply water (Kg/s)

$\dot{m}_1$ = mass flow rate of 5 Ton chiller supply water (Kg/s)

$\dot{m}_2$ = mass flow rate of 10 Ton chiller supply water (Kg/s)

m_{cri} = mass of liquid refrigerant entering condenser (Kg)

m_{cro} = mass of vapor refrigerant leaving condenser (Kg)

m_{eri} = refrigerant mass of the expansion valve outlet (Kg)

m_{ero} = mass of vapor refrigerant leaving evaporator (Kg)

M = mutual inductance (H)

M_{cri} = mass flow rate of liquid refrigerant entering condenser (Kg/s)

M_{cro} = mass flow rate of vapor refrigerant leaving condenser (Kg/s)

M_{cw} = mass flow rate of condenser water (Kg/s)

M_{eri} = refrigerant flow rate of the expansion valve outlet (Kg/s)

M_{ero} = mass flow rate of vapor refrigerant leaving evaporator (Kg/s)

M_{ew} = mass flow rate of chilled water (Kg/s)

N = compressor motor speed (RPS)

n = polytropic exponent

P_s = compressor suction pressure (Pa)

P_d = compressor discharge pressure (Pa)

Q_c = ideal heat absorbed by refrigerant (KJ/s)

Q_r = ideal heat rejected by refrigerant (KJ/s)

Rr = rotor resistance (Ω)

Rs = stator resistance (Ω)

T_{cot} = condenser outside mean temperature (°C)

T_{cr} = condenser refrigeration temperature (°C)

T_{ct} = condenser wall mean temperature (°C)

T_{cw} = condenser water temperature (°C)

T_{eot} = evaporator outside tube mean temperature (°C)

T_{etsh} = mean tube temperature of evaporator superheat section (°C)

T_{er} = evaporator refrigeration temperature (°C)

T_{et} = evaporator tube wall mean temperature (°C)

T_{ew} = chilled water temperature (°C)

T_{ewsh} = water temperature of evaporator superheat section (°C)

T_i = integral gain

T_{mech} = mechanical load torque (Nm)

T_{sh} = superheat temperature of evaporator superheat section (°C)

U1 = stator equivalent two-phase voltage applied in X axis (V)

U2 = stator equivalent two-phase voltage applied in Y axis (V)

u_{sa} = single phase A voltage (V)

u_{sb} = single phase B voltage (V)

u_{sc} = single phase C voltage (V)

V_{cl} = clearance volume of the cylinder (m^3)

V_d = maximum volume of the cylinder (m^3)

V_o = expansion valve opening percent (%)

$V_p(t)$ = proportional controller output

V_s = refrigerant specific volume in compressor suction port (m^3/kg)

$V_i(t)$ = integral controller output

i_x = stator equivalent two-phase current applied in X axis (A)

i_y = stator equivalent two-phase current applied in Y axis (A)

fl_a = flux linkage in rotor phase a (Web)

fl_b = flux linkage in rotor phase b (Web)

av = motor angular velocity (radian/s)

ap = motor angular position (radian)

Greek letters

ρ_{eri} = density of evaporator refrigerant saturated liquid (Kg/ m^3)

ρ_{et} = density of the evaporator tubes (Kg/m^3)

ρ_{ero} = density of the refrigerant density leaving the evaporator tube (Kg/m^3)

ρ_{esh} = density of superheated refrigerant vapor (Kg/m^3)

α_e = mean void fraction values of two phase sections

Δy = length of one single control volume

υ = viscosity of water (Kg/s m)

υ_l = dynamic viscosity of saturated liquid (Pa s)

ρ_l = density of saturated liquid (Kg/m^3)

ρ_v = density of saturated vapor (Kg/m^3)

Δx = difference between vapor fraction

CHAPTER 1

INTRODUCTION

1.1 Background

Compression refrigeration chillers (CRC) form an important part of Heating, Ventilating and Air-Conditioning (HVAC) systems. However, the chillers are also the major energy-consuming equipments in buildings. There is a great economic incentive in developing proper chiller capacity control methods and thus realizes more energy savings. With the development of automatic control technologies and the use of industrial controllers in HVAC field, especially the variable frequency drive motors to regulate the speed for chiller capacity control, larger energy savings could be achieved.

The operation of the chillers for start/stop and capacity control was entirely manual in the early systems. As thermostats, electronic capacity controls and time scheduled operation were adopted in the chiller control systems, more accurate controls emerged with significant potential for energy savings. Since 1980s, direct digital controller (DDC), computer simulation and variable frequency drive technology were extensively utilized in the field of chiller capacity control. Garland (1980), Williams (1984), Johnson (1985), Lau (1985), Stephan (1985), and Braun (1987, 1988, and 1989) presented their research results in the field of chiller capacity and optimal control.

To this end, in order to develop capacity control strategies, appropriate dynamic models of each component of CRC and the overall model are needed. Therefore, in this thesis component models of thermostatic expansion valve (TXV), evaporator, compressor and condenser have been adapted and modified to study the dynamic response of CRC. Also a squirrel cage induction motor dynamic model was used to simulate the variable frequency modulated motor speed. In this model, the refrigerant mass flow rate was

controlled by the variable speed motor under part load conditions. Open loop responses of each control loop were presented and explained. For closed loop control, responses to step changes in loads and setpoints were given. Furthermore, a sub-optimal control technique was applied for solving the multiple chiller capacity control problems.

1.2 Motivation and objectives

The term "capacity control" is used in this thesis to refer to the active means of modulating the refrigerant mass flow rate by compressor motor rotor speed to limit the capacity of vapor compression refrigeration system.

For better chiller controls it is necessary to modulate chiller capacity to match actual load condition. However, this has been done by running the compressor in a cyclic on-off manner. It is well known that these frequent start-up and shut-down transients result in poor energy efficiency. The variable frequency drive technology offers the possibilities for improving the part-load system performance and energy efficiency of chiller systems. Therefore, to this end, the major objectives of this thesis are

(i) to develop a dynamic model of variable speed compression refrigeration chiller (CRC) suitable for control analysis and design.

(ii) to develop a variable frequency squirrel cage induction motor controller to modulate the refrigerant mass flow rate of chiller systems.

(iii) to design a PI control strategy for modulating the capacity of CRC systems to achieve good supply water temperature control.

(iv) to determine optimal setpoint temperature profiles as a function of chiller cooling load.

(v) to carry out simulation runs to test the developed control strategy under various operating conditions.

Another practical problem faced by building managers is how to determine the best operation method of sequencing of multiple chillers. Therefore, another objective of this thesis is to develop an optimal control technique for the operation of multiple chillers such that the overall system Coefficient of Performance (COP) of multiple chillers is improved by matching the chiller capacity with predicted cooling loads.

1.3 Organization of thesis

In Chapter 2, a literature survey of previous studies conducted on steady state and dynamic models of the refrigerating systems, chiller capacity control methods are reviewed. Then, the dynamic models and their open loop simulation results of the overall chiller system are presented in Chapter 3. Methodologies for closed loop control and simulation results are presented in Chapter 4. The multiple chiller control strategies and simulation results are described in Chapter 5. Finally, conclusions of this study along with the recommendations for the future research are presented in Chapter 6.

CHAPTER 2

LITERATURE REVIEW

2.1 Steady state models

Fiscker and Rice (1980) reported a heat pump model developed at Oak Ridge National Laboratory (ORNL). The authors presented a FORTRAN-IV computer program to predict the steady-state performance of conventional vapor compression electrically driven air-to-air heat pumps in both heating and cooling modes. The heat pump model requires the following conditions as the user inputs: 1) system operating conditions, 2) compressor characteristics, 3) refrigerant flow control devices, 4) fin–and-tube heat exchanger parameters, 5) fan and indoor duct characteristics, and 6) refrigerants. The model can compute 1) system capacity and COP, 2) compressor and fan motor energy consumption, 3) coil outlet air dry-bulb and wet-bulb temperatures, 4) air-side and refrigerant-side pressure drops, 5) a summary of the refrigerant-side states throughout the cycle and 6) overall compressor efficiencies and heat exchanger effectiveness. However, the model being steady state can not predict the refrigerant charge inventory i.e. how much refrigerant is in the heat exchangers and the compressor as a function of time.

Dabiri and Rice (1981) developed a heat pump simulation model (HPSM) based on the ORNL heat pump model. This compressor model is based on the manufacturers' empirical performance curves. Two additional models of heat pump components are presented: one is a refrigerant mass flow rate model and another is the degree of superheat model. The detail analysis shown includes 1) the effect of superheat on refrigerant mass flow rate and 2) the effect of superheat on compressor power. Corrections for the effect of superheat level on refrigerant mass flow rate and compressor

power are developed. These results suggest that each compressor map should be calibrated with the heat pump test data to ensure simulation accuracy.

Krakow and Lin (1983) presented a computer model for the simulation of multiple source heat pump system. The model permits the simulation of heat pump systems with reciprocating compressors and includes compressor model, condenser model, evaporator model, suction line liquid subcooling heat exchanger model, expansion valve model, and accumulator model. The computer model can determine steady state performance characteristics of a heat pump interacting with environment. In the program the heat pump is specified by parameters defining the capacities and efficiencies of its components and control parameters. The model is based on experimental investigations of a multiple source heat pump system for cold climates.

Allen and Hamilton (1983) reported a steady-state model (NBS model) for reciprocating water chillers of 10 to 200 Ton. There are two kinds of models in their paper: one is a full-load water chiller model; another is a part-load water chiller model. Both models are obtained by applying basic physical laws. The full-load water chiller model can be applied when compressors and cylinders are operating. On the other hand, the part-load water chiller model can be employed when compressors are cycled on and off and/or cylinders are unloading. The authors also examined two other existing water chiller models: DOE-2 and BLAST water chiller models. By comparing with the NBS, DOE-2 and BLAST models, following conclusions were made: 1) The DOE-2 model is the simplest one, requiring only two equations and four constants, but it also has the largest predictive error because of not accounting for temperature variation. 2) The BLAST

model consists of five equations and 14 coefficients, but the model also has a large predictive error because of neglecting temperature effects on the power. 3) The NBS model consists of five equations and 12 constants, and the model accounts for the temperature effects, condenser leaving water temperature and evaporator leaving water temperature. The NBS model has the smallest predictive error among the three models.

Krakow and Lin (1987) presented an improved version of their previous model (Krakow and Lin 1983). The new model is based on analyzing steady-state performance characteristics of a heat pump. The new model considers additional means of refrigerant mass flow rate controls and capacity controls by the following four ways: expansion valves responding to the superheat degree of the refrigerant downstream of the evaporator, capillary tubes, and expansion valves responding to the evaporator pressure, and limited refrigerant charge. The model can also predict the transition between refrigerant-dominant modes of operation of capillary-tube-controlled heat pumps. The authors think that the model is sufficiently accurate for the analysis of heat pumps with various refrigerant mass flow rate control means. However, they agree that further refinement of the component models will improve the overall accuracy of the heat pump model.

Hamilton and Miller (1990) reported a general steady state model for simulating an air-conditioning system. The system model consists of various standard components such as evaporator, compressor, condenser, capillary tube, and evaporator and condenser fans. The equations describing each component in the system are based on a hypothetical steady-state condition and consist of an energy balance and a mass balance conditions.

The evaporator and condenser models include the air mass flow rates and the evaporator model accounts for the mass flow rate of the water condensing on the coils. The system dealt with in the paper is formed by connecting the components in a particular pattern such that the input of one component is the output of the previous component. The study is mainly focused on system design.

Cecchini and Marchal (1991) presented a simulation model of refrigerating and air-conditioning system, which is based on a mathematical model of the thermodynamic cycle and experimental datum. The simulation includes the compressor model, evaporator model, thermostatic expansion valve model and condenser model. The models focus on: 1) the refrigerant thermodynamic cycle, which is the same for all types of equipments, 2) the heat exchange laws for external fluids (water, air) at evaporator and at the condenser. 3) A comparison between computed results and experimental datum is presented. An additional benefit of the model is claimed that it can predict the performance of a wide variety of equipments from a limited test data

Popovic and Shapiro (1995) presented a simple semi-empirical compressor model based on thermodynamics principles and a large database. The goal of their paper is to develop a simple accurate model of reciprocating compressors, which can be utilized in refrigeration system simulation. There are three models discussed in this paper. In the compressor model, compressor mass flow losses are accounted by effective suction and discharge pressure drops. The procedure to estimate the level of effective pressure drops, which represent compressor performance parameters, is outlined. In the polytropic exponent model, the polytropic exponent correlations based on the experimental data are

given for each refrigerant. In the energy losses model, energy losses are related to the required compression work rate that includes mass flow losses. The model predicts mass flow and compressor power within 10% of relative error.

Kim and Bullard (2001) developed a simple physical model for hermetic reciprocating compressors. In the paper, pressure losses along the refrigerant path are neglected, and a compression process is assumed as an isentropic process. The model consists of three sequential steps: 1) mass flow rate, 2) compressor work, and 3) compressor shell heat transfer and discharge temperature. The model can also estimate mass flow rate and compressor power consumption with error less than 3%.

Jin and Spitler (2002) presented a water-to-water heat pump model, which is suitable for use in building energy analysis and HVAC system simulation programs. The model is based on the basic thermodynamic principles and heat transfer relations. The model includes several unspecified parameters that are estimated from catalog data. A thermostat signal is used as an input parameter to the model to indicate which set of parameters (heating mode and cooling mode) will be used. Also, the objective function evaluation takes advantage of the fact that the heat transfer rates are known, using the catalog data as an initial guess, minimizing the difference between the predicted and measured heat-transfer rates. Then the model outputs the temperatures for each of the fluid streams, cooling and heat capacity, and COP of the system.

Liaw et al. (2002) presented a detail model to analyze a small air-conditioning system. In the model, a constraint of fixed suction superheat at the evaporator, which is often seen in the previous models, is released. Detailed simulations of each component, namely,

expansion device, evaporator, compressor and condenser are presented. The influence of complex circuitry design for both condenser and evaporator is incorporated into this model. The author investigated the influence of the number of circuits and various arrangements, and offered the following conclusion: the system performance is related to the refrigerant flow distribution in each circuit; more uniform the refrigerant flow in the circuitry, better the overall system performance.

2.2 Transient models

Dhar (1978) presented a detailed mathematical model of vapor compression refrigeration system. The author described the basic components, which are compressor, condenser, expansion device, evaporator and accumulator. A mathematical model of a refrigeration system involves development of equations that predicts the movement of refrigerant in the system and the state change of refrigerant in the system components against time. The influence of various metal masses on the system response is also taken into account. These models are simulated for window type room air conditioners. The numerical results and predicted responses of the system agree with the real system performance. The author pointed out the need for refinement of the simulation model.

Chi (1979) reported a computer model DEPAC for the design and performance analysis of chillers. The model includes four sub-models, which are compressor model, condenser model, evaporator model, and cooling tower model. The mathematical equations for the models are based on the heat and mass transfer theories. The models are applicable for selecting operation parameters for an existing chiller plant as well as required design parameters for a new plant, and are also a tool for studies in energy conservation.

Yasuda et al. (1983) presented a vapor compression refrigeration system mathematical model to predict the transient behavior of a single-cylinder reciprocating compressor, a shell-and-tube condenser, a thermostatic expansion valve, and a dry evaporator. The basic equations of the model components are derived from the mass and energy conservation theories. Simulation and experimental results are compared for three cases of transient behavior following positive and negative step changes in the static superheat of the expansion valve. The results show good agreement regarding values and response trends.

Macarthur (1984) described a detailed mathematical model of vapor compression heat pump. The model developed is based on energy conservation principles. The component models are composed of compressor, condenser, evaporator, accumulator, and expansion device. The heat pump model can predict the spatial values of temperature and enthalpy as functions of time for the two heat exchangers. The temperature and enthalpy in other component are simulated using lumped-parameter model. Simulation results show that the model is internally consistent. However, in order to improve the model accuracy the corrections that define the heat transfer coefficients and pressure drop calculations have to be used.

Crawford and Shirey (1987) reported a dynamic model of a residential heat pump. The model can provide quantitative predications of heat pump capacity and coefficient of performance (COP) as functions of outside temperature, so it is especially useful for heat pump system analysis. The model is directly derived from actual building performance data for residences that are heated and cooled with electrical heat pump.

Sami et al. (1987) presented an improved computer program to simulate the dynamic response of heat pumps. The mathematical formulation of this model is based on mass,

momentum, and energy balances. The equations for each control volume are written based on the conservation of mass, energy, and momentum principles. Besides the main models of the computer program, other detailed models are also presented to study the side effects of the various phenomena associated with heat pump operations, such as, thermodynamic properties of refrigerants, pressure drop, and heat transfer coefficients. Numerical results show that the proposed model predicts fairly well the heat pump dynamic response compared to the experimental data.

He et al. (1998) presented a lumped-parameter model to describe the dynamics of vapor compression cycles. The Linear-Quadratic Gaussian (LQG) technique is applied to coordinate compressor speed and expansion valve opening. The evaporator is divided into two sections: two-phase section and superheat section. The sum of refrigerant stored in the evaporator and condenser is constant. However, the parameter, mean void fraction values in the two-phase section of evaporator and condenser needs to be estimated by the empirical equations.

Shah et al. (2004) presented a dynamic model of multi-evaporator air-conditioning cycles. The model includes expansion valve, compressor and dual-evaporator system. In order to use the linear control design techniques, the model structure is linearized about an operating condition. Open loop responses of a typical system for in different system actuators are simulated. The open loop behaviors observed in these simulation studies indicate the effect of cross-coupling between dynamic variables of different evaporators. The closed loop control strategies based on the model and the system characteristics are also discussed, and the comparison of two control strategies for control of pressure and superheat of the two evaporators is also presented.

2.3 Chiller capacity and optimal control

Garland (1980) outlined a method for evaluation of energy savings during selecting a compressor with or without capacity controls or a multiplicity of compressor with or without capacity control. The reduced capacity can be achieved by means of cylinder unloading. The author obtained the following results: 1) For one compressor capacity control, the maximum energy savings will be obtained when cylinder unloading is in steps of one cylinder at a time; 2) For multiple compressors capacity control, only one of the compressors should be used for capacity changes within the capacity range of that compressor, as for the all others should be at full capacity or shutdown. The conclusion is obtained by using compressor performance datum. The COP of changeover points of converting another chiller are not considered in this paper.

Lundberg (1980) reported a capacity control system for a screw compressor, and the part operational characteristics were emphasized in this paper. First, the screw compressor capacity control system is described. Then, electronic control system, which includes compressor controller, temperature regulator, and sequence regulator is presented. Finally, the electronic valve regulator controls for the expansion valve are explained. This paper also shows how the different characteristics of the compressor and the control system are utilized in a water chiller unit with an air-cooled condenser. However, the paper concentrates on the electric control method of chiller capacity control.

Hackner et al. (1985) reported the short-term test results of equipment dynamics and the simulation model. In this paper, the use of model to determine an optimal control strategy is described. This model can control the refrigerant flow rates, temperatures, and

pressures of the HVAC system. It also controls the chilled water supply set point temperatures. The chilled water return temperature is used to determine whether a change in set temperature is desired. The operating status of the cooling tower fans are controlled by the approach temperature, which is the temperature difference between the ambient wet bulb temperature and the condenser water supply set point temperature. The optimal points to switch from operation with one chiller to operation with two chillers depend on chiller load and ambient wet bulb temperature. In practice, the optimal control strategy is to allow a chiller to meet up to its maximum chilled water load for given operating conditions.

Johnson (1985) defined and described some potential optimization routes available for minimizing the electrical energy costs of centrifugal chiller plant. While the techniques described are applicable primarily to an electric-driven centrifugal chiller plant, most are generally applicable to other drive types and refrigeration machines. The control strategies in this paper are described as they apply to electric-driven centrifugal chiller plants with cooling tower fans and associated chilled and condenser water pumps. These control strategies include the following: 1) Optimize equipment start time by matching pulldown load to chiller capacity; 2) Electrical demand reduction during chiller pulldown; 3) Multiple chillers sequence control; 4) Optimum cooling tower fan control; and 5) Reset chilled water temperature consistent with comfort requirements. The author suggested that the controller could improve the plant operation, as well as reduce the total plant energy usage.

Spethmann (1985) reported research results about the optimized control of multiple chillers. The plant system includes centrifugal chillers with integral condensers, primary chilled water pumps with distribution piping, and evaporative cooling towers with condenser water pumps. The purpose of the paper is to find out the optimal control points between the lowest possible condenser water temperature and the highest possible chilled water temperature. The following conclusion are obtained from this paper: 1) Optimized selection of multiple chillers is best done by using measurement of condenser water temperature and chilled water temperature; 2) Selection of similar chillers can be done by a predetermined sequence and changeover decision line; and 3) Dissimilar chiller selection is best done by an on-line analysis.

Lau et al. (1985) presented a minicomputer monitor and control system. The simulation models are separated into a plant model and a chilled water load model. The components in the plant model are chillers, pumps, cooling towers, valves and pipes. In order to get the site chilled water load model, the site is broken into 15 zones. The chiller and cooling models are made specific for this study using manufacturer's data and the other models are the control functions. Optimal control strategies for the number of chillers, cooling tower fan speeds, and condenser pump flow rates are developed.

Braun et al. (1987) presented an investigation of performance and control characteristics of control system at an airport project. A simple and empirical models of chiller, pumps and cooling tower is utilized in the paper. The performance associated with the use of variable speed chiller control is compared with that of fixed speed vane control. When variable speed fans are employed for the cooling tower, it is desirable to operate as many

cells as possible. If variable-speed condenser pumps are utilized, the optimal operating point occurs at points such that the thermal capacities of the air and water streams are equal. The model can also be used to evaluate the optimal condenser water and tower airflow rates.

Braun et al. (1989) developed an optimal control scheme for chilled water systems. Optimization techniques are applied to analyze the control of chilled water systems. The following useful results were obtained: 1) Operate all variable speed tower fans at identical fan speeds; 2) For multi-speed tower fans, increase the lowest speed tower fans first when add tower capacity and reverse for removing capacity; 3) The sequencing of variable speed pumps should be directly coupled to the sequencing of chillers to give peak pump efficiencies for each possible combination of operating chillers; 4) Multiple chillers should have identical chilled-water set temperatures, and the evaporator and condenser water flows for multiple chillers should be divided according to the chiller's relative cooling capacities; and 5) All parallel air handlers should have identical supply air set point temperature.

The above literature review shows that most models are steady state type. And the dynamic models are mainly used for finding optimal control schemes. However, speed control of compressor is not adequately addressed. Therefore, in this thesis a feedback control scheme augmented with optimal chilled water setpoints is presented for improving the overall control ability and COP of chiller systems.

CHAPTER 3

DYNAMIC MODELING AND OPEN LOOP SIMULATION RESULTS

3.1 Basic compression refrigeration cycle and system components

The components employed in the basic vapor compression refrigeration system are illustrated in Figure 3.1. The system consists of a single cylinder compressor, a condenser, an expansion valve, and an evaporator. The refrigerant flowing in the system may be assumed to follow an ideal cycle of the pressure-enthalpy diagram as shown Figure 3.2.

The cycle consists of a reversible adiabatic (constant enthalpy) compression process (1-2), a reversible constant pressure, de-superheating, condensation and sub-cooling process (2-3), an irreversible adiabatic (constant enthalpy) expansion process (3-4), and a reversible constant pressure evaporation process (4-1).

Refrigerant leaves the evaporator at point '1' as a low pressure, low temperature and superheated vapor and enters the compressor where it is compressed adiabatically. At point '2', it leaves the compressor as a high temperature, high pressure and superheated vapor and enters the condenser where it is condensed at a constant pressure. At point '3', refrigerant leaves the condenser as a high pressure, medium temperature and saturated liquid and enters the expansion device where it expands adiabatically. At point '4', refrigerant enters the evaporator as a low pressure, low temperature and low quality vapor where it is evaporated at '1''. At point '1'', it is superheated as the superheated vapor into the compressor.

From Figure 3.2, the amount of heat removed by the evaporator from the cooled space of refrigerant is

$$Q_c = H_1 - H_4 \qquad (3.1.1)$$

Since the process (3-4) is an ideal adiabatic expansion, so that we have $H_4=H_3$

where

Q_c is the heat absorbed by refrigerant (KJ/s)

H_1 is the enthalpy of the superheat vapor (KJ/kg)

H_3 is the enthalpy of refrigerant entering the expansion valve (KJ/kg)

H_4 is the enthalpy of refrigerant entering the evaporator (KJ/kg)

The work of compression of refrigerant flowing is

$$W = H_2 - H_1 \tag{3.1.2}$$

where

H_2 the refrigerant enthalpy in compressor discharge port (KJ/kg)

The amount of heat rejected is

$$Q_r = H_2 - H_3 \tag{3.1.3}$$

where

Q_r is the heat rejected by refrigerant (KJ/s)

A convenient measure of the performance of a complete cooling system is the Coefficient of Performance of a basic vapor compression system, given by

$$COP=\frac{Q_c}{W} \tag{3.1.4}$$

where

COP is the Coefficient of Performance, (dimensionless)

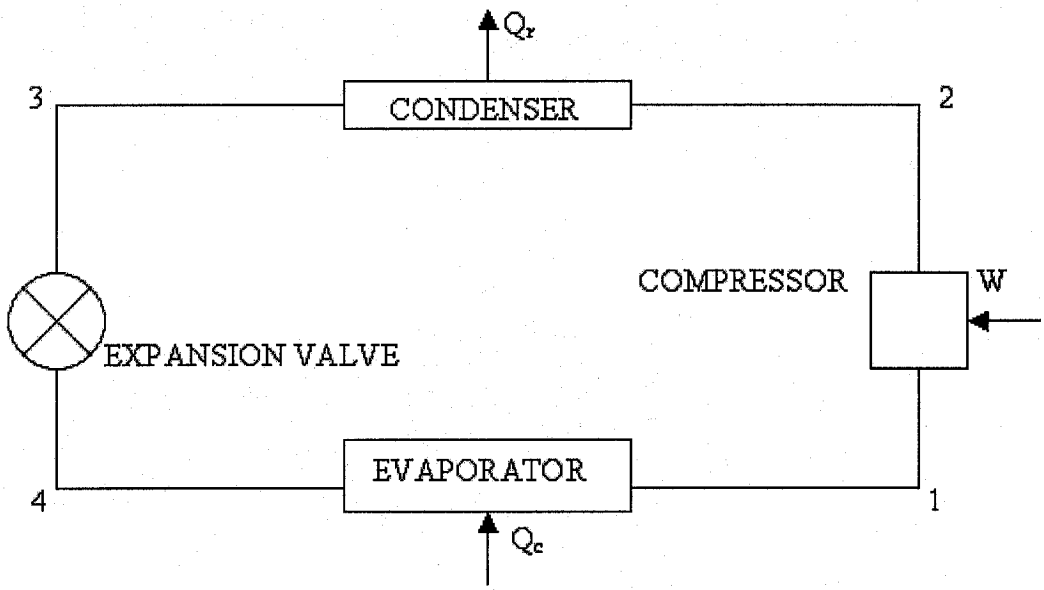

Figure 3.1 Vapor compression system schematic diagram

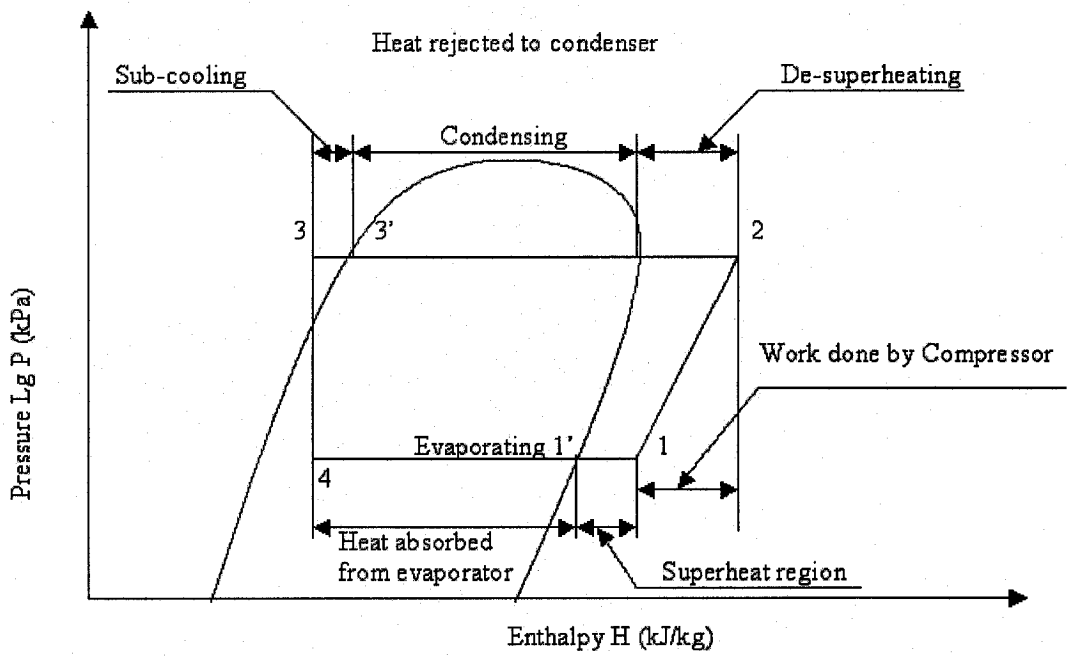

Figure 3.2 Refrigeration pressure-enthalpy diagram

3.2 Dynamic model

Many analytical models of individual refrigeration system components are available to analyze the performance of individual component. The state of refrigerant enthalpy, temperature, or pressure in each component is established by writing the conservation of mass and energy balance equations which correlate the refrigerant properties. The overall system model can be developed by combining these basic equations. The mathematical model of the refrigeration system therefore consists of a set of algebraic and ordinary differential equations. The analytical model can be formulated by representing the continuous physical process occurring in the system. Each system component is represented by one or more separated control volumes. The mathematical modeling of the system components and overall refrigeration system will be presented in the following section. The components utilized in the paper are shown in Figure 3.3. The components are simulated in this paper include an evaporator, a compressor, a condenser, and an expansion valve.

3.3 Expansion valve model

For the expansion valve section, which plays a primary role in controlling the liquid mass rate into the evaporator, the steady state description is utilized because the time constant involved in the valve motion is considered to be very small when compared with that of the refrigerating system. The refrigerant flow rate through the Thermostatic Expansion Valve (TXV) can be obtained from the orifice flow equation (ASHREA Fundamental Handbook 1997)

$$M_{eri} = C_v A_v V_o \sqrt{(P_d - P_s)\rho_{eri}} \qquad (3.3.1)$$

where

M_{eri} is the refrigerant flow rate of the expansion valve outlet (Kg/s)

C_v is the orifice coefficient

A_v is the expansion valve area (m^2)

V_o is the expansion valve opening percent (%)

P_s is the compressor suction pressure (Pa)

P_d is the compressor discharge pressure (Pa)

ρ_{eri} is the density of evaporator refrigerant saturated liquid (Kg/ m^3)

L_e is the length of evaporator (m) in Figure 3.3

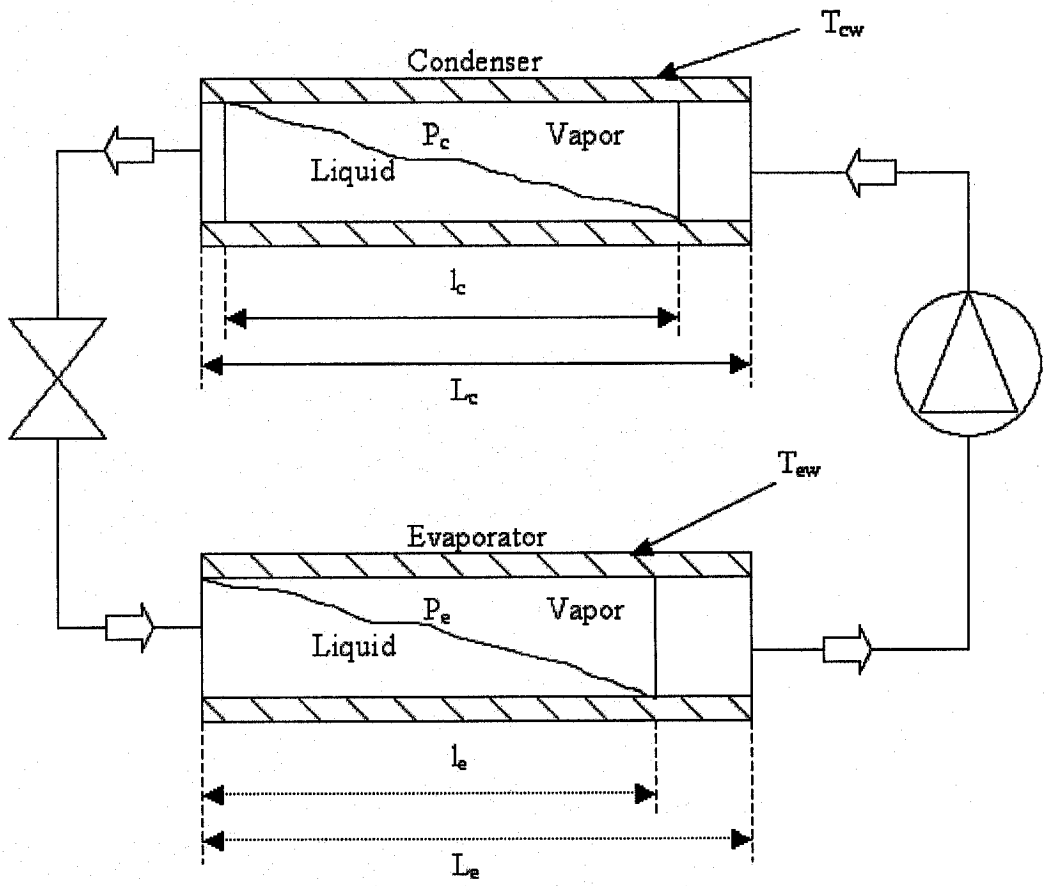

Figure 3.3 Refrigeration system diagram

The expansion valve parameters used in simulation are listed in Table 3.1

Table 3.1 5 Ton chiller expansion valve parameters

Symbol	Magnitude	Units
C_v	0.75	dimensionless
A_v	0.000507	m^2

3.4 Evaporator model

The shell-and-tube evaporator is utilized in this study based on the model developed by (He et al. 1998). The mathematical model of describing evaporator includes two-phase section (liquid and vapor) equations and superheated vapor section equations. Basic equations are derived from consideration of mass and energy balance principles. The energy balance in the evaporator tube yields the following equation

$$\rho_{et} A_{es} l_e C_{et} \frac{dT_{et}}{dt} = h_{ei} A_{ei} (T_{er} - T_{et}) + h_{eo} A_{eo} (T_{ew} - T_{et}) \qquad (3.4.1)$$

where

T_{et} is the evaporator tube wall mean temperature (°C)

T_{er} is the evaporator refrigerant temperature (°C)

T_{ew} is the chilled water temperature (°C)

h_{ei} is heat transfer coefficient between the refrigerant and the evaporator tube wall ($KJ/sm^2°C$)

h_{eo} is heat transfer coefficient between the chilled water and the evaporator tube wall ($KJ/sm^2°C$)

A_{ei} is heat transfer area of the evaporator tube inside (m^2)

A_{eo} is heat transfer area of the evaporator tube outside (m^2)

A_{es} is cross section area of the evaporator tubes (m^2)

ρ_{et} is the density of the evaporator tubes (Kg/m^3)

C_{et} is the specific heat of the evaporator tubes (KJ/kg°C)

l_e is the length of the evaporator tubes two phase sections (m)

The energy balance equation for the chilled water is given by

$$M_{ew}C_{ew}\frac{dT_{ew}}{dt} = h_{eo}A_{eo}(T_{et} - T_{ew}) + h_{eot}A_{eot}(T_{eot} - T_{ew}) \tag{3.4.2}$$

where:

T_{eot} is the evaporator outside tube mean temperature (°C)

h_{eot} is heat transfer coefficient between the water and the evaporator outside wall ($KJ/sm^2°C$)

A_{eot} is the area of the evaporator outside tubes (m^2)

M_{ew} is the mass flow rate of chilled water (Kg/s)

C_{ew} is the specific heat of the chilled water (KJ/kg°C)

Considering a lumped capacity model of refrigerant, the refrigerant mass flow rate equations in two-phase section of evaporator are given as follows

$$\frac{\partial}{\partial t}(m_{eri} + m_{ero}) = M_{eri} - M_{ero} \tag{3.4.3}$$

where

M_{ero} is the mass flow rate of vapor refrigerant leaving evaporator (Kg/s)

The refrigerant mass of saturated liquid and saturated vapor can be respectively expressed as

$$m_{eri} = A_{eic}\rho_{eri}l_e(1-\alpha_e) \tag{3.4.4}$$

$$m_{ero} = A_{eic}\rho_{ero}l_e\alpha_e \tag{3.4.5}$$

where

ρ_{ero} is the density of the refrigerant leaving the evaporator tube (Kg/m^3)

A_{eic} is the cross section area of inner tube (m^2)

α_e is the mean void fraction value of two phase section

α_e can be estimated based on thermodynamics tables, as discussed in He et al. (1998).

The energy balance equation in the evaporator refrigerant can be expressed as

$$\frac{d}{dt}(m_{eri}H_l + m_{ero}H_v) = h_{ei}A_{ei}(T_{et} - T_{er}) - M_{ero}H_{eo} + M_{eri}H_{ei} \tag{3.4.6}$$

where

H_{ei} is the enthalpy of liquid refrigerant entering evaporator (KJ/kg)

H_{eo} is the enthalpy of gas refrigerant leaving evaporator (KJ/kg)

H_{ev} is the enthalpy of saturated vapor refrigerant in evaporator (KJ/kg)

H_{el} is the enthalpy of saturated liquid refrigerant in evaporator (KJ/kg)

Applying the mass and energy principles to the entire evaporator, the following expression holds for vapor density:

$$A_{eic}l_e\frac{d\rho_{ero}}{dt} = M_{eri}\alpha_e - M_{ero} + \frac{h_{ei}\pi D_{ei}l_e(T_{et} - T_{er})}{H_{elv}} \tag{3.4.7}$$

where

H_{elv} is the enthalpy of liquid and gas refrigerant in evaporator(KJ/kg)

Applying the chain rule to the derivative and replacing α_e by $\frac{(H_v - H_l)}{H_{elv}}$, the above equation can be rewritten as:

$$A_{eic} l_e \frac{d\rho_{ero}}{dP_e} \frac{dP_e}{dt} = M_{eri} \frac{H_v - H_l}{H_{elv}} - M_{ero} + \frac{h_{ei} \pi D_{ei} l_e (T_{et} - T_{er})}{H_{elv}} \quad (3.4.8)$$

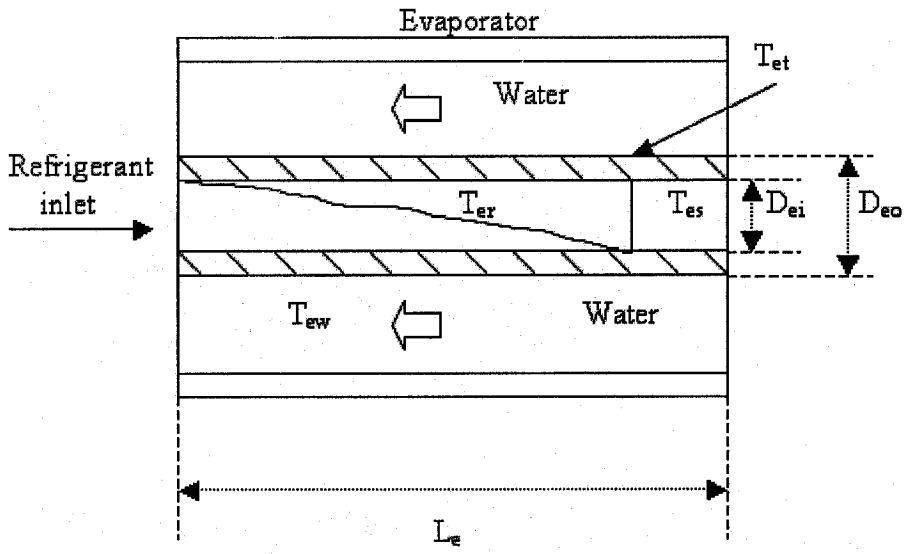

Figure 3.4 Evaporator model diagram

The evaporator parameters used in simulation are listed in Table 3.2

Table 3.2 5 Ton chiller evaporator parameters

Symbol	Magnitude	Units
A_{ei}	0.2026	m^2
A_{eo}	0.6472	m^2
L_e	12.0	m
l_e	10.5	m
C_p	0.6	KJ/kg K

3.5 Superheat model

The superheat region can be considered as two individual control volumes (Yasuda et al.1983). The superheated vapor refrigerant can be assumed incompressible therefore we can express the energy balance equation as

$$\rho_{esh} C_{esh} A_{eic} \frac{\partial T_{sh}(t,y)}{\partial t} + \frac{M_{ero} C_{esh}}{\Delta y} \partial T_{sh}(t,y) = h_{esh} D_{ei} \pi [T_{etsh}(t,y) - T_{sh}(t,y)] \qquad (3.5.1)$$

where

T_{sh} is the superheat temperature in the evaporator superheat section (°C)

T_{etsh} is the mean tube temperature of the evaporator superheat section (°C)

h_{esh} is the equivalent heat transfer coefficient between tube wall and refrigerant in superheat section (KJ/s m^2 K)

D_{ei} is the diameter of evaporator inner tube (m)

ρ_{esh} is the density of superheated refrigerant vapor (Kg/m^3)

C_{esh} is the specific heat of superheated refrigerant vapor (KJ/kg K)

The energy balance equation for tube wall in the superheat section is:

$$\rho_{et} C_{et} A_{es} \frac{\partial T_{etsh}(t,y)}{\partial t} = h_{eo} D_{eo} \pi [T_{ewsh}(t,y) - T_{etsh}(t,y)] - h_{esh} D_{ei} \pi [T_{etsh}(t,y) - T_{sh}(t,y)] \qquad (3.5.2)$$

where

T_{ewsh} is the water temperature of evaporator superheat section (°C)

D_{eo} is the diameter of evaporator outer tube (m)

The energy balance on chilled water in the superheat section is given as

$$\rho_{ew} C_{ew} A_{eoc} \Delta y \frac{\partial T_{ewsh}(t,y)}{\partial t} = M_{ew} C_{ew} [T_{ew} - T_{ewsh}(t,y)] - h_{eo} D_{eo} \pi \Delta y [T_{ewsh}(t,y) - T_{etsh}(t,y)] \qquad (3.5.3)$$

where

A_{eoc} is the cross section area between inner tube and outside tube(m^2)

By using the finite difference technique, the above three Equations, 3.5.1, 3.5.2, and 3.5.3 can respectively be converted into the ordinary differential equations. These are

$$\rho_{esh}C_{esh}A_{eic}\frac{dT_{sh}(i)}{dt}+\frac{M_{ero}C_{esh}}{\Delta y}(dT_{sh}(i+1)-dT_{sh}(i))=h_{esh}D_{ei}\pi[T_{etsh}(i)-T_{sh}(i)] \quad (3.5.4)$$

$$\rho_{et}C_{et}A_{es}\frac{dT_{etsh}(i)}{dt}=h_{eo}D_{eo}\pi[T_{ewsh}(i)-T_{etsh}(i)]-h_{esh}D_{ei}\pi[T_{etsh}(i)-T_{sh}(i)] \quad (3.5.5)$$

$$\rho_{ew}C_{ew}A_{eoc}\Delta y\frac{dT_{ewsh}(i)}{dt}=M_{ew}C_{ew}[T_{ew}-T_{ewsh}(i)]-h_{eo}D_{eo}\pi\Delta y[T_{ewsh}(i)-T_{etsh}(i)] \quad (3.5.6)$$

where

i from 1 to 2

the length of superheat section is $l_s=L_e-l_e$

Δy is the length of one single control volume.

3.6 Condenser model

The condenser was divided into three sections, a superheated vapor section, a condensation two-phase section, and a sub cooling section. However, the two-phase section of condenser is longer than the others. So, the storage capacitance is greater for mass and thermal energy of two-phase section than for other section. The heat exchange of condenser is dominated by two-phase section (He et al. 1998). The shell-and tube condenser is utilized in this thesis. Basic equations are derived from the physical laws of mass and energy conservation for refrigerant, tube wall, and condenser water. See Figure 3.5

The energy balance equation in the condenser tube is given as

$$\rho_{ct} A_{cs} l_c C_{ct} \frac{dT_{ct}}{dt} = h_{ci} A_{ci} (T_{cr} - T_{ct}) + h_{co} A_{co} (T_{cw} - T_{ct}) \quad (3.6.1)$$

where

T_{ct} is the condenser wall mean temperature (°C)

T_{cr} is the condenser refrigeration temperature (°C)

T_{cw} is the condenser water temperature (°C)

l_c is length of condenser two phase section (m)

h_{ci} is heat transfer coefficient between the refrigeration and the condenser wall ($KJ/sm^2°C$)

h_{co} is heat transfer coefficient between the condenser water and the condenser wall ($KJ/sm^2°C$)

A_{ci} is heat transfer area of the condenser tube inside (m^2)

A_{co} is heat transfer area of the condenser tube outside (m^2)

C_{ct} is the specific heat of the condenser tubes (KJ/kg°C)

The energy balance equation for the condenser water is given as

$$M_{cw} C_{cw} \frac{dT_{cw}}{dt} = h_{co} A_{co} (T_{ct} - T_{cw}) + h_{cot} A_{eot} (T_{cot} - T_{cw}) \quad (3.6.2)$$

where

C_{cw} is the specific heat of condenser water (KJ/kg°C)

M_{cw} is the mass flow rate of condenser water (Kg/s)

T_{cot} is the condenser outside mean temperature (°C)

h_{cot} is heat transfer coefficient between the water and the condenser outside wall ($KJ/sm^2°C$)

A_{cot} is the area of the condenser outside tubes (m^2)

Assuming a lumped capacity model of refrigerant, the refrigerant mass flow rate equations in two-phase section of condenser are given as

$$\frac{d}{dt}(m_{cri} + m_{cro}) = M_{cri} - M_{cro} \tag{3.6.3}$$

The refrigerant mass of saturated liquid and saturated vapor can be respectively expressed as

$$m_{cri} = A_{cic}\rho_{cri}l_c(1-\alpha_c) \tag{3.6.4}$$

$$m_{cro} = A_{cic}\rho_{cro}l_c\alpha_c \tag{3.6.5}$$

where

ρ_{cro} is the density of the refrigerant density leaving the condenser tubes two phase sections (Kg/m^3)

ρ_{cri} is the density of the refrigerant density entering the condenser tubes two phase sections (Kg/m^3)

A_{cic} is the cross section area of inner tube(m^2)

α_c is the mean void fraction values of two phase sections

The energy balance equation on refrigerant in the condenser can be expressed as

$$\frac{d}{dt}(m_{cri}H_v + m_{cro}H_l) = h_{ci}A_{ci}(T_{ct} - T_{cr}) - M_{cro}H_{co} + M_{cri}H_{ci} \tag{3.6.6}$$

M_{cri} is the mass flow rate of liquid refrigerant entering condenser (Kg/s)

M_{cro} is the mass flow rate of vapor refrigerant leaving condenser (Kg/s)

H_{ci} is the enthalpy of liquid refrigerant entering condenser(KJ/kg)

H_{co} is the enthalpy of gas refrigerant leaving condenser(KJ/kg)

H_{cvap} is the enthalpy of saturated vapor refrigerant (KJ/kg)

H_{cliq} is the enthalpy of saturated liquid refrigerant (KJ/kg)

By analysis to the evaporator, the pressure equation in the condenser is given as

$$A_{eic} l_c \frac{d\rho_{cro}}{dP_c} \frac{dP_c}{dt} = M_{cro} - \frac{h_{ci} \pi D_{ci} l_c (T_{cr} - T_{ct})}{H_{clv}} \tag{3.6.7}$$

where

H_{clv} is the enthalpy of liquid and gas refrigerant in condenser(KJ/kg)

The condenser parameters used in simulation are listed in Table 3.3

Table 3.3 5 Ton chiller condenser parameters

Symbol	Magnitude	Units
A_{ci}	0.45	m^2
A_{co}	0.93	m^2

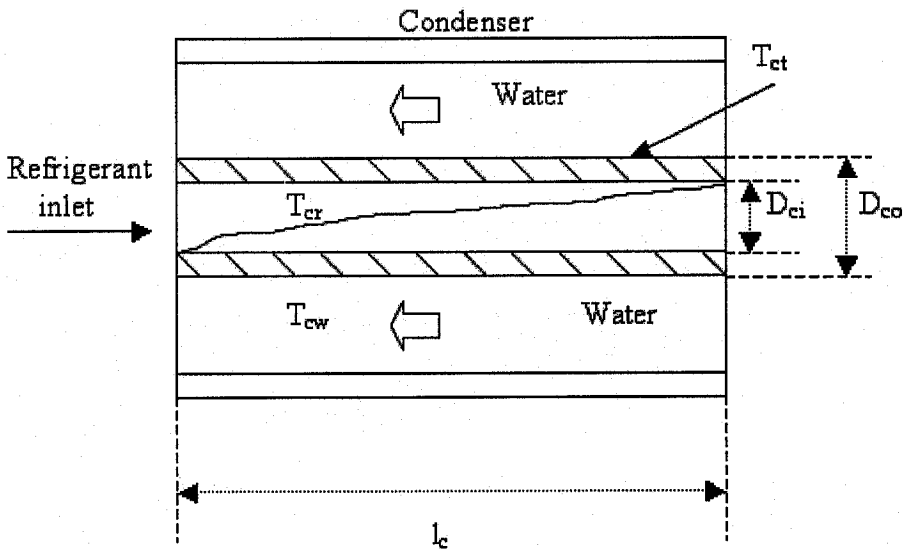

Figure 3.5 Condenser model diagram

3.7 Heat transfer coefficient

To calculate the heat transfer coefficient in different mediums and materials, first, the heat transfer coefficients are classified as heat transfer between the water and tube outer wall, heat transfer between gas refrigerant and tube inner wall and heat transfer between two-phase refrigerant and tube inner wall. These equations were adapted from ASHRAE Fundamentals Handbook (1997).

3.7.1 Waterside heat transfer coefficient

The waterside film heat transfer coefficient is based on the bulk temperature. The equation is

$$\frac{h_{co}D}{k} = 0.023\left(\frac{GD}{\upsilon}\right)^{0.8}\left(\frac{\upsilon C_p}{k}\right)^{0.4} \qquad (3.7.1)$$

where:

D is inside tube diameter, m

k is thermal conductivity of water, W/m°C

G is mass velocity of water, Kg/s m^2

C_p is specific heat of water, KJ/kg°C

υ is viscosity of water, Kg/s m

3.7.2 Refrigerant side heat transfer coefficient of condensation

The refrigerant side heat transfer coefficient equation is

$$\frac{h_{ci}D}{k_l} = 0.1(\frac{C_p \upsilon_l}{k_l})^{\frac{1}{3}}(\frac{h_{fg}}{C_p \Delta t})^{\frac{1}{6}}\left[\frac{DG_v}{\upsilon_l}(\frac{\rho_l}{\rho_v})^{\frac{1}{2}}\right]^{\frac{2}{3}} \quad (3.7.2)$$

where:

υ_l is dynamic viscosity of saturated liquid, Pa s

h_{fg} is latent heat, KJ/kg mol

G_v is vapor mass velocity, Kg/ sm^2

ρ_l is density of saturated liquid, Kg/m^3

ρ_v is density of saturated vapor, Kg/m^3

k_l is liquid thermal conduct, w/m°C

3.7.3 Refrigerant side heat transfer coefficient of evaporation

The refrigerant side heat transfer coefficient of evaporation is given by the following equation

$$h_{ei} = 0.0082(\frac{k_l}{D})[(\frac{GD}{\upsilon_l})^2(\frac{J\Delta x h_{fg}}{L})]^n \quad (3.7.3)$$

McAdams (1954) recommends the n for heating and cooling is 0.4 for 6K superheat at exit, and others recommend exponents of 0.4 for heating and 0.3 for cooling.

3.7.4 Superheat region heat transfer coefficient of evaporation

The superheat region heat transfer coefficient of evaporation is given by the following equation

$$h_{esh} = 155.2c(\frac{G^{0.8}}{D^{0.2}}) \quad (3.7.4)$$

where

h_{esh} is the superheat region heat transfer coefficient, KJ/m^2 s°C

c is 0.00197 for vapor at 0°C

The heat transfer coefficient parameters used in simulation are listed in Table 3.4

Table 3.4 Heat transfer coefficient parameters

Symbol	Magnitude	Units
h_{co}	2.28	KJ/s m^2 K
h_{eo}	1.66	KJ/s m^2 K
h_{eio}	2.42	KJ/s m^2 K
h_{ci}	3.86	KJ/s m^2 K
h_{ei}	1.99	KJ/s m^2 K
h_{esh}	0.87	KJ/s m^2 K

3.8 Compressor model

The compressor is one of the most important components in a compression refrigerant system. In this study, the compressor model only consists of one single- cylinder reciprocating compressor. The clearance volumetric efficiency η_v can be expressed as follows (ASHREA Fundamental Handbook 1997)

$$\eta_v = 1 - \frac{Vcl}{Vd}[(\frac{Pd}{Ps})^{\frac{1}{n}} - 1] \quad (3.8.1)$$

where

V_{cl} is the clearance volume of the cylinder (m^3)

V_d is maximum volume of the cylinder (m^3)

Mass flow rate through the compressor is written as:

$$M_{ero} = \rho_{esh} V_d N \eta_v \quad (3.8.2)$$

where

N is the compressor motor speed (RPS)

ρ_{esh} is the refrigerant density of the compressor suction (Kg/ m^3)

Work done by compressor is given by

$$W = \frac{n}{n-1} P_s V_s [(\frac{P_d}{P_s})^{\frac{n-1}{n}} - 1] \quad (3.8.3)$$

where

W is the work of compression (KJ/kg)

P_s is the compressor suction pressure (Pa)

P_d is the compressor discharge pressure (Pa)

V_s is the refrigerant specific volume in compressor suction port (m^3/kg)

n is the polytropic exponent.

Although the polytropic exponent n must be determined experimentally, it may be approximated by the isentropic exponent k when other data are not available. Typical valves are n=1.30 for R-134a. The compressor parameters used in simulation are listed in Table 3.5

Table 3.5 5 Ton chiller compressor parameters

Symbol	Magnitude	Units
V_{cl}	0.0003	m^3
V_d	0.007	m^3
N	20	RPS
n	1.3	dimensionless

3.9 Alternating Current (AC) induction motor model

Conventional chillers use a constant speed motor to drive the compressor. Since the variable speed motor can offer large energy savings under part-load running conditions, it is extensively used by many chiller manufacturers in recent years. The variable-speed compressor uses an inverter drive to convert a fixed frequency alternating current into one with adjustable voltage and frequency, which allows the variation of the rotating speed of the compressor motor. Typical operating frequency varies between 15 and 150Hz. The induction motor is the most widely used motor type in the HVAC&R industry, because of its good self-starting capability, simple and rugged structure, low cost and reliability, etc. A mathematical model of induction motor adapted from Gokdere (1999) is presented in this study. The modeling method is based on its equivalence with the symmetrical rotary, AC three-phase, and asynchronous squirrel-cage induction motor. The magnetic saturation effects and the core losses are not taken into account in the model. The model is based on equivalent two-phase induction motor whose dynamic equations are given as follows Gokdere (1999)

$$\frac{di_x}{dt} = \varepsilon \cdot \beta \cdot fl_a + \beta \cdot np \cdot fl_b \cdot av - \gamma \cdot i_x + \frac{U1}{\chi \cdot Ls} \tag{3.9.1}$$

$$\frac{di_y}{dt} = \varepsilon \cdot \beta \cdot fl_b + \beta \cdot np \cdot fl_a \cdot av - \gamma \cdot i_y + \frac{U2}{\chi \cdot Ls} \tag{3.9.2}$$

$$\frac{dfl_a}{dt} = -\varepsilon \cdot fl_a - np \cdot fl_b \cdot av + \varepsilon \cdot M \cdot i_x \tag{3.9.3}$$

$$\frac{dfl_b}{dt} = -\varepsilon \cdot fl_b + np \cdot fl_a \cdot av + \varepsilon \cdot M \cdot i_y \tag{3.9.4}$$

$$\frac{dav}{dt} = mu \cdot (fl_a \cdot i_y - fl_b \cdot i_x) - (\frac{f}{J}) \cdot av - \frac{T_{mech}}{J} \tag{3.9.5}$$

$$\frac{dap}{dt} = av \tag{3.9.6}$$

where

i_x is the stator equivalent two-phase current applied in X axis (A)

i_y is the stator equivalent two-phase current applied in Y axis (A)

fl_a is the flux linkage in rotor phase a (Web)

fl_b is the flux linkage in rotor phase b (Web)

av is the motor angular velocity (radian/s)

ap is the motor angular position (radian)

U_1 is the stator equivalent two-phase voltage applied in X axis (A)

U_2 is the stator equivalent two-phase voltage applied in Y axis (A)

T_{mech} is the mechanical load torque (Nm)

Rs is the stator resistance (Ω)

Rr is the rotor resistance (Ω)

Ls is the stator self inductance (H)

Lr is the rotor self inductance (H)

M is the mutual inductance (H)

f is the viscous friction coefficient (Nm/Ωs)

J is the rotor moment of inertia (Kg m m)

Fre is the frequency (Hz)

$$\varepsilon = \frac{R_r}{L_r}$$

$$\chi = 1 - \frac{M^2}{L_r L_s}$$

$$\beta = \frac{M}{L_s L_r \chi}$$

$$\gamma = \frac{R_r M^2}{L_s L_r^{\ 2} \chi} + \frac{R_s}{L_s \chi}$$

$$mu = 2np \frac{M}{3JL_r}$$

np is the number of pole-pairs (dimensionless)

A 7.5Kw, 3-phase, 3 poles, rated speed 1200RPM, 230V Y connection induction motor was simulated. The power supply is symmetrical, so the three voltage of phase A, phase B and phase C are displaced by 120° from each other. The three voltage values are respectively shown in the follows:

$$u_{sa} = \frac{220}{\sqrt{3}} \sin(2\pi \cdot Fre \cdot t) \tag{3.9.7}$$

$$u_{sb} = \frac{220}{\sqrt{3}} \sin(2\pi \cdot Fre \cdot t + \frac{2}{3}\pi) \tag{3.9.8}$$

$$u_{sc} = \frac{220}{\sqrt{3}} \sin(2\pi \cdot Fre \cdot t - \frac{2}{3}\pi) \tag{3.9.9}$$

Equivalent-two phase values of three-phase voltages are obtained by applying the following three-phase conversion

$$\begin{bmatrix} U_1 \\ U_2 \end{bmatrix} = \begin{bmatrix} 3/2, 0, 0 \\ 0, \sqrt{3}/2, -\sqrt{3}/2 \end{bmatrix} \begin{bmatrix} U_{sa} \\ U_{sb} \\ U_{sc} \end{bmatrix} \tag{3.9.10}$$

The equivalent three-phase values of the two-phase currents are calculated from

$$\begin{bmatrix} i_{sa} \\ i_{sb} \\ i_{sc} \end{bmatrix} = \begin{bmatrix} 2/3, 0 \\ -1/3, 1/\sqrt{3} \\ -1/3, 1/\sqrt{3} \end{bmatrix} \begin{bmatrix} x_1 \\ x_2 \end{bmatrix} \tag{3.9.11}$$

The above equations were solved for various operating conditions. The outputs such as stator three-phase currents (amperes), stator three-phase voltages (volts), angular velocity (radians/second), angular position (radians), and mechanical load torque (N.M) were obtained by integrating the above set of equations. The motor parameters used in simulation are listed in Table 3.6

Table 3.6 7.5 Kw AC induction motor parameters

Symbol	Magnitude	Units
R_s	0.3	Ohm
R_r	0.15	Ohm
L_s	$15.5/(2\pi \cdot Fre)$	H
L_r	$15.2/(2\pi \cdot Fre)$	H
M	$15.0/(2\pi \cdot Fre)$	H
f	0.001	N·m /Rad·S
J	3.89	Kg·m·m

3.10 Open loop simulation results

The mathematical model developed above in this chapter is applied to a 5 Ton reciprocating compression refrigeration chiller. The physical dimensions of the chiller components are listed in Table 3.1-3.6. The dynamic characteristics of the chiller system are simulated for changes in cooling load, compressor motor speed and mass flow rate.

Figure 3.6 shows the variation in suction and discharge pressures with time. After the motor is started, the suction pressure, P_s, drops rapidly at first and then gradually approaches a steady value of about 191 KPa. At the same time, the discharge pressure, P_d, immediately rises at first and then gradually approaches a steady value about 1138 KPa.

Figure 3.7 shows the temperatures of the chilled water, evaporator tube wall and refrigerant as functions of time in the evaporator. The temperature curves of chilled water and evaporator tube wall move with the same trend with a little difference during the whole process. The steady-state time is about 380s, and the final temperatures are 6.0°C and 4.9°C, respectively. However, the evaporator refrigerant temperature reaches quickly steady state compared with the other two, and the final value is -10.4°C. As it is expected, the evaporator tube wall temperature and chilled water temperature lag the refrigerant temperature.

The temperature responses against time in condenser are shown in Figure 3.8. The steady state values of the condenser refrigerant and the condenser tube wall have smaller difference, and are 41.7°C and 41.2°C respectively. Approaching steady-state times are about 450s.The condenser water temperature's final value is about 33°C, and its steady-state time is far larger than that of the condenser refrigerant and condenser tube wall.

Figure 3.9 shows the mass flow rate as a function of time through the compressor and thermostatic expansion valve (TXV). At the initial condition, both of mass flow rates are equal to zero. As soon as the compressor is started, compressor mass flow rate increases to its maximum value. The process time is about 20s to 30s, and this is because of the motor start up feature that it needs 22s to achieve its maximum speed. After the first time step, the compressor delivers refrigerant to the condenser against a rapidly increasing pressure difference of suction and discharge pressures. As such, the compressor mass flow rate gradually decreases to its steady state value. Similarly, the mass flow rate through the TXV firstly increases and then gradually achieves the same steady state value.

Figure 3.10 shows the relationship of superheat degree as a function of time. It is noted that when the cooling load is increased, if the TXV keeps the same opening, the superheat increases to higher degree. The reason is that superheat vapor will absorb more heat from the increasing cooling load, so superheat degree will be increased. However, if the superheat of refrigerant in the evaporator increases, the expansion valve opening should also increase to admit more liquid into the evaporator, and thus reduces the superheat to the desired degree.

Figure 3.11 shows the transient relationship of voltage, current, and flux linkage of the induction motor at a rated frequency 60Hz. The stator current and rotor flux linkage show a large value when the motor is energized. During the time the motor accelerates from zero speed to the rated speed, the current and flux linkage remain close to the high level. They drop off rapidly as the motor continues to accelerate, and settle down to their steady state value. These figures match the Electromagnetic Transients Program (EMTP) simulation results of Ali Hussein (1995).

Figure 3.12 shows the motor speeds as a function of time at different frequencies, 60Hz (rated frequency), 45Hz and 30Hz respectively. At the rated frequency 60Hz, the motor speed is 1195RPM. Due to the physical properties of asynchronous induction motor, slip rate of motor, usually within 2%, causes the difference between rated speed 1200RPM and actual speed 1195RPM. As the frequencies are reduced to 45Hz and 30Hz, the motor speeds are also decreased to 896RPM and 597RPM, respectively. The motor steady state time is about 22s.

Figure 3.13 shows the compressor mass flow rate as a function of time. A higher motor speed can translate into higher refrigerant mass flow. For example, while the motor speed

is 1195RPM, the refrigerant mass flow rate is 0.12 Kg/s; while the motor speeds are 896RPM and 597RPM, the refrigerant mass flow rates are 0.095 Kg/s and 0.058 Kg/s, respectively.

Figure 3.14 shows the chilled water temperature as a function of different motor speeds. The results can be obtained from the curves that lower chilled water temperature needs higher motor speed. When the chilled water temperatures are decreased from 9.2°C to 6.1°C, the motor speeds increase from 597RPM to 1195RPM.

The steady state time of chilled water temperature responses is about 400s. These figures show the time responses of refrigeration system. The results show expected trends and thus give an indication that the model equations are yielding acceptable results.

Another observation that can be made is that the dynamic responses of compressor speed, evaporator and condenser pressures, and refrigerant flow are faster than chilled water temperature responses. Thus the overall systems consist of both fast and slow system responses.

The developed model was also used to study steady state performance of chiller system. Several simulation runs were made at various capacity operating conditions. These are plotted in Figures 3.15, 3.16 and 3.17.

These figures show the operating performance and balance points of the chiller system between such operating variables such as evaporator and condenser pressures, refrigeration capacity and coefficient of performance. The simulated system capacity ranged between 8 to 18Kw with corresponding COP's ranging between 3.0 to 4.8 respectively. Such performance curves are useful in assessing the good operating range of system.

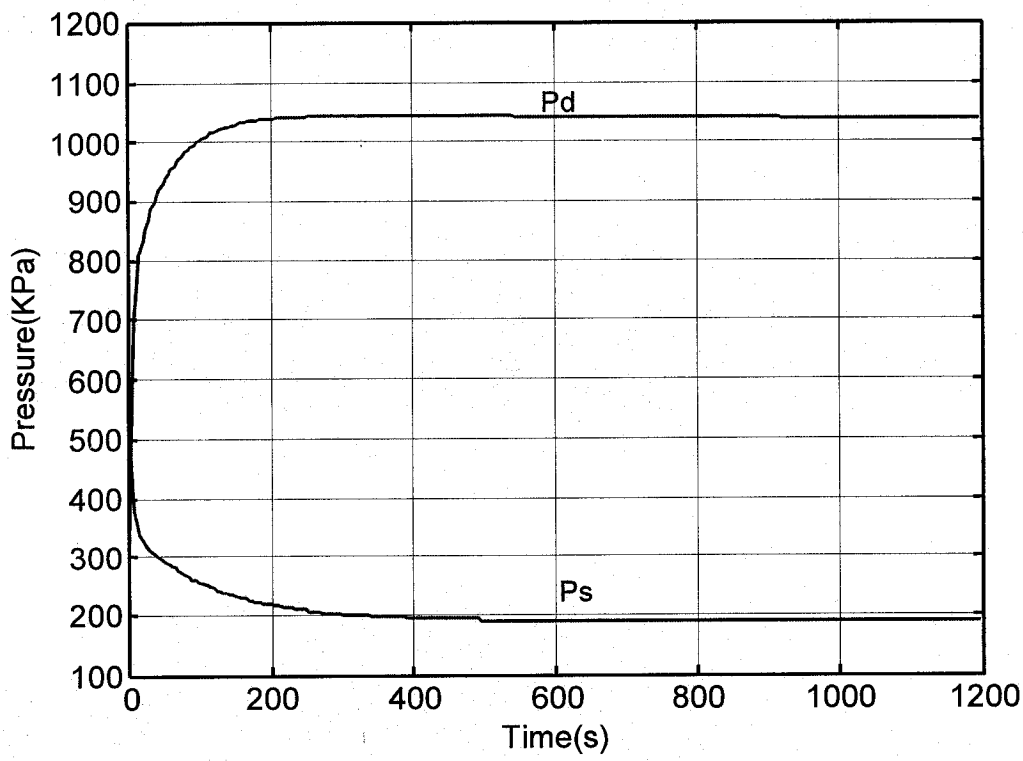

Figure 3.6 Condenser and evaporator pressures as functions of time

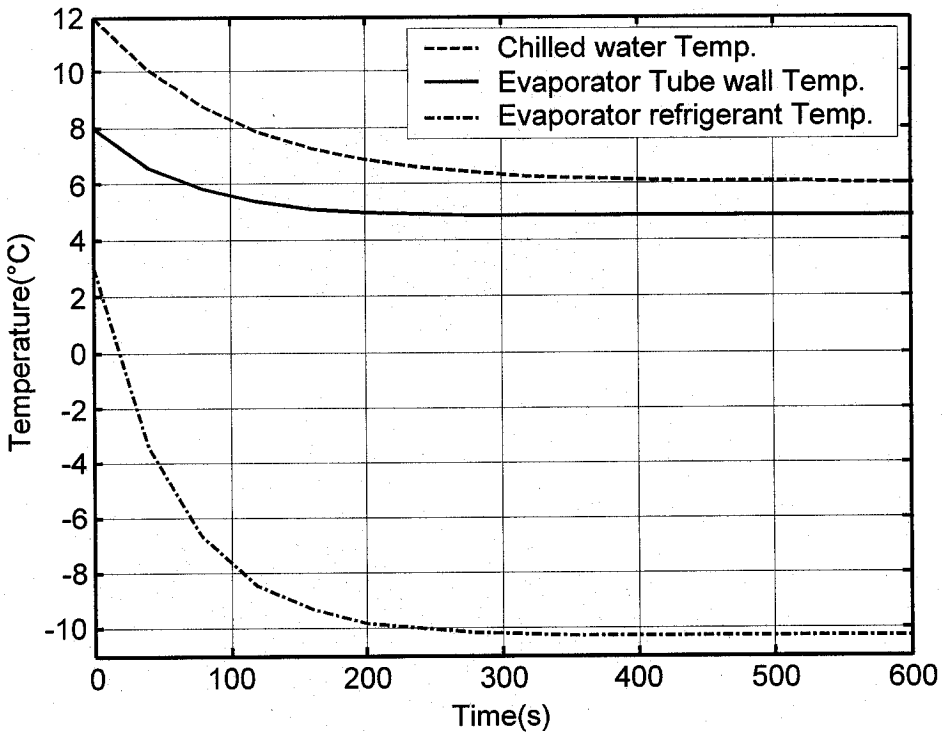

Figure 3.7 Temperatures in evaporator as functions of time

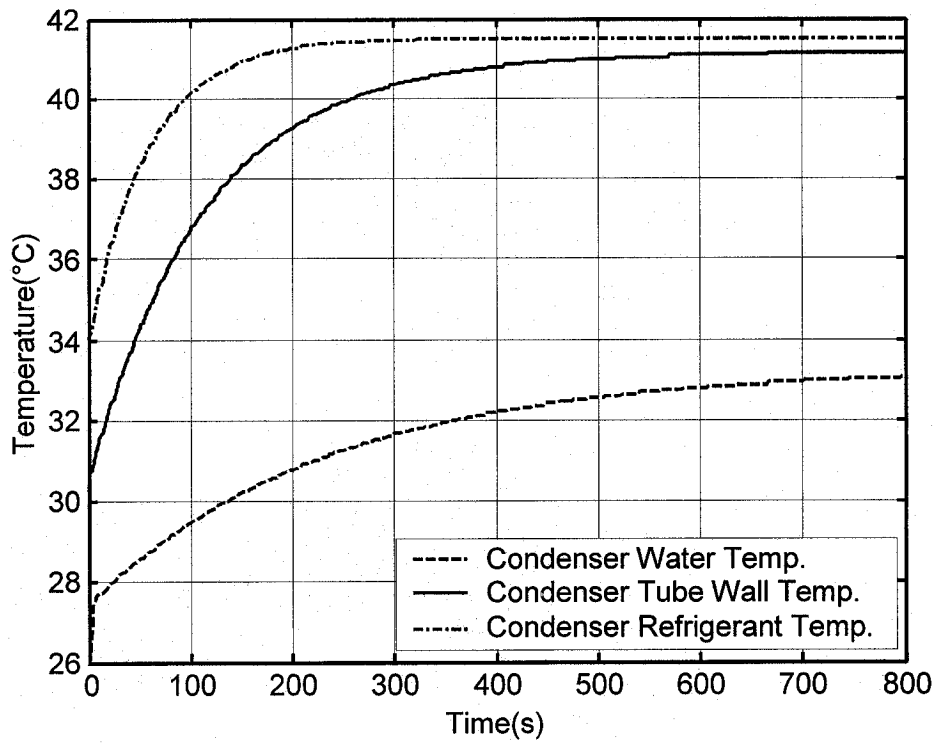

Figure 3.8 Temperatures in condenser as functions of time

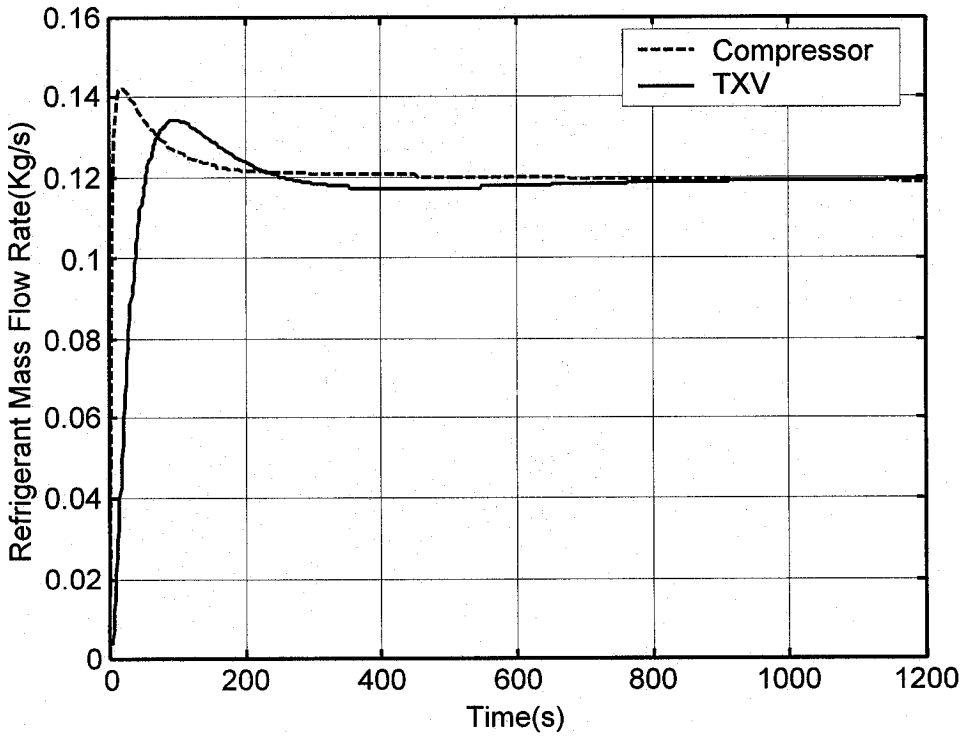

Figure 3.9 TXV and compressor mass flow rates as functions of time

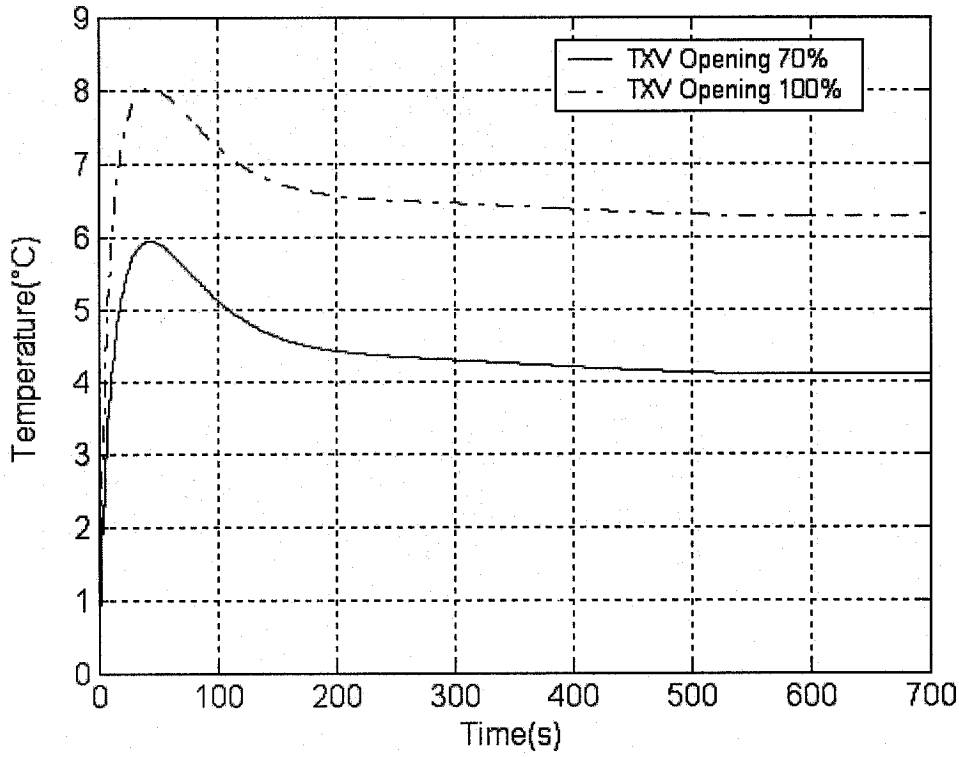

Figure 3.10 Degrees of superheat as functions of time

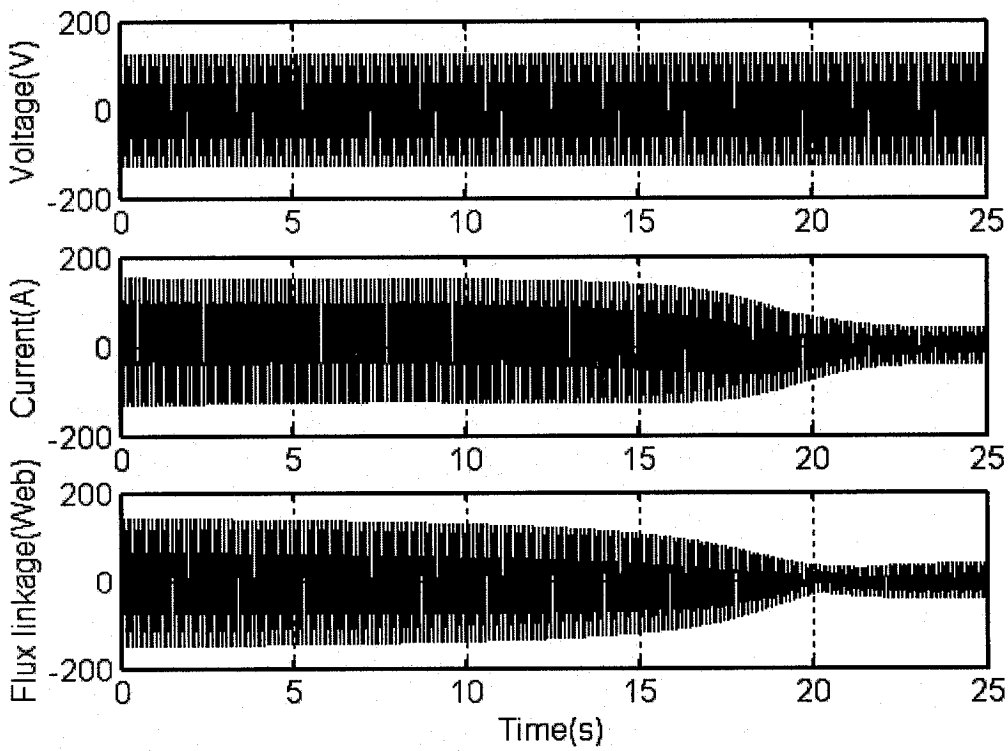

Figure 3.11 Transient relationships with voltage, current, and flux linkage

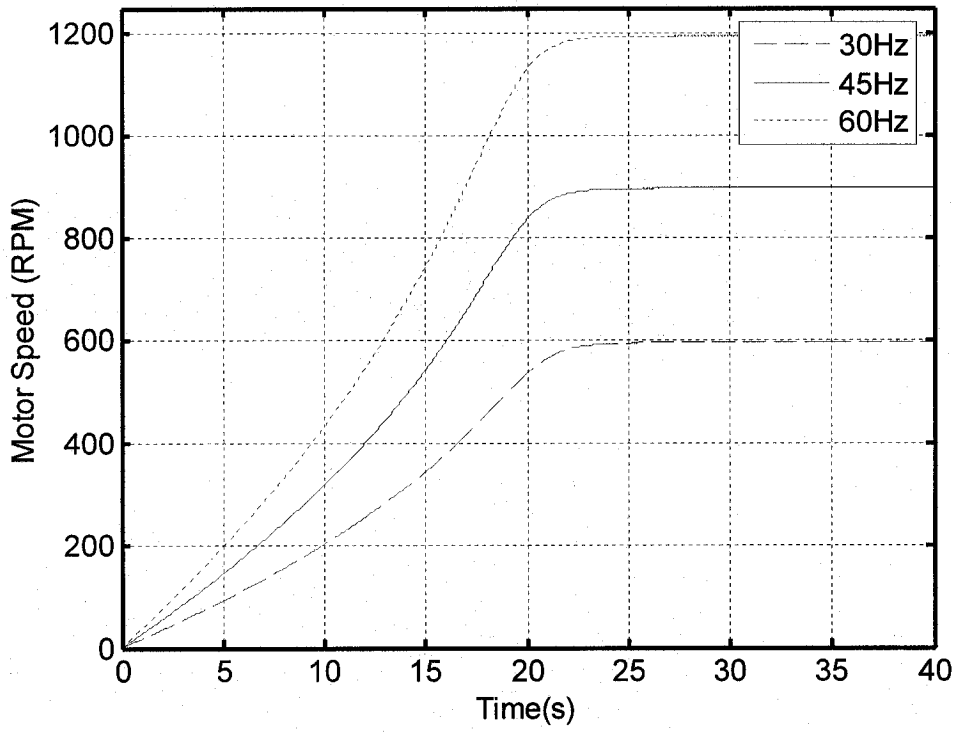

Figure 3.12 Motor speed as a function of time

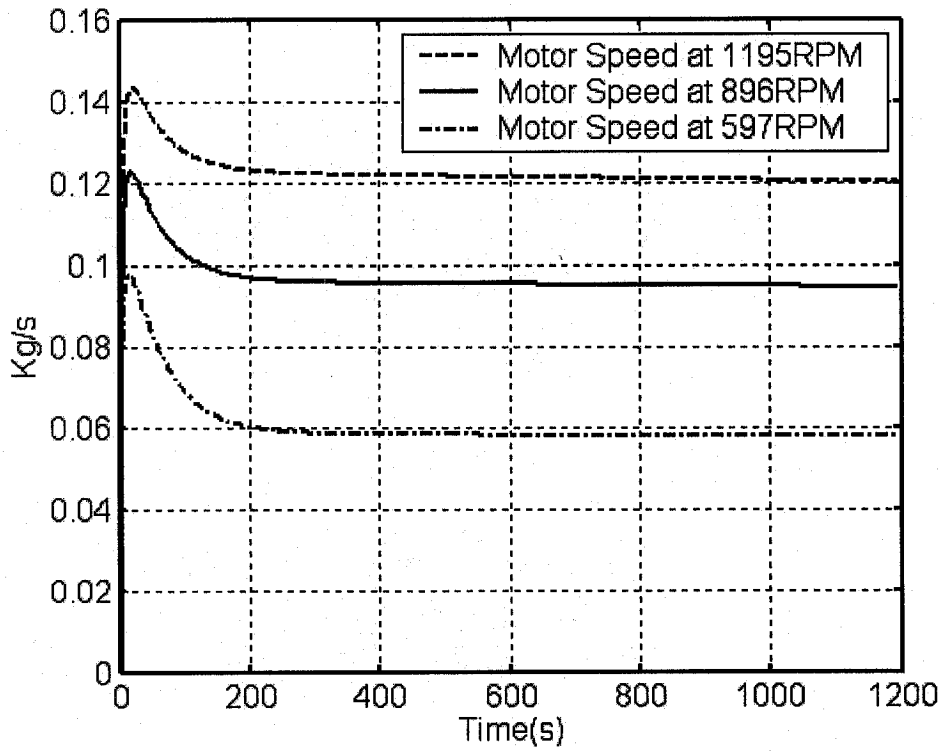

Figure 3.13 Refrigerant mass flow rate as a function of time

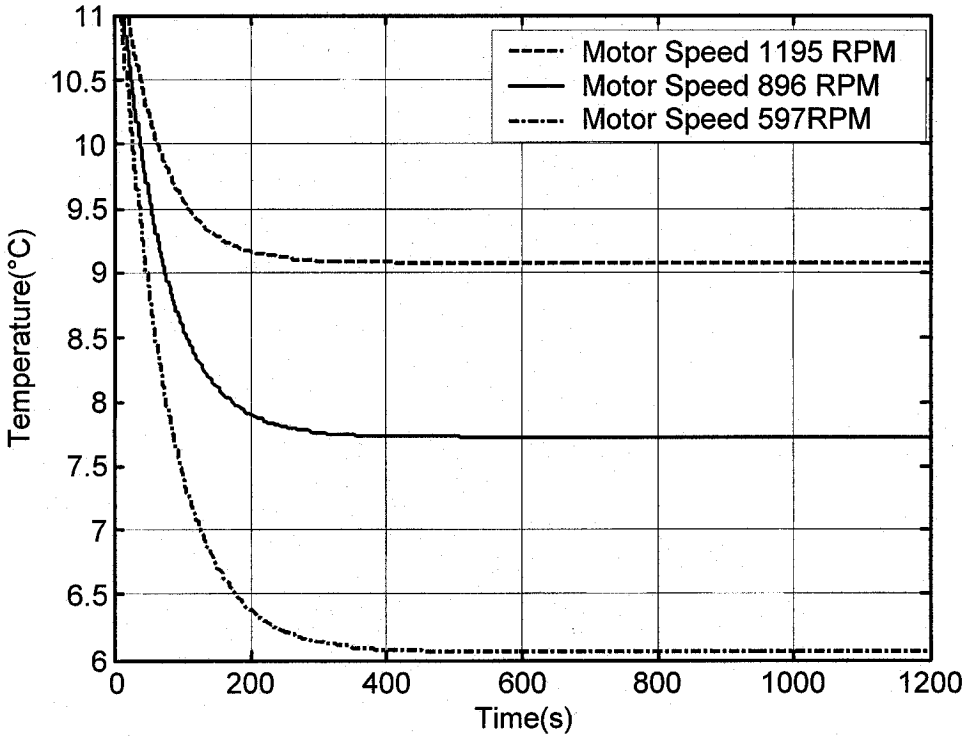

Figure 3.14 Chilled water temperature as a function of time

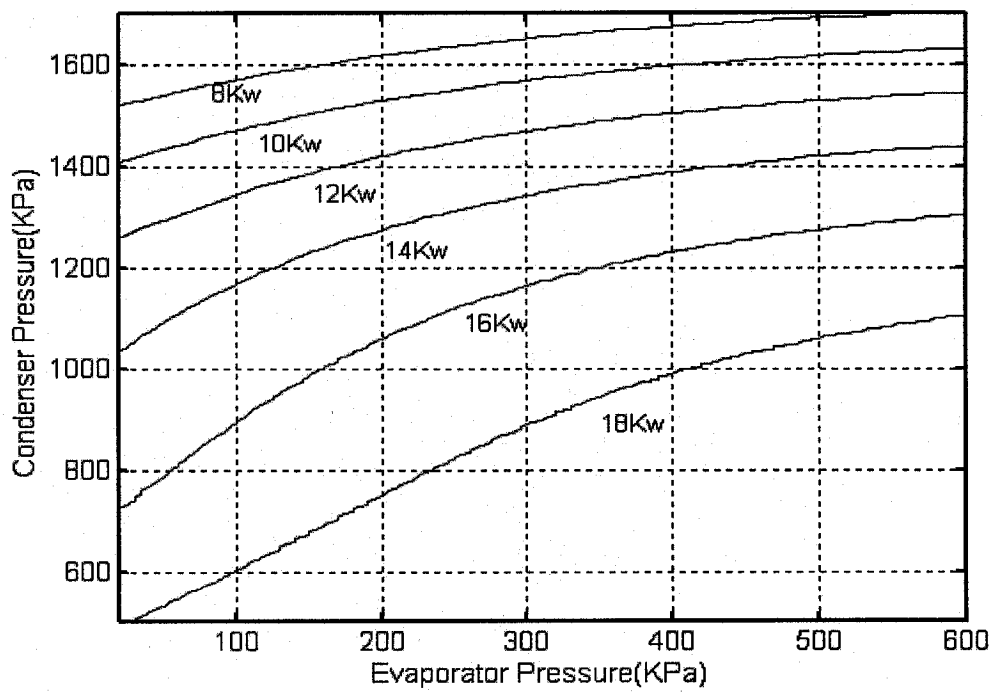

Figure 3.15 Refrigeration system cooling capacity performance curves

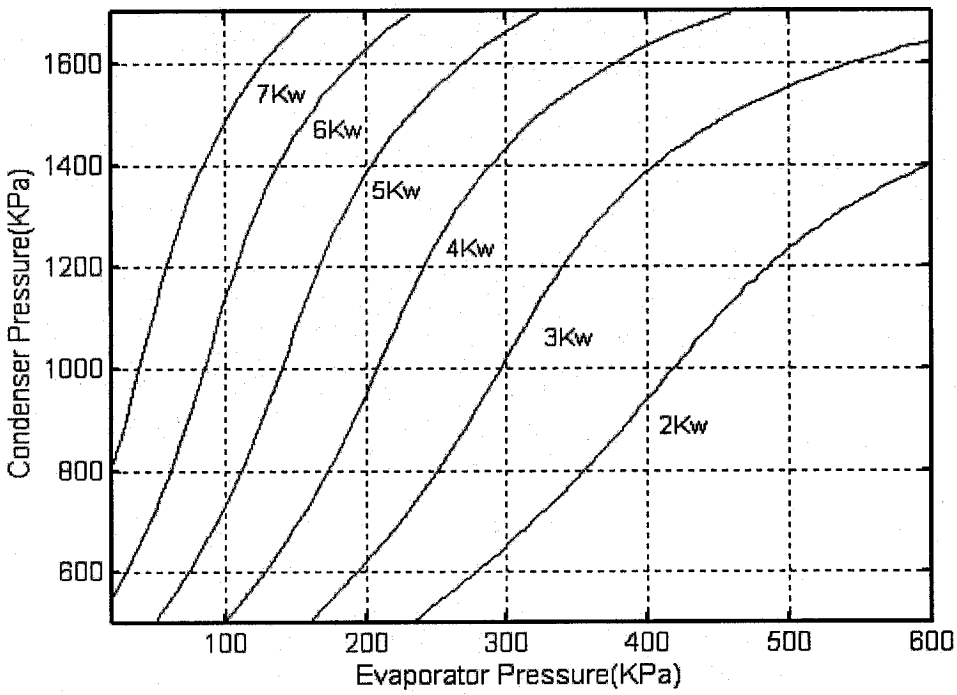

Figure 3.16 Refrigeration system compressor work performance curves

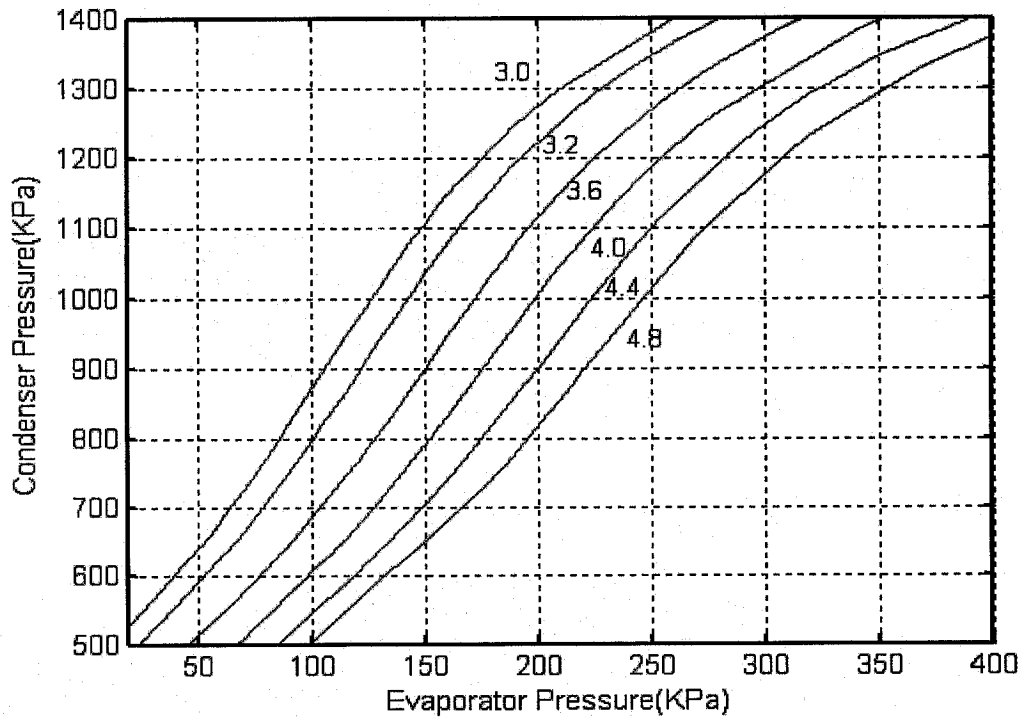

Figure 3.17 Refrigeration system COP performance curves

CHAPTER 4

PI CONTROL OF REFRIGERATION SYSTEMS

4.1 Introduction

The proportional-integral (PI) control has been widely utilized in the field of HVAC control. A typical control system includes the controller, actuator, a system or a process and one or several sensors. The variables to be controlled such as temperature, pressure, speed or refrigerant mass flow rate are obtained from sensors and compared with setpoint values. If there is a difference between the controlled variable value and the setpoint, the controller will receive an error signal and adjust the position of the actuator to eliminate the error. The following Figure 4.1 is a typical feedback control system block diagram.

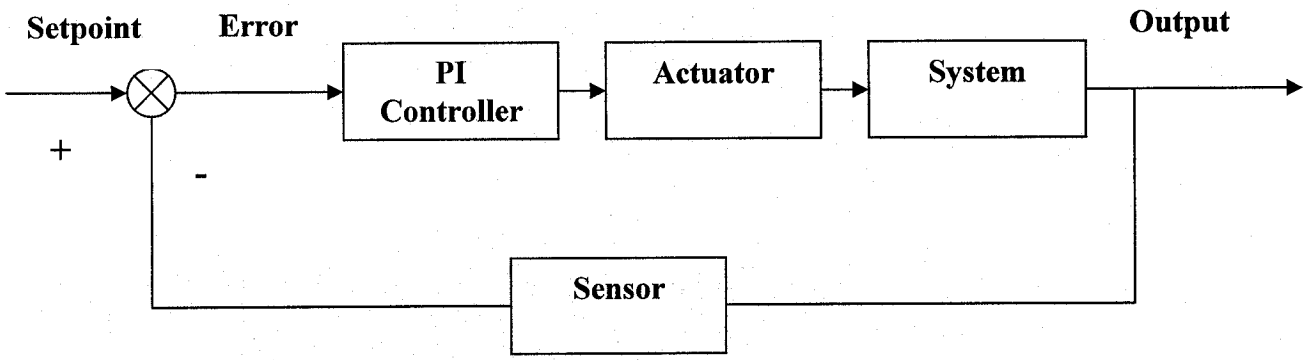

Figure 4.1 Typical feedback control system block diagram

In a PI controller, there are two kinds of control actions, such as proportional control and integral control. Proportional controller is one in which the control action is proportional to the error between the sensed and set values of controlled variation. Its mathematical equation can be expressed as follow

$$V_p(t) = K_p e(t) \tag{4.1.1}$$

where

$V_p(t)$ is the proportional controller output

K_p is the proportional gain

$e(t)$ is the error

Proportional action usually cannot eliminate the error completely in which the stable state value has an offset with the setpoint. When the offset is unacceptable, an additional feature can be incorporated, namely the integral control. The integral mode integrates with respect to time the deviation between the controlled variable and the setpoint, and based on the magnitude of this integral it determines the adjustment to the control signal. The integral control mathematical equation can be expressed as follow

$$V_i(t) = \frac{1}{T_i} \int e(t)dt \tag{4.1.2}$$

where

$V_i(t)$ is the integral controller output

T_i is the integral gain

After combining with Equation 4.11 and 4.12, the PI control equation becomes

$$V(t) = K_p e(t) + \frac{1}{T_i} \int e(t)dt \tag{4.1.3}$$

It is quite common that derivative (D) action is not applied in HVAC control system, so the derivative action is not discussed in this thesis.

The actual actuator in the vapor compression refrigeration closed loop control system is an AC inductive motor, the adjusted system is the vapor compression refrigeration system, and the adjusted volume is refrigerant mass flow rate. As for the sensor used in the control, it is a resistance temperature detector (RTD) or thermocouple sensor. The closed loop system output is chilled supply water temperature, and the input is the setpoint temperature. Figure 4.2 shows the block diagram for closed loop control of vapour compression chiller system

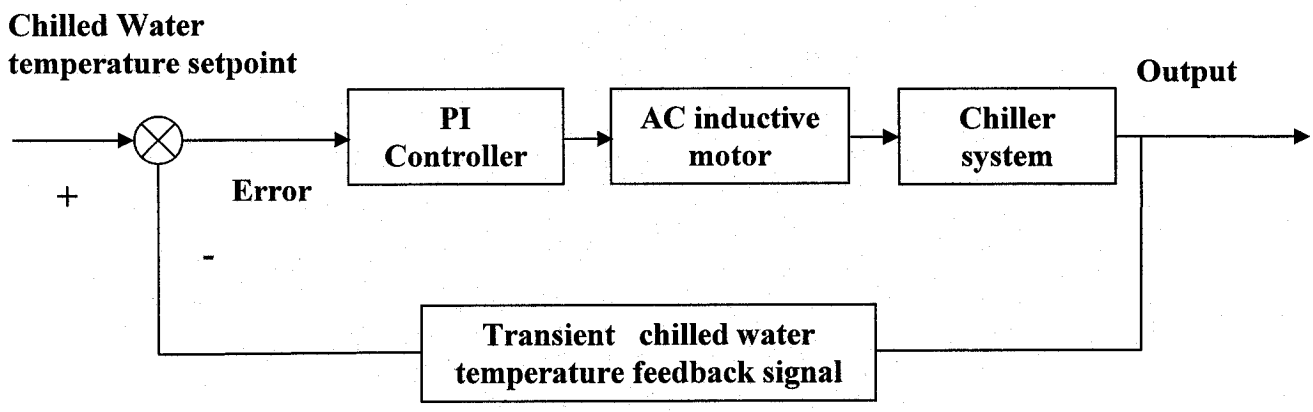

Figure 4.2 Chiller capacity closed loop control system block diagram

In this chapter the following issues will be studied: 1) system control strategy, 2) control configuration, 3) closed loop system response with setpoint and AC motor VFD speed changes, 4) closed loop system response with disturbances changes, 5) closed loop system response with supply water temperature control, and 6) simulation results

4.2 CRC control strategy

The feedback control scheme of CRC is depicted in Figure 4.2. The AC inductive motor block diagram includes six dynamic equations, which describe the AC motor stator current, the flux linkage in rotor phases, angular velocity and angular position. (see Chapter 3). When the motor input frequency is changed, the motor speed is also changes. The input to the motor is motor frequency, and the output of the model is motor rotor speed. Similarly, the chiller system block includes eight dynamic equations, which have been described in Chapter 3. When the AC motor speed is varied, the refrigerant mass flow rate is also changed. Therefore, the chilled water temperature is changed to track the setpoint temperature. The feedback path sends the temperature output value back to the comparison block. The feedback value, namely actual output chilled supply water temperature will be compared with the setpoint temperature, and the difference or the error between the two values will be adjusted by the PI controller to eliminate the error. The chilled water temperature control process for the vapor compression refrigeration system in respectively to an increase in frequency is depicted in flowchart in Figure 4.3. The motor in the refrigeration system is a 7.5 KW VFD AC inductive motor, and its rated speed is 1200 RPM at rated input frequency of 60HZ. The refrigeration system is a 5 Ton reciprocating chiller, with an evaporator, a compressor, a condenser, and the thermostatic expansion valve. The design parameters of this chiller were given in Chapter 3. The chilled supply water temperature ranged from 6°C to 12°C.

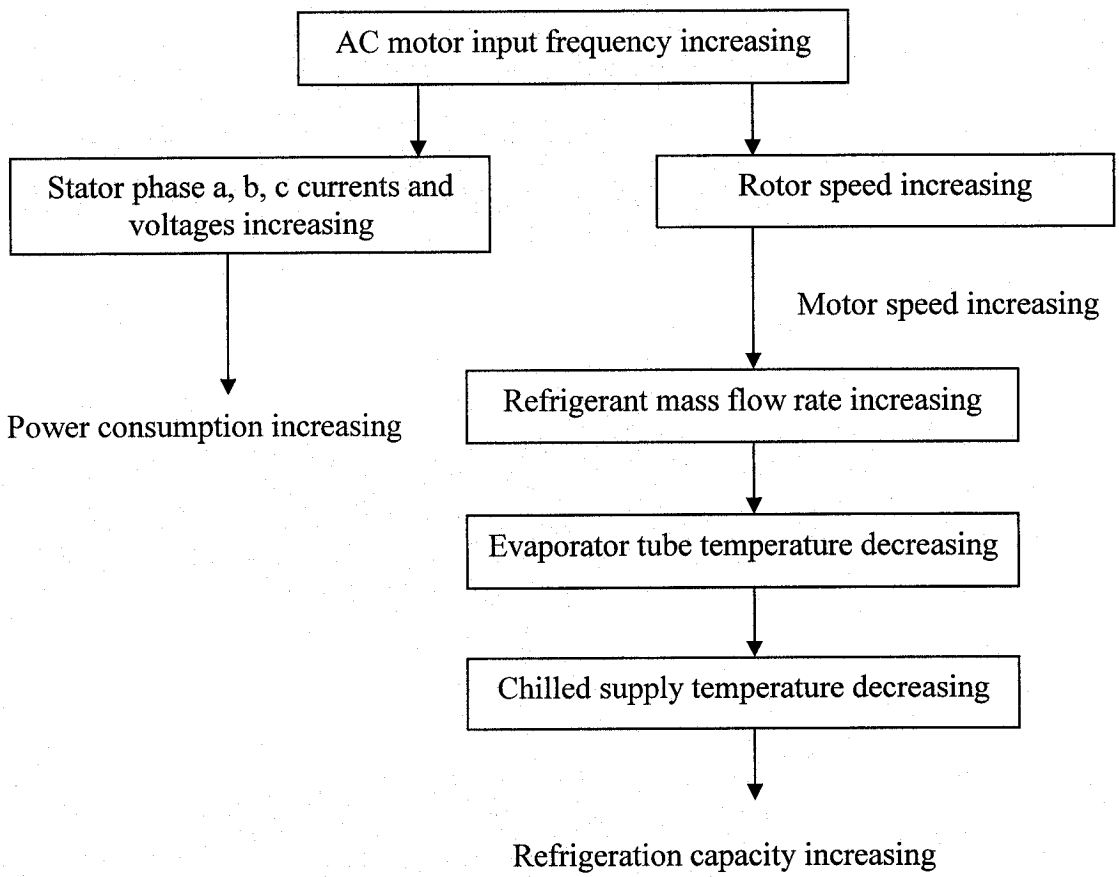

Figure 4.3 Refrigeration system capacity control flowchart

4.3 Closed loop system response with setpoint and motor speed changes

The Figure 4.4 is a closed loop system block diagram with the setpoint temperature changed by the AC motor VFD speed control. The first block is the PID control model, the second block is the motor VFD model, the third block is the refrigeration system compressor block and the fourth is chiller evaporator and condenser block. The controlled output and feedback signal are the chilled supply water temperature. The error

is the difference between the setpoint and feedback signal. These blocks and controlled parameters make up the whole temperature feedback control system. In the following simulation cases, the setpoint temperatures are changed from 6°C and 8.0°C, and the resulting motor rotor speed and frequency responses were observed. The system steady state times and final temperatures were recorded.

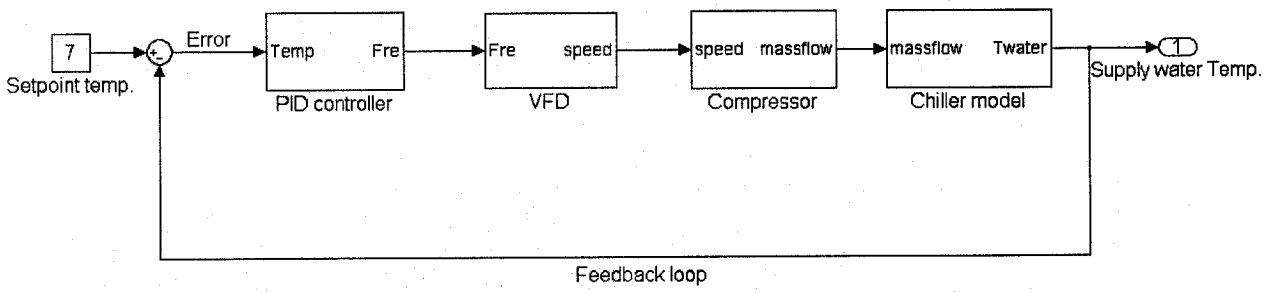

Figure 4.4 Closed loop refrigeration system with setpoint changed block diagram

In case 1, the setpoint temperature is at 6°C, and system simulation time is one hour. Figure 4.5 shows the chilled supply water temperature response tracking the setpoint temperature 6°C. The system steady state time is about 0.2 hour, and the maximum overshoot is about 4°C. The final value is 6.04°C which is very close to the setpoint temperature. Figures 4.6 and 4.7 show respectively the corresponding motor rotor speed and input frequency responses. This simulation corresponds to the rated design conditions. In other words for the supply water temperature of 6°C, the corresponding motor input frequency should be its rated frequency, namely 60Hz. We could see from Figure 4.7 that the steady state value of frequency is 60Hz. However, due to the motor

rotor slip rate, the steady state motor rotor speed is 1178 RPM rather than 1200RPM. Figure 4.8 shows that the refrigerant mass flow rate response closely follows the dynamic responses of motor rotor speed. The final value is about 0.12 Kg/s reaching steady state in 0.2 hours.

In case 2, the setpoint temperature is 8.0°C, and system simulation time is also one hour. Figures 4.9, 4.10, 4.11, 4.12 show respectively the closed loop responses of supply water temperature, motor rotor speed, input frequency and refrigerant mass flow rate. As the setpoint temperature is changed from the 6°C to 8.0°C, the motor rotor speed and input frequency are reduced to 785 RPM and 39 Hz respectively. However, the system steady state time, 0.25 hour is longer than the one in case 1. The reason is that the PI parameters are not changed when the setpoint temperature is changed from the 6°C to 8.0°C. By choosing better PI parameters, the steady state time could be decreased. The system final value temperature is 8.0°C, which is the same as the setpoint temperature. The refrigerant mass flow rate under this part load condition reduces to 0.078 Kg/s.

In the above case1 and case 2, the PI control parameters were kept constant. By comparing the systems response times, steady state errors, and maximum overshoot of the two cases, it is noted that although there are slight differences in dynamic responses, the differences are small and are acceptable. On the other hand, slight variations in steady state time do not affect the steady state simulation results to analyze the relationship among motor rotor speed, changed setpoint temperatures, and system capacity. For these reasons, it was decided to use constant set of PI parameters in all other simulation runs in this thesis.

When we compare Figures 4.6 and 4.10, it is easy to conclude that the motor rotor speed at setpoint temperature 8.0 °C is lower than that of the setpoint temperature 6°C. It is well known that by decreasing the speed using VFD significant energy savings could be realized.

4.4 Load-matching optimal setpoint control strategy

A practical problem faced by plant operation engineers is to predict the chiller loads as accurately as possible and thus set the supply water temperature appropriate for the load. In the event the supply water temperature setpoint in chosen either higher or lower than necessary, it could lead energy losses. In order to address this issue, an optimization methodology for determining optimal setpoint is proposed here. The optimal setpoints so determined serve as setpoint trajectories for PI controller.

The main energy consuming device in a CRC is the electrical power of compressor motor for running chiller under different load condition. Operating the chiller at as high a COP as efficiency as possible at the given load and through selecting optimal setpoints we can achieve significant energy savings. If a CRC control loop can track an energy optimal setpoint profile, significant energy savings can be realized. To this end, a constrained optimization problem was formulated and solved. The method of steady state multi-variable constraint optimization is utilized to find out the optimal setpoint T_{sw}. The optimization approach includes defining an objective function and specifying the limit bounds of control parameters. Since the electrical power consumption of CRC is a function of cooling load and T_{sw}, therefore, the objective function in the optimization problem should consider the effects of T_{sw}, P_{eva}, P_{con}, I, U and COP etc.

If we assume building's internal load remains more or less constant and thus the building's total cooling can be assumed to be a function of outdoor temperature. So, we could obtain a function of outside temperature. By using the methodology described by Cho and Zaheeruddin (2002), building cooling load as a function of outdoor temperature was determined (Figure 4.14). A multi-variable constraint optimization problem was solved to obtain optimal operating setpoints based on such building outside cooling load model.

4.4.1 Steady state optimization

To obtain the optimal setpoints, first, it is necessary to define an objective function which includes all of energy consumption elements. Then, describe constraint relationships together with upper and lower bounders. The optimization problem so formulated could be solved using available software packages in Matlab.

The aim of the optimization is to minimize the objective function in order to save electrical power consumption. The optimization problem was defined as the minimization of compressor work

$$J = \frac{n}{n-1} P_s V_s [(\frac{P_d}{P_s})^{\frac{n-1}{n}} - 1] \tag{4.4.1}$$

Subject to steady state model equations as given below

$$M_{ero} = C_v A_v V_o \sqrt{(P_d - P_s)\rho_{eri}} \tag{4.4.2}$$

$$T_{sw} = \frac{(1.99A_{ei}h_{eot}A_{eot} + 1.66A_{eo}h_{eot}A_{eot})T_{eot} - 3.32A_{ei}A_{eo}T_{er}}{(1.99A_{ei}h_{eot} + 1.66A_{eo}h_{eot}A_{eot} - 3.32A_{ei}A_{eo})} \tag{4.4.3}$$

$$T_{er} = (\frac{h_{eot}A_{eot}}{1.66A_{eo}} + \frac{h_{eot}A_{eot}}{1.99A_{ei}})T_{eot} + (1 - \frac{h_{eot}A_{eot}}{1.66A_{eo}} + \frac{h_{eot}A_{eot}}{1.99A_{ei}})T_{ew} \tag{4.4.4}$$

$$H_{ei} = (\alpha_e - 1)H_{elv} - \frac{H_{eo}}{M_{ero}} + \frac{1.99A_{ei}T_{er}}{M_{ero}}) \tag{4.4.5}$$

$$H_{eo} = (\alpha_e - 1)H_{elv} - \frac{H_{ei}}{M_{ero}} + \frac{1.99A_{ei}T_{er}}{M_{ero}}) \tag{4.4.6}$$

$$T_{cr} = (1 + \frac{h_{\cot}A_{\cot}}{2.28A_{co}} + \frac{h_{\cot}A_{\cot}}{3.86A_{ci}})T_{cw} - \frac{(3.86A_{ci} + 2.28A_{co})h_{\cot}A_{\cot}}{8.8A_{ci}A_{co}}T_{\cot} \tag{4.4.7}$$

$$T_{cw} = \frac{8.8A_{ci}A_{co}T_{cr} + (3.86A_{ci} + 2.28A_{co})h_{\cot}A_{\cot}T_{\cot}}{8.8A_{co}A_{ci} + 3.86A_{ci}h_{\cot}A_{\cot} + 2.28A_{co}h_{co}A_{\cot}} \tag{4.4.8}$$

$$H_{ci} = H_{co} - A_i H_{clv} + \frac{(3.86A_{ci}^2 - A_{ci})T_{cr}}{M_{cro}} \tag{4.4.9}$$

$$H_{co} = A_i H_{clv} - H_{co} - \frac{(3.86A_{ci}^2 - A_{ci})T_{cr}}{M_{cro}} \tag{4.4.10}$$

$$M_{cro} = A_{cic}\rho_{cro}L_c\alpha_c \tag{4.4.11}$$

$$i_x = \frac{(\frac{R_r}{L_r} \cdot \frac{M}{L_s L_r\left(1 - \frac{M^2}{L_s L_r}\right)} \cdot fl_a + \frac{M}{L_s L_r\left(1 - \frac{M^2}{L_s L_r}\right)} \cdot np \cdot fl_b \cdot av + \frac{U1}{\left(1 - \frac{M^2}{L_r L_s}\right) \cdot Ls})}{(\frac{R_r M^2}{L_s L_r^2(1 - \frac{M^2}{L_s L_r})})} \tag{4.4.12}$$

$$i_y = \frac{(\frac{R_r}{L_r} \cdot \frac{M}{L_s L_r\left(1 - \frac{M^2}{L_s L_r}\right)} \cdot fl_b + \frac{M}{L_s L_r\left(1 - \frac{M^2}{L_s L_r}\right)} \cdot np \cdot fl_a \cdot av + \frac{U2}{\left(1 - \frac{M^2}{L_r L_s}\right) \cdot Ls})}{(\frac{R_r M^2}{L_s L_r^2(1 - \frac{M^2}{L_s L_r})})} \tag{4.4.13}$$

$$fl_a = \frac{np \cdot fl_b \cdot av + \frac{R_r}{L_r} \cdot M \cdot i_x}{\frac{R_r}{L_r}} \tag{4.4.14}$$

$$fl_b = \frac{np \cdot fl_a \cdot av + \frac{R_r}{L_r} \cdot M \cdot i_y}{\frac{R_r}{L_r}} \tag{4.4.15}$$

$$av = \frac{2np\frac{M}{3JL_r} \cdot (fl_a \cdot i_y - fl_b \cdot i_x) - \frac{T_{mech}}{J}}{(\frac{f}{J})} \tag{4.4.16}$$

$$\begin{bmatrix} U_1 \\ U_2 \end{bmatrix} = \begin{bmatrix} 3/2,0,0 \\ 0,\sqrt{3}/2,-\sqrt{3}/2 \end{bmatrix} \begin{bmatrix} U_{sa} \\ U_{sb} \\ U_{sc} \end{bmatrix} \tag{4.4.17}$$

$$\begin{bmatrix} i_{sa} \\ i_{sb} \\ i_{sc} \end{bmatrix} = \begin{bmatrix} 2/3,0 \\ -1/3,1/\sqrt{3} \\ -1/3,1/\sqrt{3} \end{bmatrix} \begin{bmatrix} i_x \\ i_y \end{bmatrix} \tag{4.4.18}$$

The upper and lower bounders of these variables were selected and are given in Table 4.1.

Table 4.1 Boundary conditions of variables for optimization parameters

Variable	P_{con}	P_{eve}	T_{sw}	T_{cr}	T_{er}	T_{cw}	H_{ei}	H_{eo}
Unit	KPa	KPa	°C	°C	°C	°C	KJ/kg	KJ/kg
Lower bounders	700	100	6	36	-26	25	16	231
Upper bounders	1100	290	12	44	-1	32	50	248
Variable	H_{ci}	H_{co}	i_{sa}	i_{sb}	i_{sc}	u_{sa}	u_{sb}	u_{sc}
Unit	KJ/kg	KJ/kg	A	A	A	V	V	V
Lower bounders	269	109	5	5	5	45	45	45
Upper bounders	232	83	60	60	60	127	127	127

4.4.2 Optimization results

The optimization results obtained are summarized in this section. The optimal chilled supply water temperature (T_{sw}) and COP are shown in Figure 4.15. This relationship shows optimal chilled water temperature and COP as a function of cooling load. When cooling load increases, optimal chilled water temperature and COP decrease simultaneously. For example, when cooling load increases from 40% to 80%, Tsw and COP decrease from 9.2°C and 6.5 to 6.8°C and 3.9°C respectively.

Figure 4.16 shows optimal trajectory between condenser and evaporator pressures. Figure 4.17 shows the corresponding compressor work as a function of supply water temperature (T_{sw}). With the increase of supply water temperature, the motor electrical consumption decreases. For this reason, chiller COP increases at low load conditions.

4.4.3 Closed loop system response with step change in cooling load

The optimal setpoint profiles shown in Figure 4.15 were used as variable setpoint for PI controller and closed CRC system responses were simulated. The results are discussed in

this section. First, results for step change in cooling load are presented. It was assumed that the anticipated cooling load is 85% of design value. The anticipated load is used to compute the optimal setpoint. Figure 4.18 shows the output capacity response. The steady state chiller capacity is 4.45USRt and reaches steady state in 0.2 hour. The condenser pressure and evaporator pressure final values are respectively 1180KPa and 235KPa. These results are shown in Figures 4.19 and 4.20. Figure 4.21 shows the chilled supply water temperature response, and its final value is about 7.2 °C. Similarly the compressor work and COP responses are depicted Figures 4.22 and 4.23 respectively.

It is possible that the anticipated cooling load may not exactly match the actual load. In such cases the chosen setpoint may not be optimal, thus some mismatch is likely to occur. However, even with this limitation it is still the best way to save energy by steering the chiller setpoints towards approaching part-load conditions. Since this process could take more than an hour to reach part load conditions in an actual system, the proposed strategy when implemented effectively takes care of gradually changing the setpoint as the chiller load approaches the part load condition.

4.4.4 Closed loop system response with anticipated daily cooling loads

In this case, the single chiller operation will be simulated to match different predicted cooling loads over a day. The predicted cooling load profile is shown in Figure 4.24. The load profile corresponds to a building schedule beginning in the morning 7:00 to evening 21:00, and is of 14 hours duration. The predicted cooling load is assumed to be about 40% of design load during 7:00 to 9:00, increased to 60% between 9:00 to 12:00, reaching maximum load from 12:00 to 16:00, and after 16:00, the cooling load is

reduced to 40%. Given this load profile, the vapor compression refrigeration system is controlled to adjust the system capacity with the anticipated cooling load. By applying the load matching optimal setpoint control strategy, the chilled water setpoint was continuously changed according to the cooling load variations.

Figure 4.25 shows chilled supply water temperature over the 14 hours period. As the cooling load increases from morning to afternoon, the chilled supply water temperature decreases from 9.5°C to 7.6°C, and the chiller capacity increases to balance the anticipated load. After 4:00PM the load is reduced to 40% of the design value, and the corresponding chilled supply water temperature increases to 9.5 °C.

Figures 4.26 and 4.27 show respectively the compressor work and COP during the same 14 hours. The minimum COP is 4.2 between 12:00 to 16:00 under maximum cooling load. The compressor work is also maximum (3.4Kw) in the same period.

Figures 4.28 and 4.29 show the motor rotor speed and refrigerant mass flow rate responses. The responses of COP and compressor work show the energy efficiency of the control strategy. When the anticipated cooling load increases, the motor rotor speed increases. For example, when cooling load is 40%, the motor rotor speed is about 470 RPM. As the cooling load increases to 80%, the motor rotor speed also increases to 940 RPM. At the same time, the refrigerant mass flow rate changes from 0.047Kg/s to 0.097Kg/s. At lower motor rotor speed, a higher COP is achieved which contributes to better overall energy efficiency of the variable speed compression refrigeration chiller.

The simulation results show that the developed optimization methodology and the designed control system are able to regulate the chiller capacity as a function of predicted cooling load in an optimal manner to achieve a higher COP of the system.

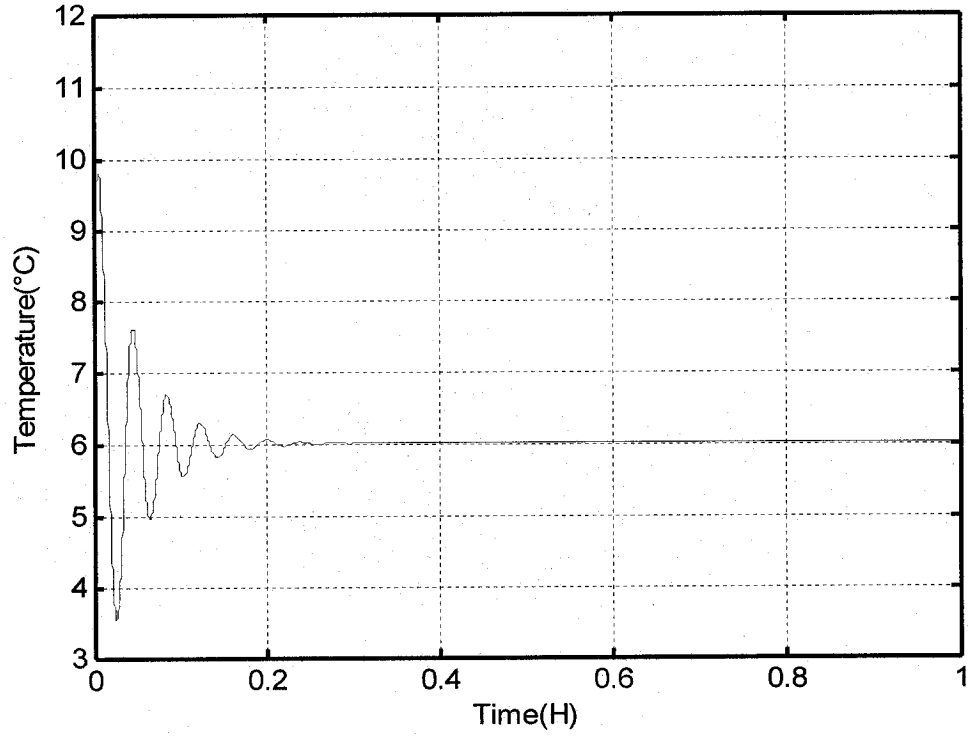

Figure 4.5 Chilled supply water temperature response at setpoint 6°C

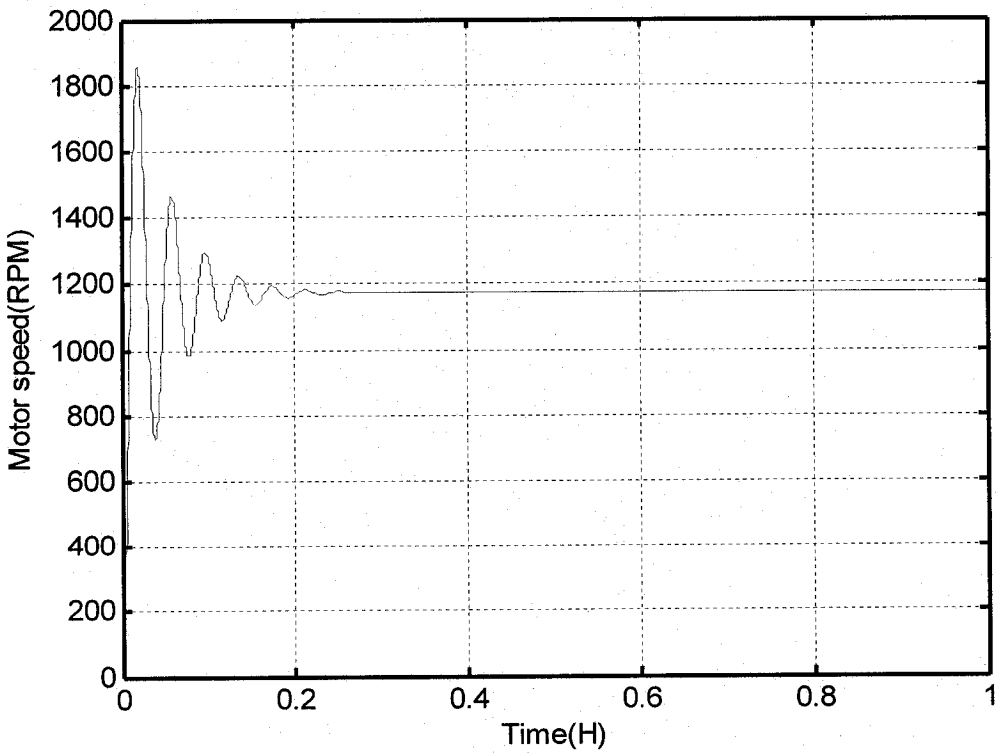

Figure 4.6 Motor speed response at setpoint 6°C

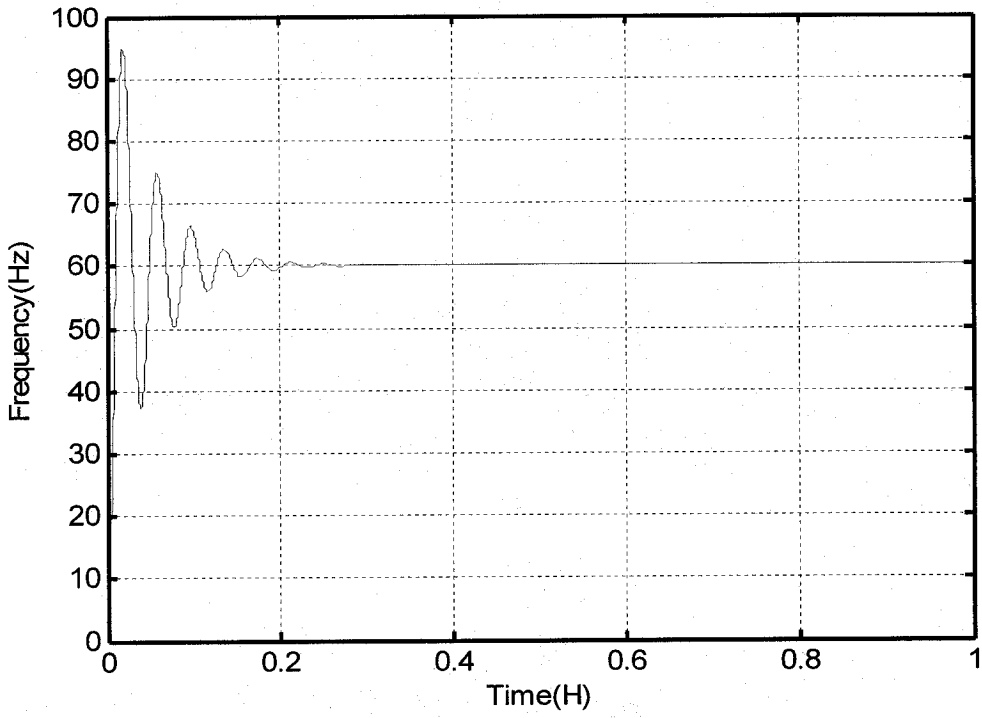

Figure 4.7 Motor input frequency response at setpoint 6°C

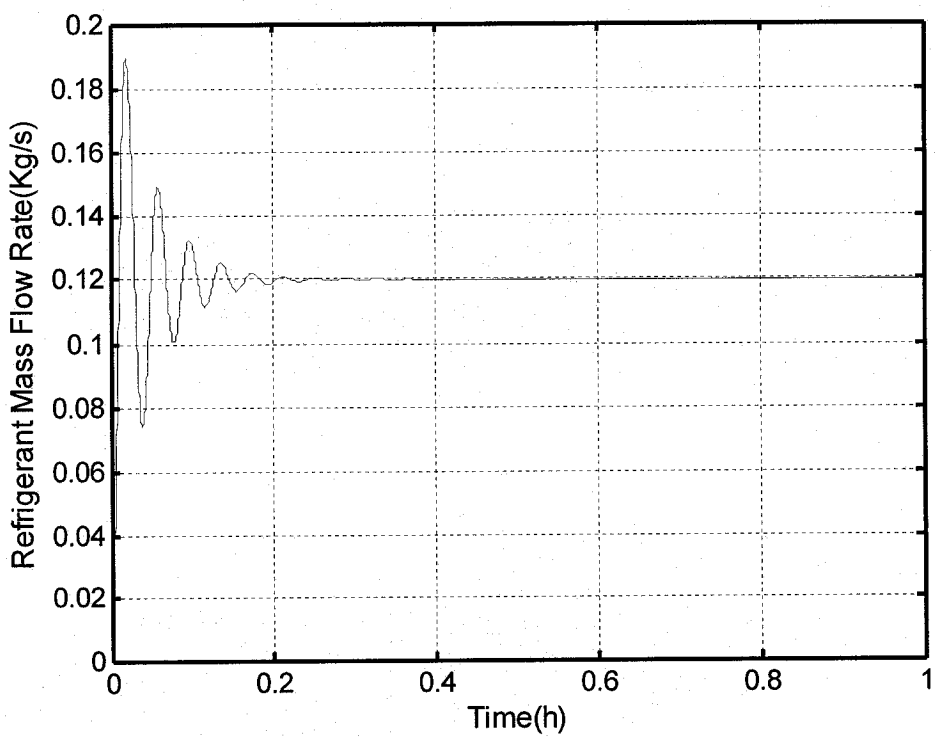

Figure 4.8 Refrigerant mass flow rate response at setpoint 6°C

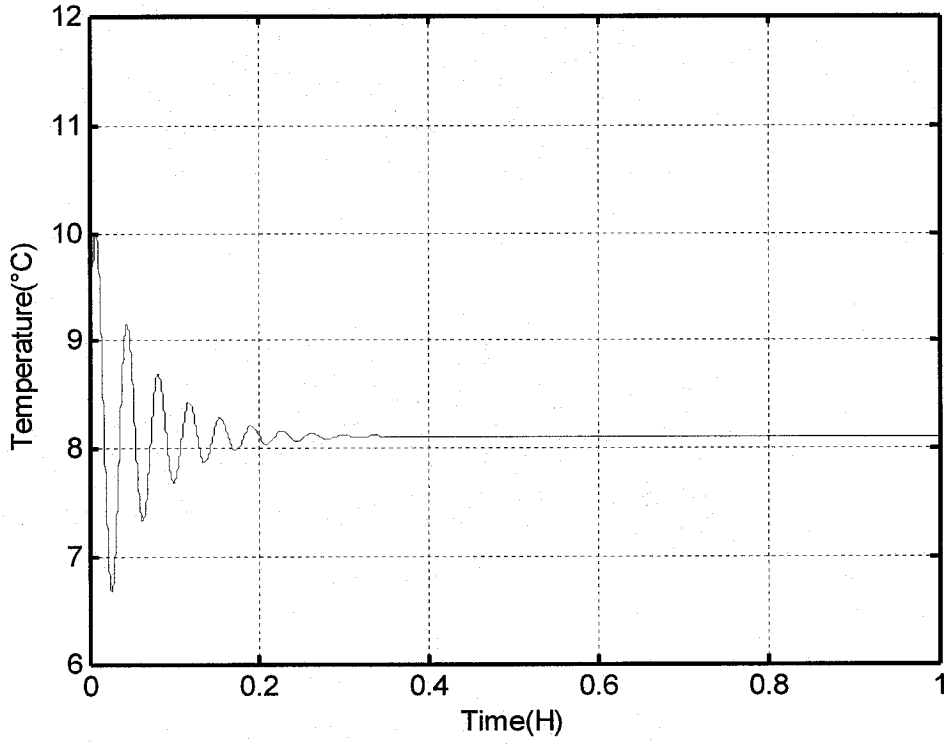

Figure 4.9 Chilled supply water temperature response at setpoint 8.1°C

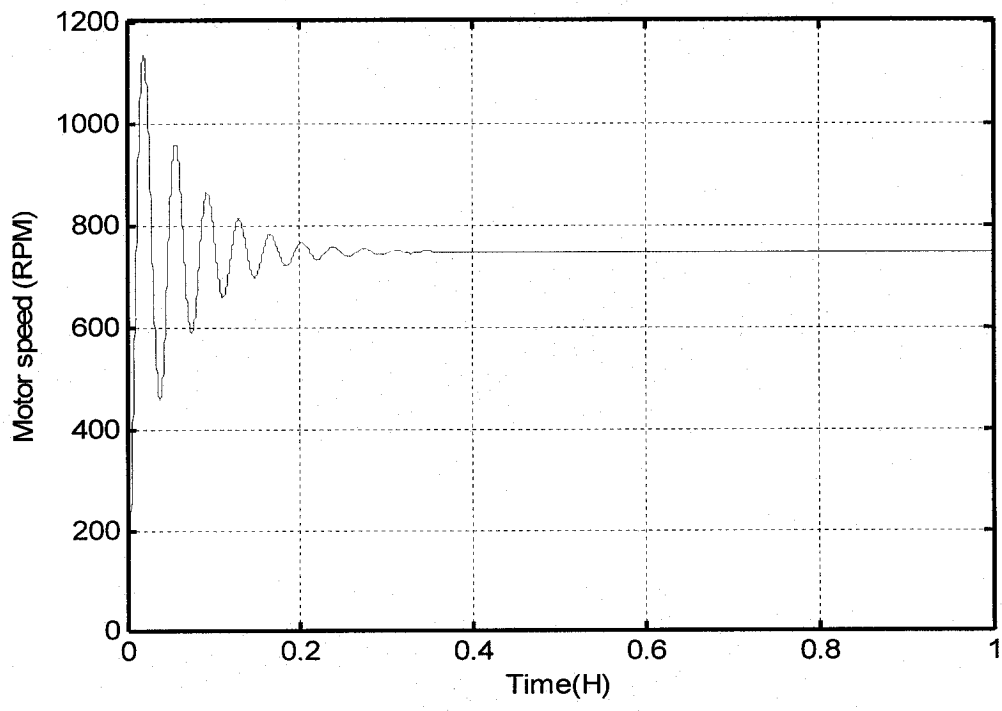

Figure 4.10 Motor speed response at setpoint 8.1°C

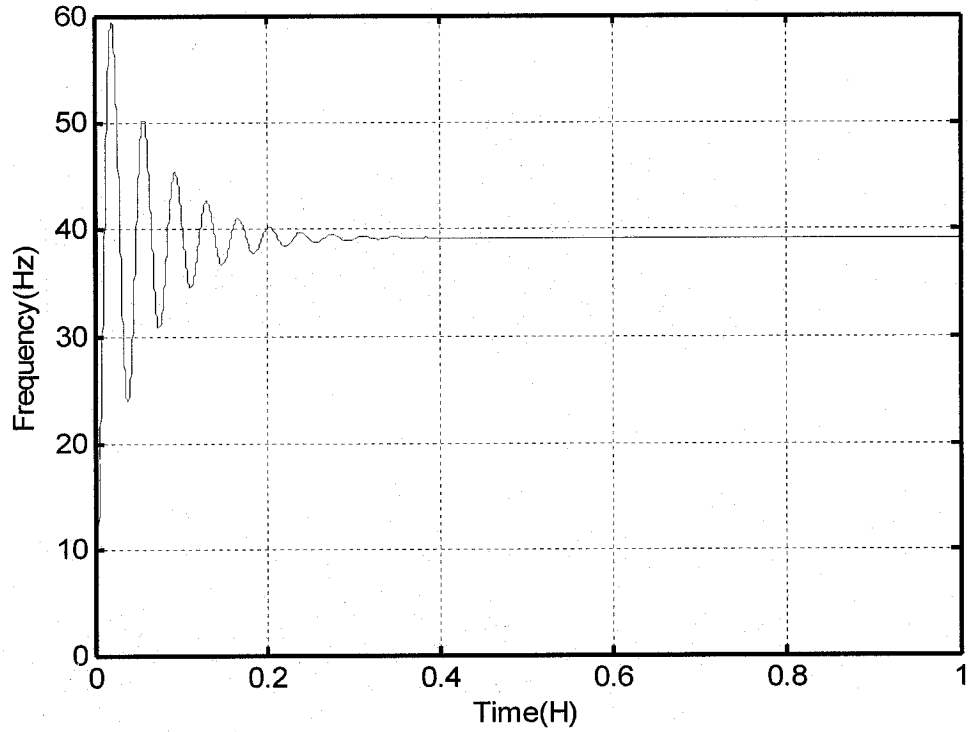

Figure 4.11 Motor input frequency response at setpoint 8.1°C

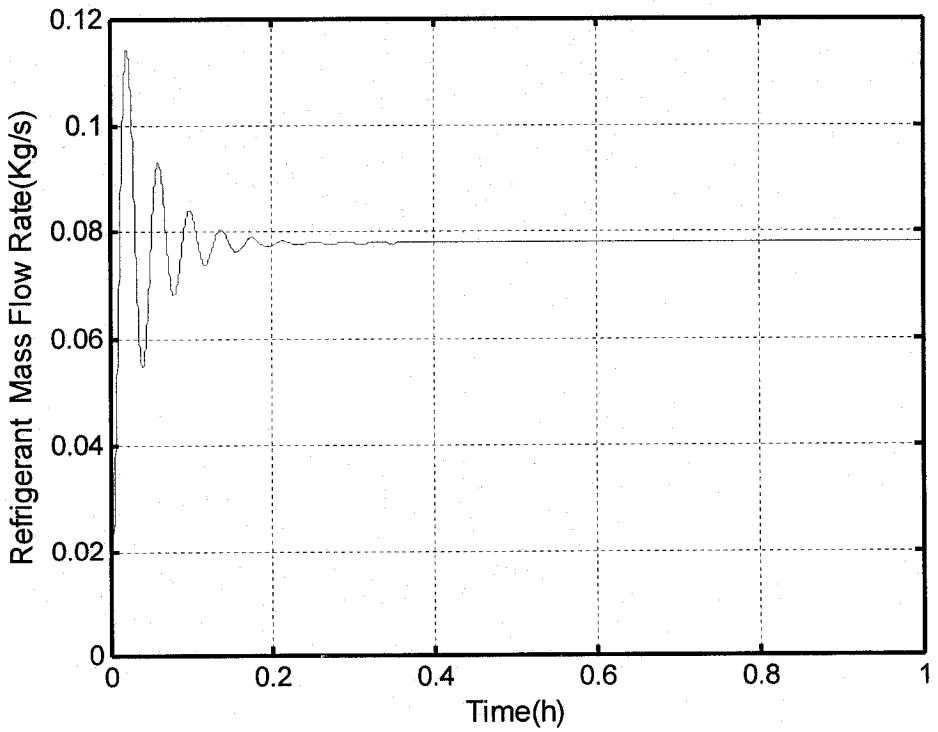

Figure 4.12 Refrigerant mass flow rate response at setpoint 8.1°C

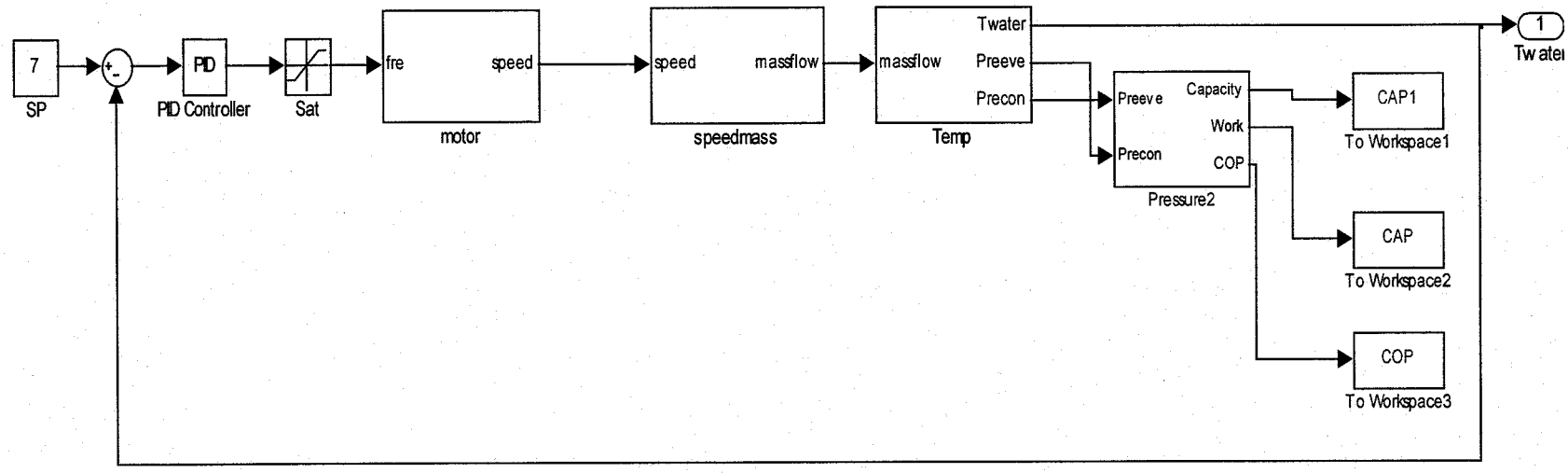

Figure 4.13 Simulation program block diagram

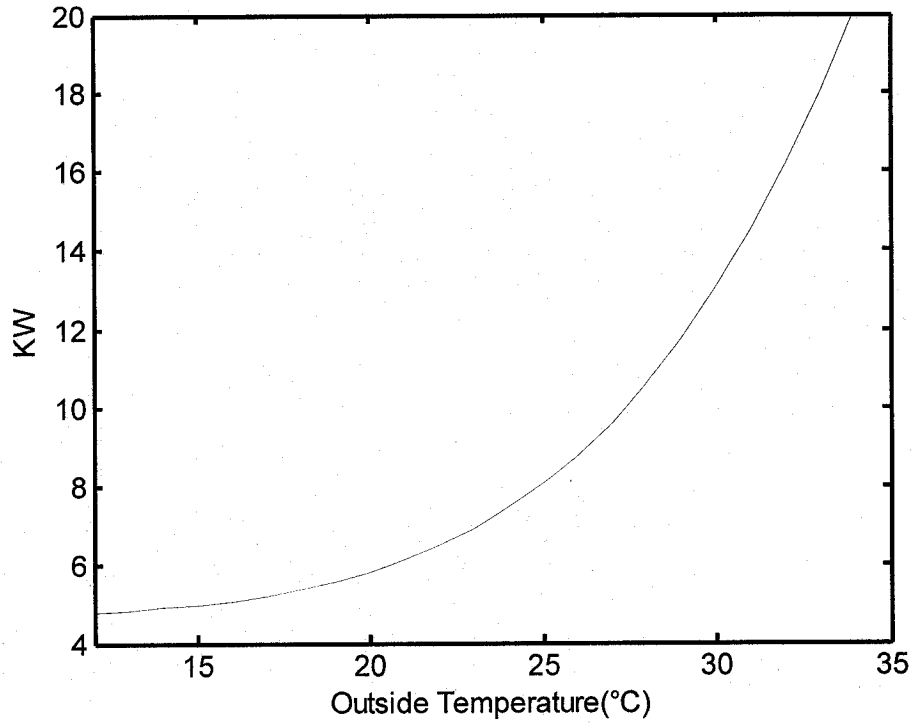

Figure 4.14 Cooling load as a function of outside temperature

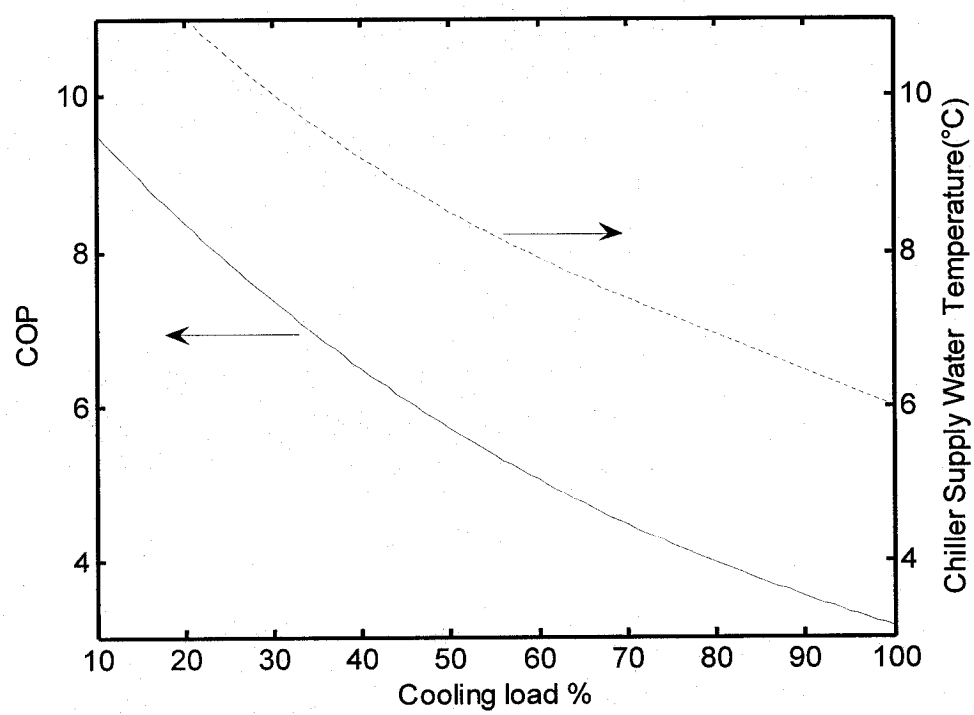

Figure 4.15 Optimal chilled supply water temperature and COP

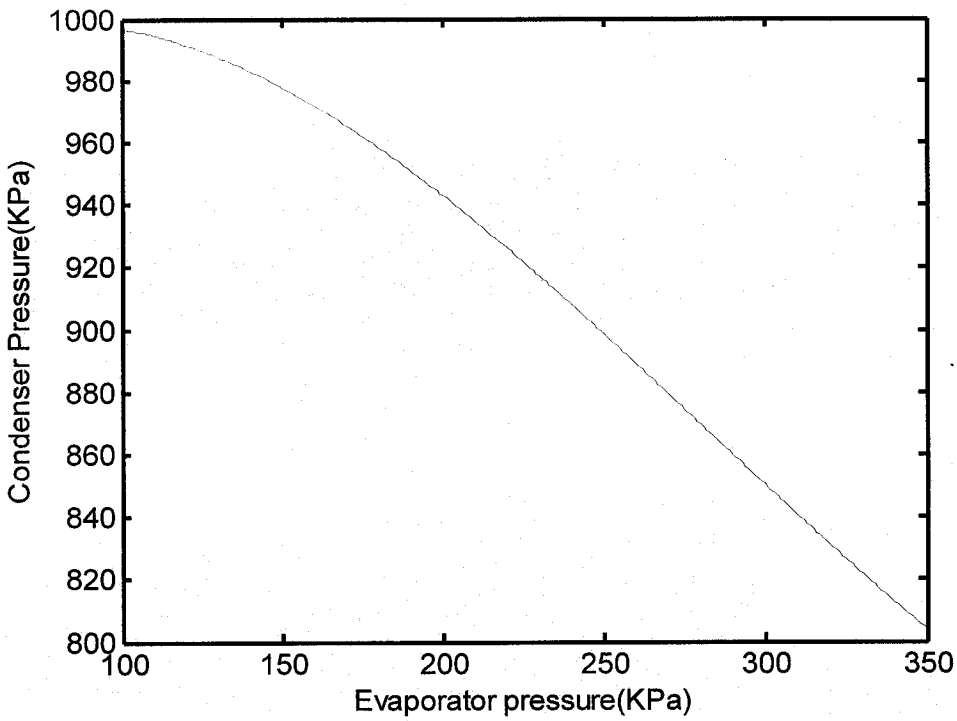

Figure 4.16 Optimal evaporator and condenser pressures

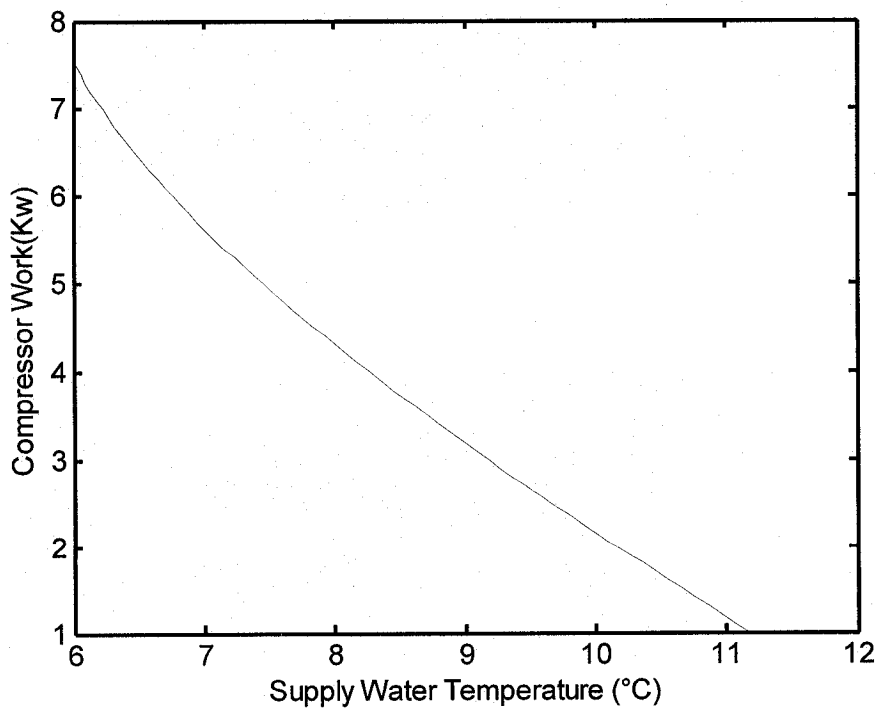

Figure 4.17 Optimal compressor work

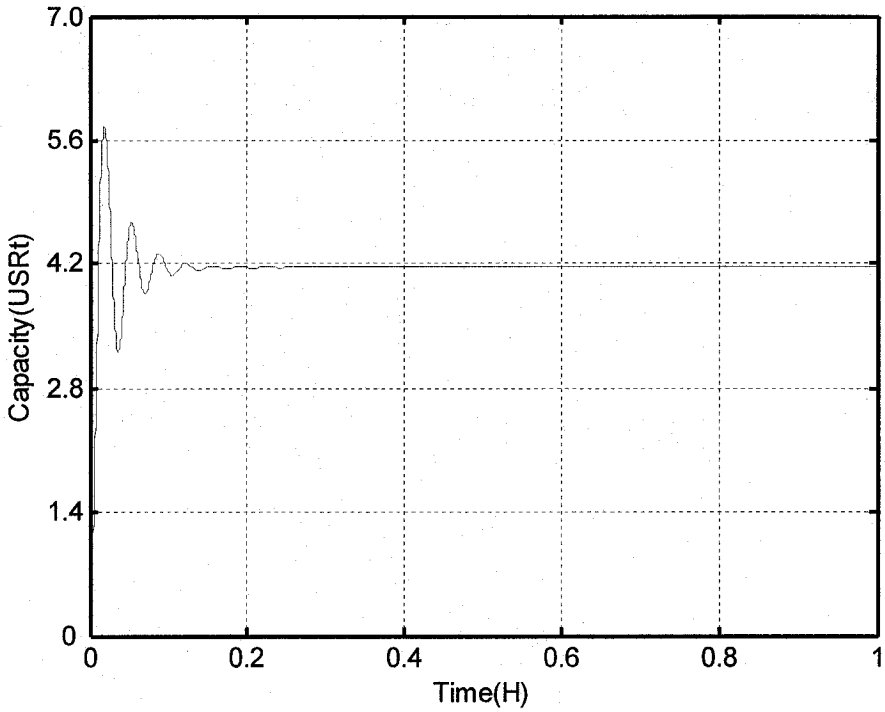

Figure 4.18 Chiller capacity response at 85% cooling load

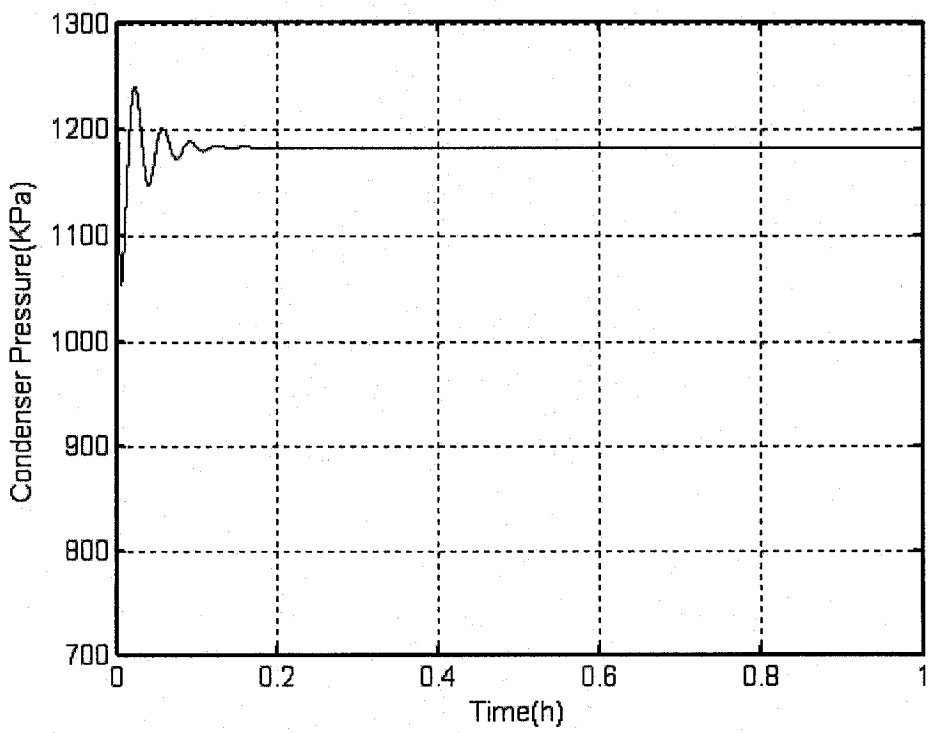

Figure 4.19 Condenser pressure response at 85% cooling load

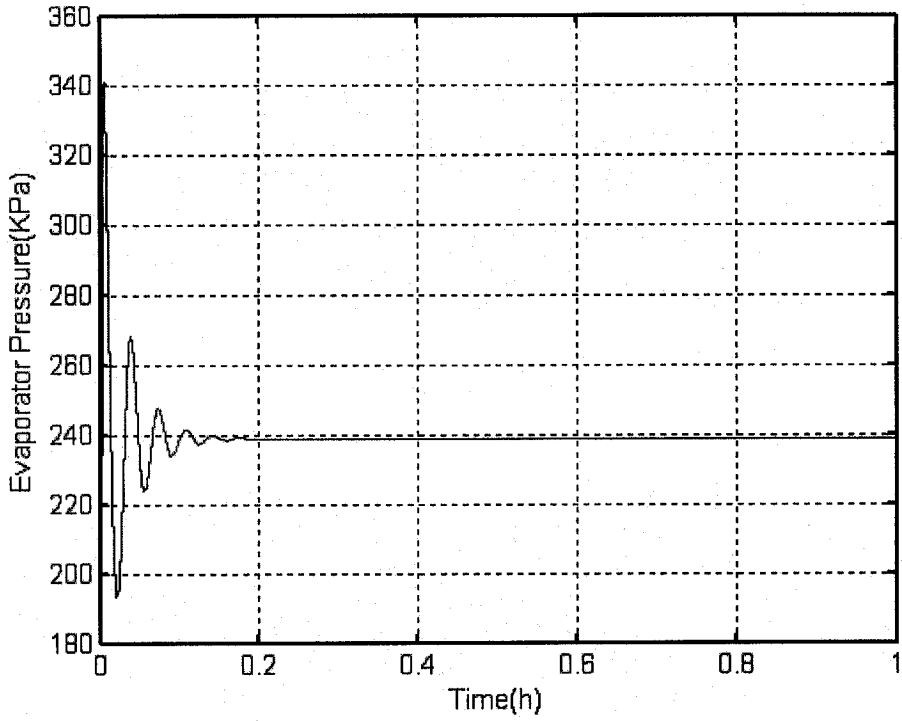

Figure 4.20 Evaporator pressure response at 85% cooling load

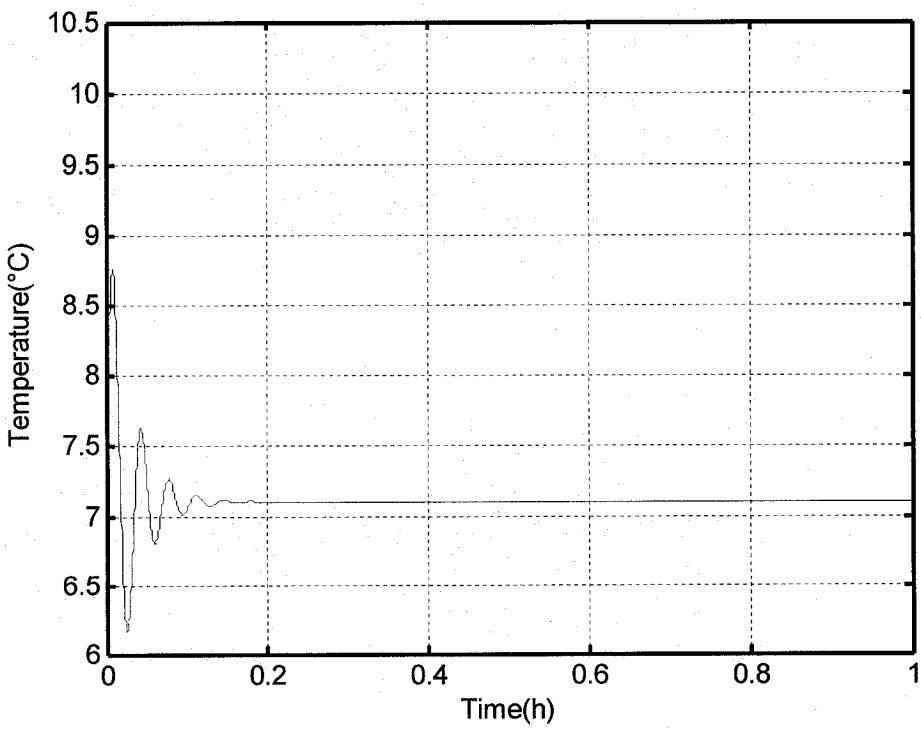

Figure 4.21 Chilled supply water temperature response at 85% cooling load

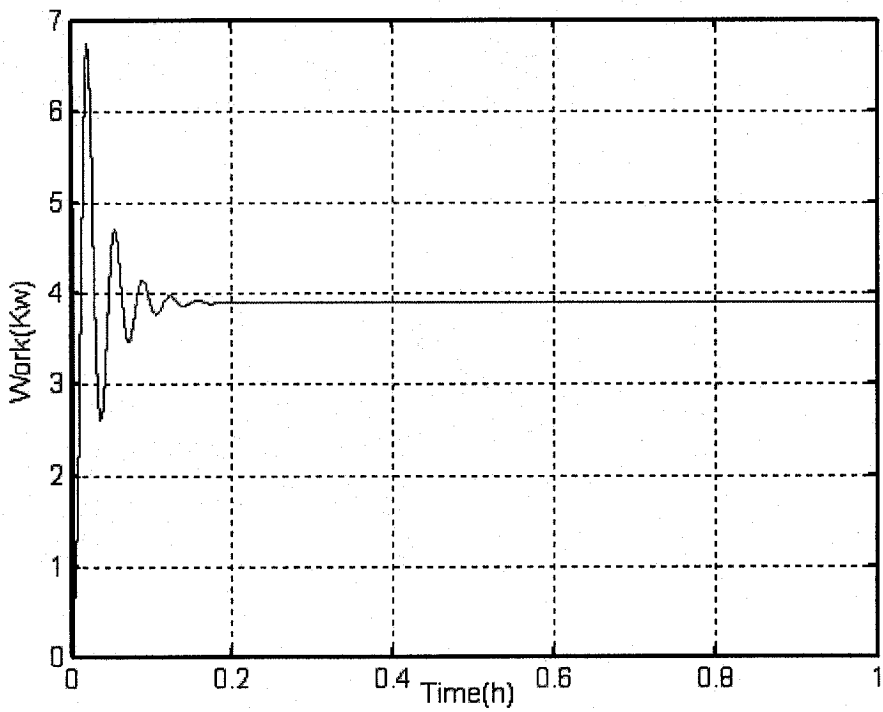

Figure 4.22 Compressor work response at 85% cooling load

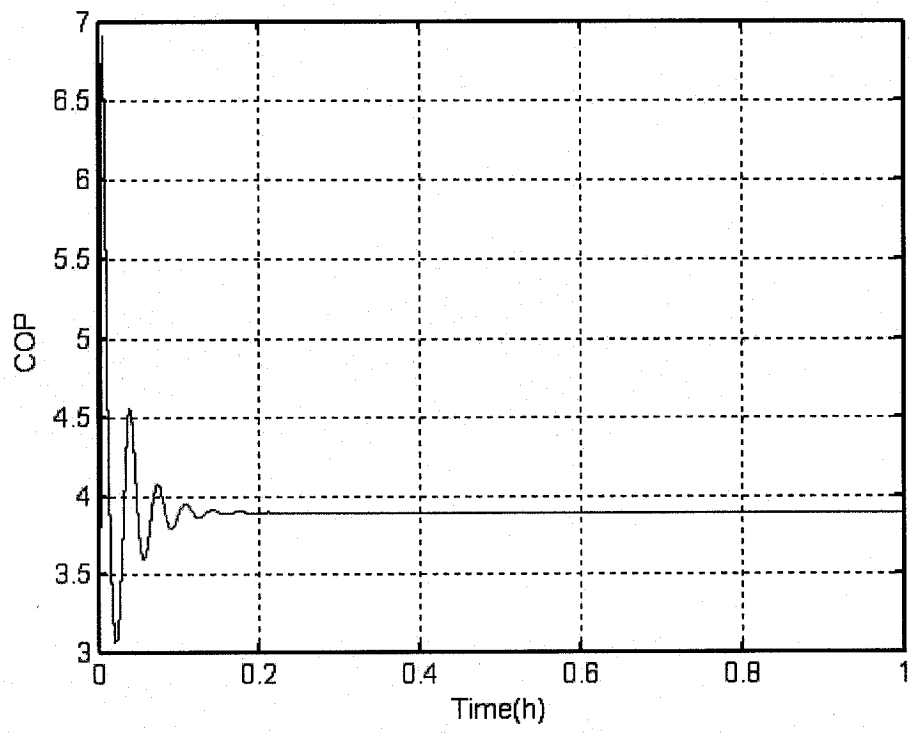

Figure 4.23 COP response at 85% cooling load

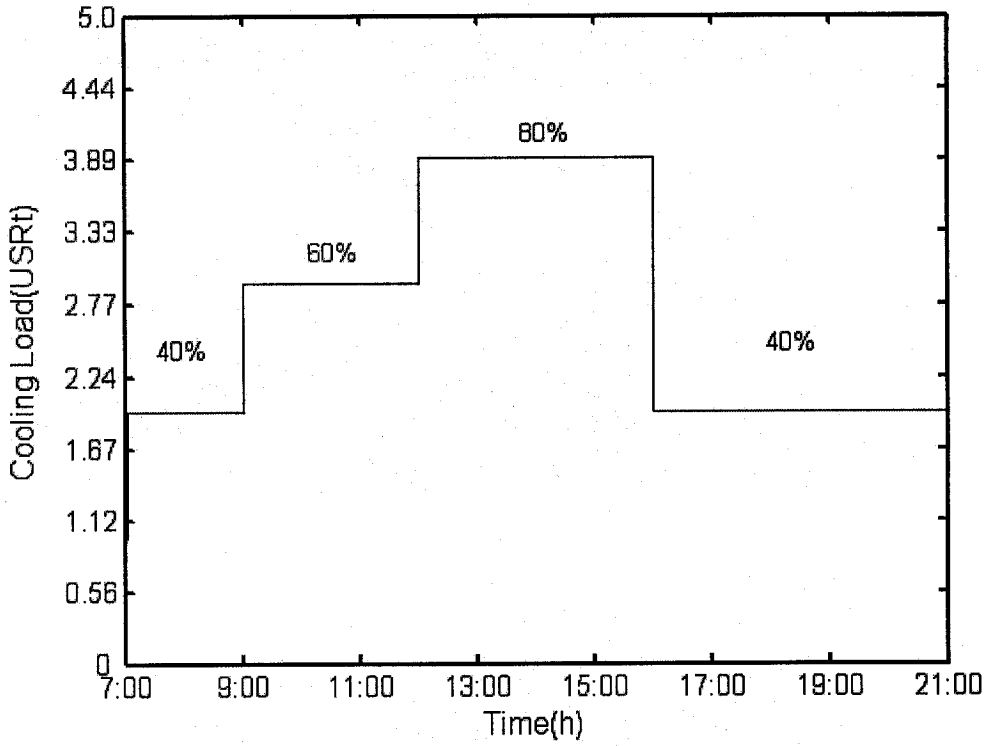

Figure 4.24 Time –of –day cooling load profile

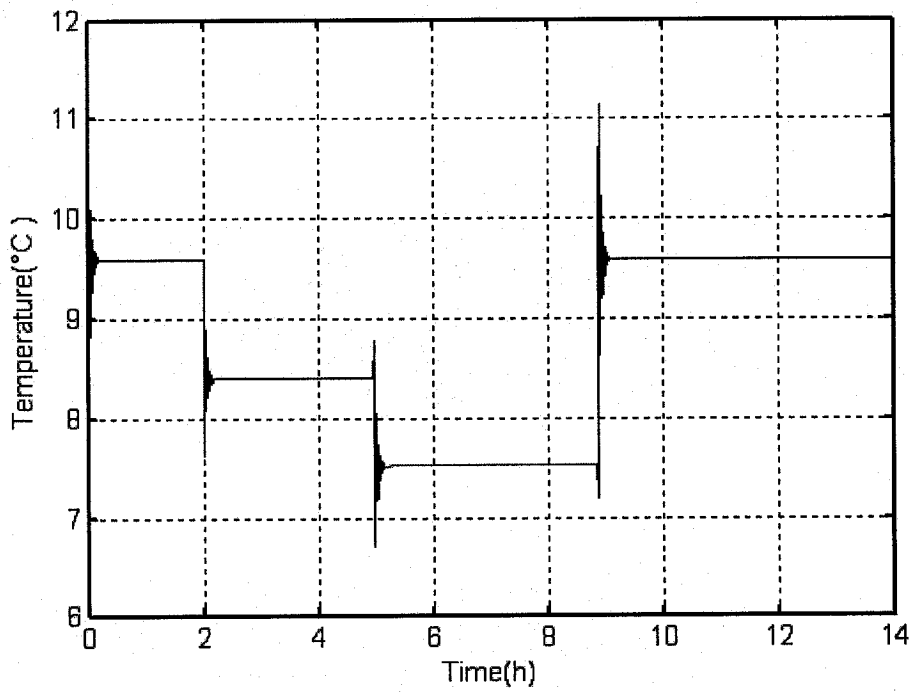

Figure 4.25 Daily chilled supply water temperature responses

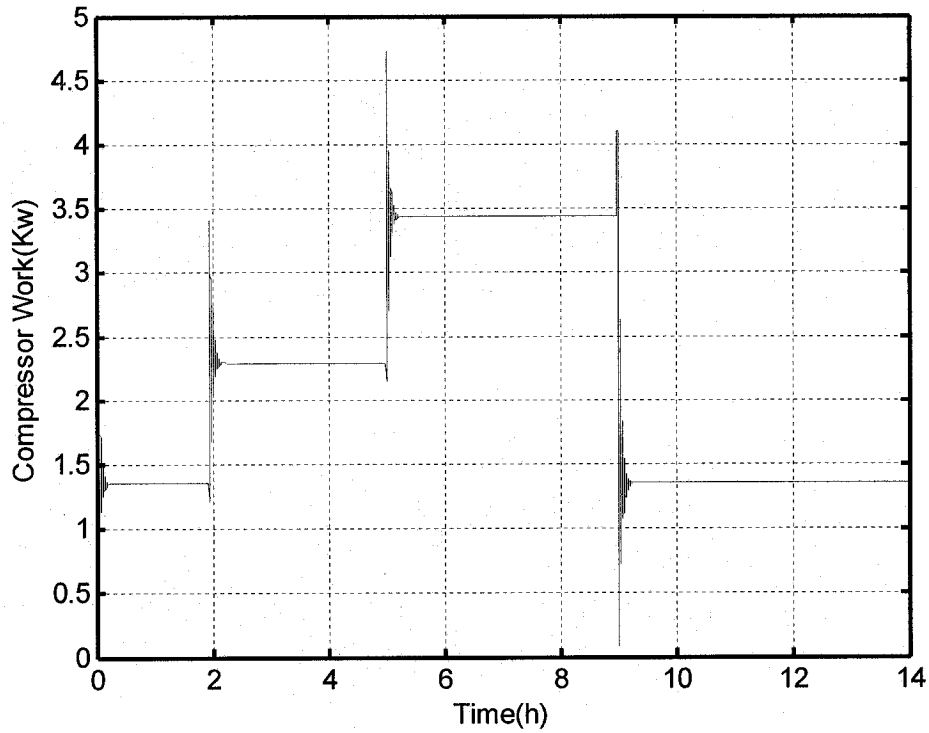

Figure 4.26 Compressor work responses over a day

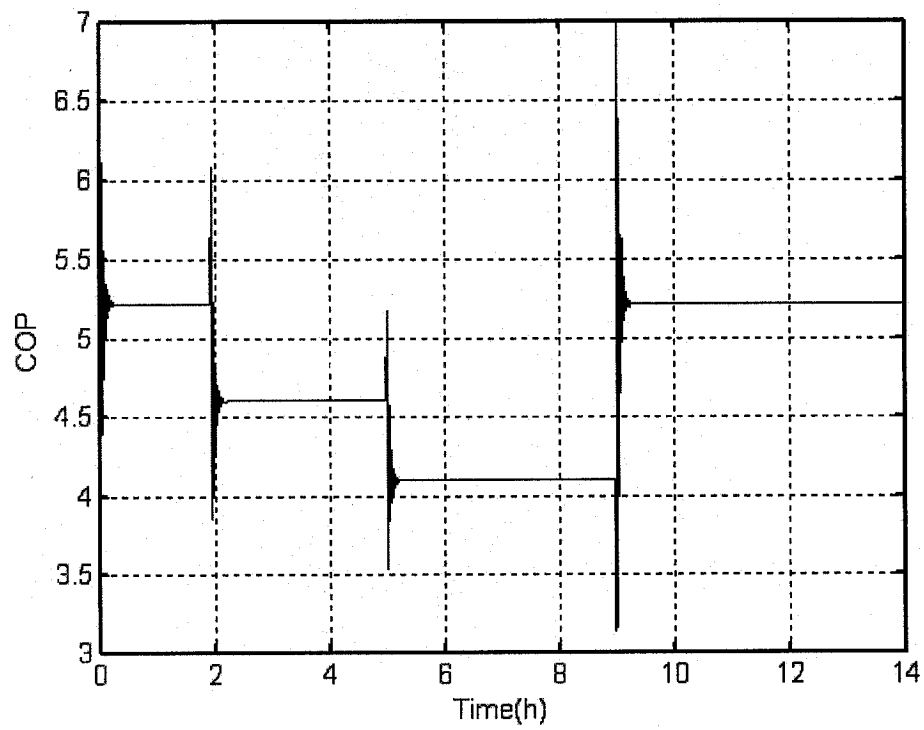

Figure 4.27 COP responses over a day

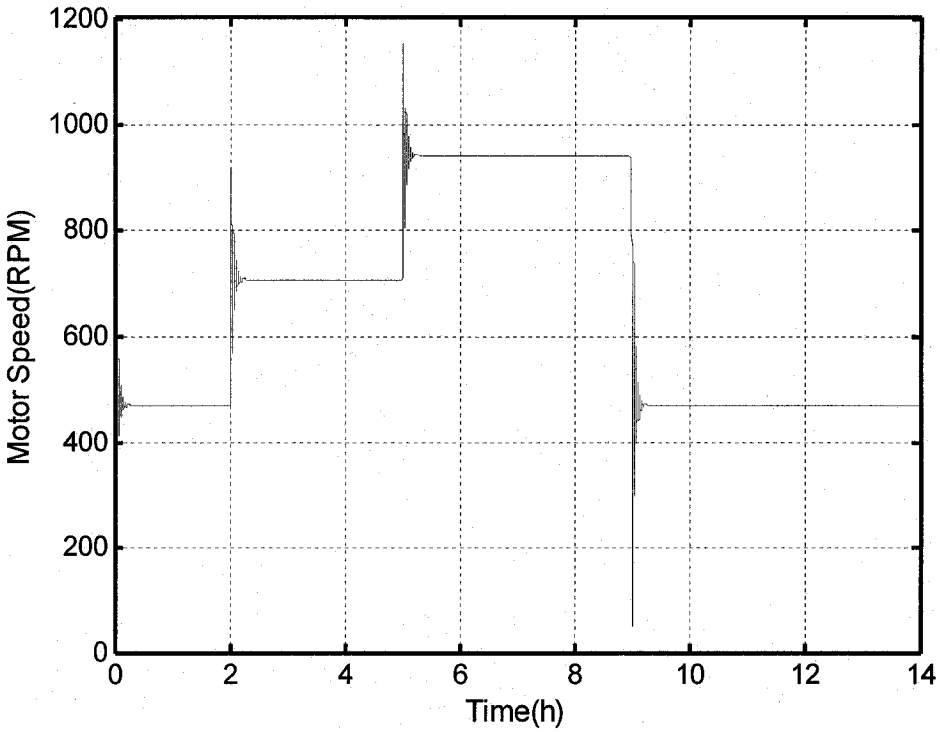

Figure 4.28 Motor rotor speed responses over a day

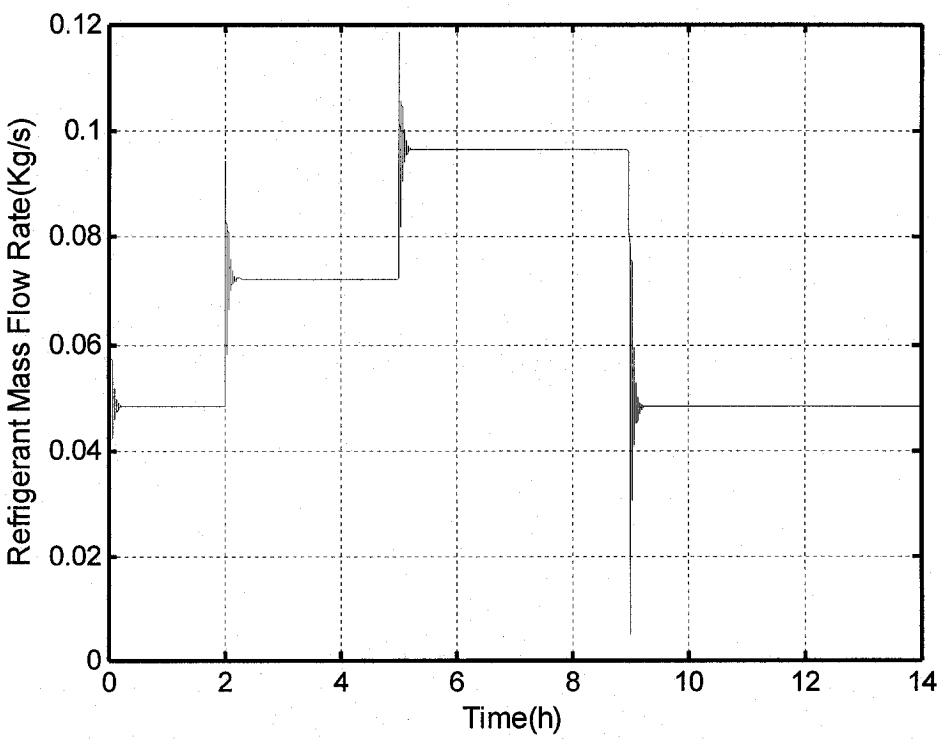

Figure 4.29 Refrigerant mass flow rate responses over a day

CHAPTER 5

MULTIPLE CHILLER CAPACITY CONTROL

5.1 Introduction

Since most buildings use multiple chillers, it is of interest to study multiple chiller capacity control strategies that result in higher overall COP of the system. The basis of multiple chiller capacity control is the sequencing of the chillers that meet the required load at the maximum COP. In a manner similar to the single chiller capacity control discussed in preceding chapter, the chiller capacity can be changed by varying compressor motor rotor speed. In the multiple chiller system, we also can modulate each chiller's compressor motor speed to match the total cooing load. For a given or anticipated load in multiple chiller system, there are a lot of capacity combinations which can satisfy the load. However, different sequencing results in different COP values. The objective of the proposed method is to select appropriate load capacity combination of multiple chillers that yields maximum COP.

This chapter is organized as follows: First the multiple chiller system configurations will be described, an example of multiple chiller temperature control is presented, then the system open loop simulation results are presented. A method of choosing multiple chiller capacity for maximum COP is developed. A closed loop control scheme for implementing maximum COP technique is developed and simulation results are presented.

5.2 System configuration

Two chillers were used to simulate multiple chiller system. One is a 5 Ton chiller which is described in the Chapter 3 and 4, and another is a 10 Ton chiller whose system parameters are given in appendix A. The two chillers are connected in parallel as shown

in Figure 5.1. The T_{sw1} and T_{rw1} are 5 Ton chiller supply water and return water temperatures respectively, and the T_{sw2} and T_{rw2} correspond to the 10 Ton chiller. The combined system supply water and return water temperatures are respectively T_{swt} and T_{rwt}.

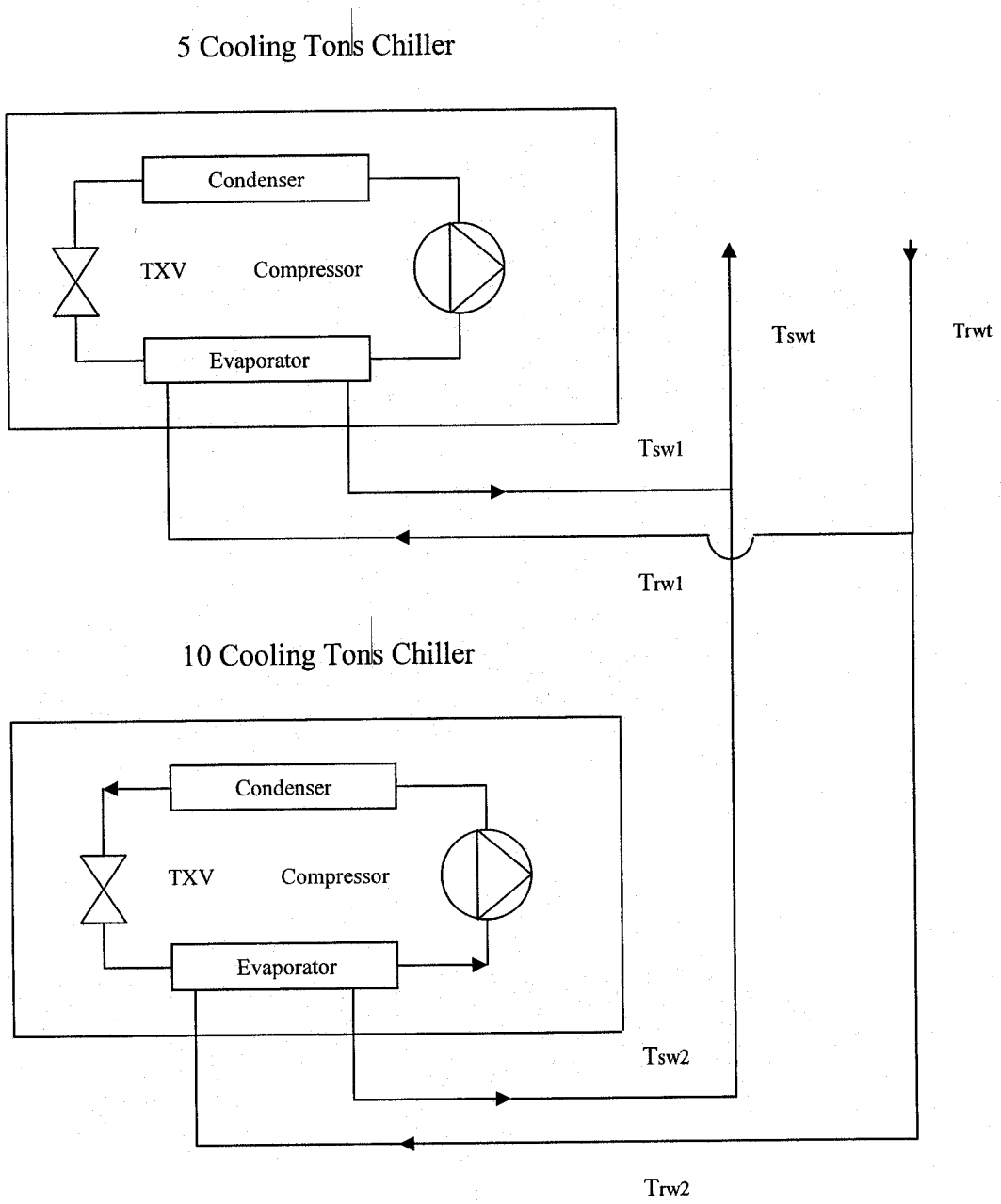

Figure 5.1 Two chiller configuration

5.3 Multiple chiller temperature control

The supply water temperature control is primary concern of operators of multiple chiller systems. For this reason, only the supply water temperature T_{swt} control was considered, irrespective the chiller capacity or system COP. To achieve this objective, the following control system configuration (Fig 5.2) was designed.

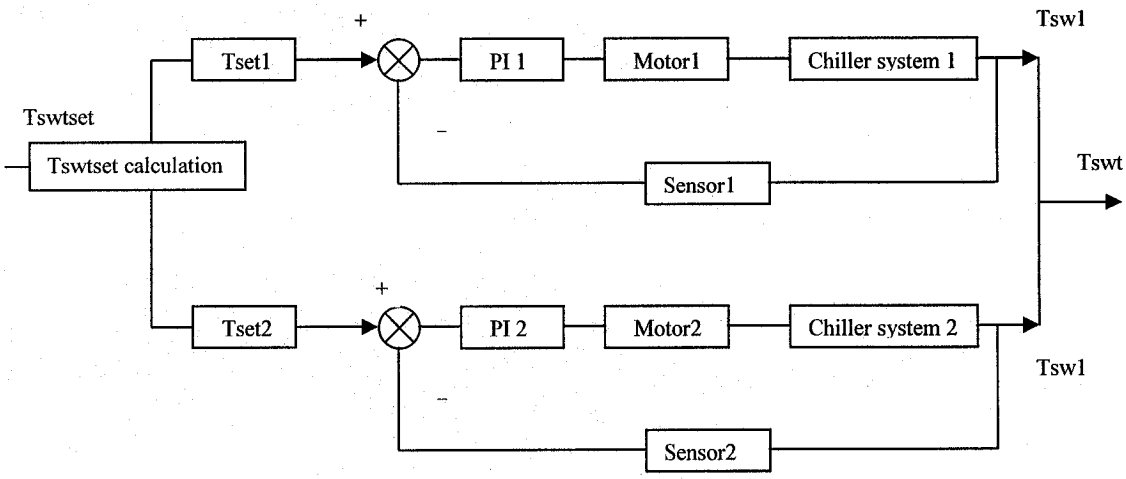

Figure 5.2 Multiple chiller temperature open loop control block diagram

In this control block diagram, the upper closed loop control block controls the 5 Ton chiller supply water temperature T_{sw1} and the lower block controls the 10 Ton chiller supply water temperature T_{sw2}. The chilled water flow rates are mixed to produce supply water temperature T_{swt}. The combined open loop setpoint temperature T_{swtset} can be obtained from following steady state equation

$$\dot{m} C_p T_{swtset} = \dot{m}_1 C_p T_{sw1set} + \dot{m}_2 C_p T_{sw2set} \tag{5.3.1}$$

$$T_{swtset} = \frac{\dot{m}_1}{\dot{m}} T_{sw1set} + \frac{\dot{m}_2}{\dot{m}} T_{sw2set} \tag{5.3.2}$$

where

$$\dot{m} = \dot{m}_1 + \dot{m}_2$$

$\dot{m}$ is mass flow rate of multiple chiller total supply water (Kg/s)

$\dot{m}_1$ is mass flow rate of 5 Ton chiller supply water (Kg/s)

$\dot{m}_2$ is mass flow rate of 10 Ton chiller supply water (Kg/s)

According to above equation, one chiller temperature setpoint can be arbitrarily assigned. For example, if we assume that the supply water temperature setpoint T_{swtset} is 8°C, then one combination that satisfies Eq.5.3.2 can be T_{sw1set} is 6.4°C and T_{sw2set} 8.8 °C. It is noted that there are a lot of choices of T_{sw1set} and T_{sw2set} which satisfy Eq (5.3.2), and only one or few combinations could yield a higher system COP. How to achieve higher COP is analyzed in the following section 5.4.

But first, by assuming one set of T_{sw1set} and T_{sw2set}, simulation runs were made to study the output responses from the multiple chiller closed loop control system. The results are depicted in Figures 5.3, 5.4 and 5.5. Figure 5.3 shows that after the initial transients the 5 Ton and 10 Ton chiller supply water temperatures reach steady state values 6.4 °C and 8.8 °C in about 20 minutes. Figure 5.4 shows the overall system supply water temperature, which attains the final value of about 8.0 °C. Under these operating conditions, the system COP was 3.8 as shown in Figure 5.5.

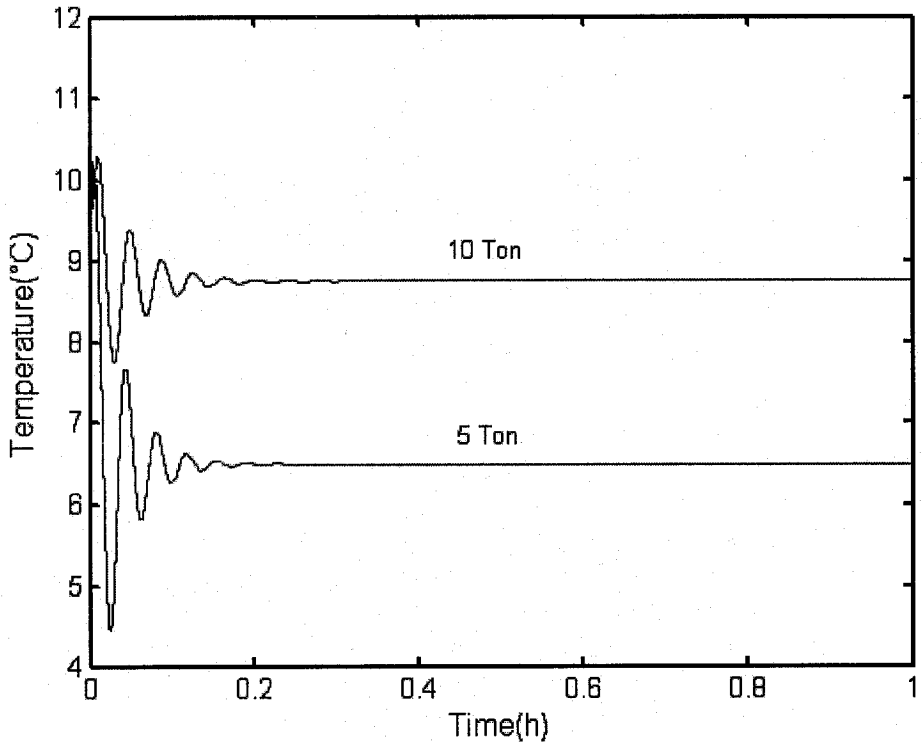

Figure 5.3 Two chillers supply water temperature responses

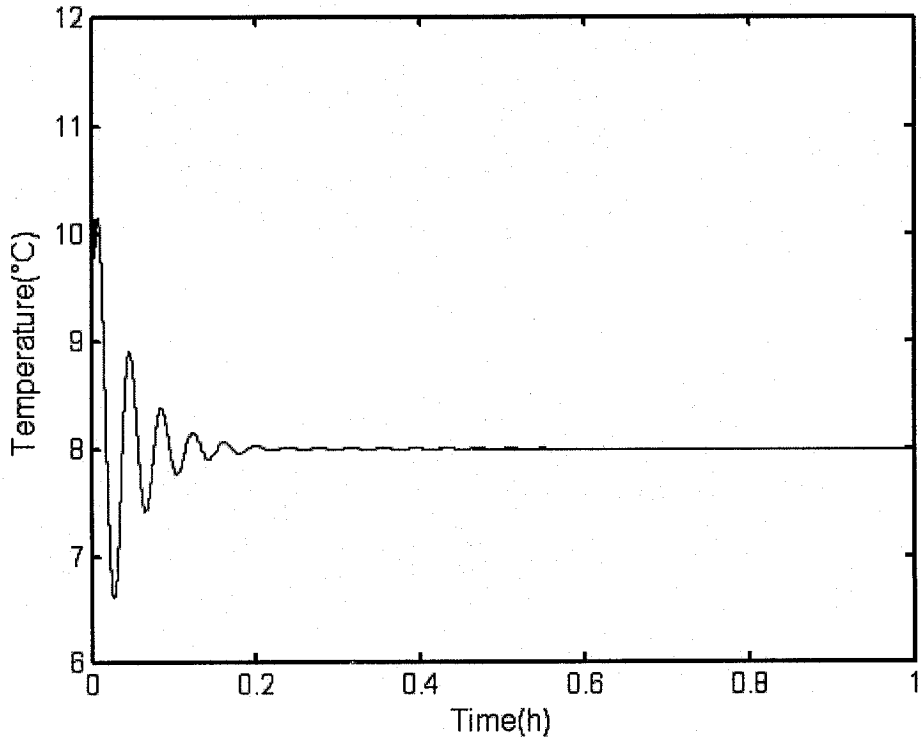

Figure 5.4 Combined supply water temperature response

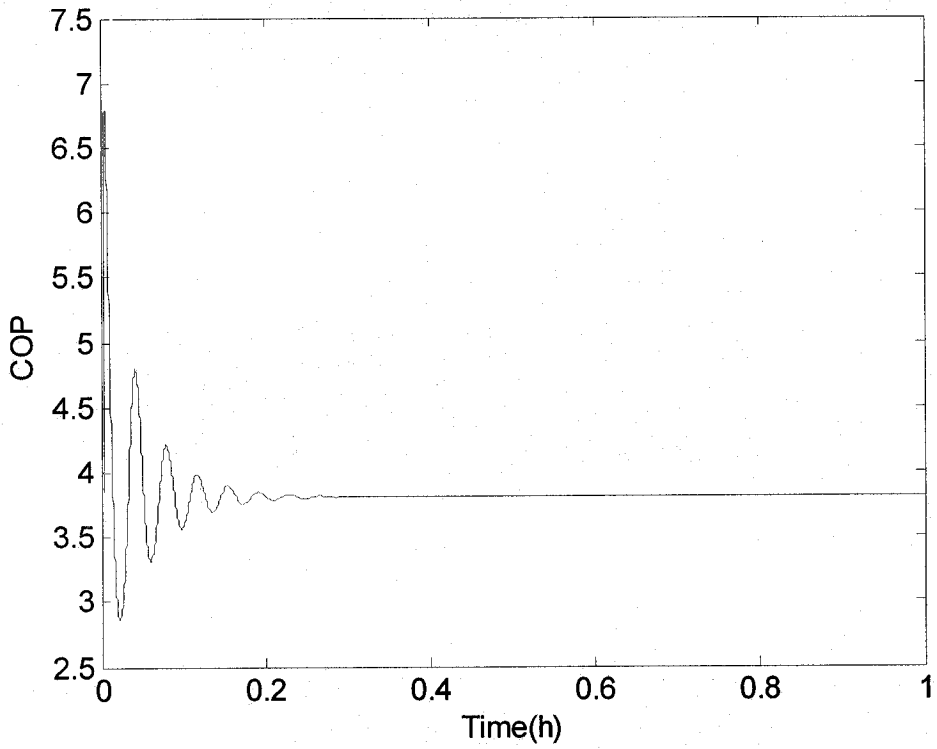

Figure 5.5 System COP response

5.4 Multiple chiller performance curves

In order to improve the energy efficiency in multiple chiller systems, the chiller operators need to consider not only the supply water temperature but also the system COP. The following steady state analysis of multiple chiller performance curves is presented which can be utilized as means of improving the COP of multiple chiller systems.

Several open loop simulation tests were done to determine the steady state balance points of combined supply water temperature (T_{swt}), COP, each chiller compressor motor speed, and each chiller capacity. The energy efficient operating parameters were extracted by analyzing these steady state results.

In the open loop simulations, conducted for a given cooling load the output values for each chiller compressor were determined. The outputs include: motor speed, combined supply water temperature (T_{swt}), each chiller supply water temperature (T_{sw1} and T_{sw2}), COP and each chiller capacity. These results are depicted in Figures 5.6(a-i) along with the COP values. Typical values of combined supply water temperatures ranging from 6.5 °C to 10.5°C were selected for the simulation runs. For example, for a supply water temperature of 6.5 °C, the 5 Ton chiller capacity was varied from 20% to 120% and 10 Ton chiller capacity from 20% to 120%, and the COP values were recorded. Among these COP values, the maximum COP and the corresponding loads were identified. For example from Figure 5.6 a, when 5 Ton chiller operates at 70.75% capacity and the 10 Ton chiller is at 102.13%, for supply water temperature of 6.5 °C, the maximum COP is 3.33. In other words, the maximum COP and its matching capacities can be obtained for different supply water temperature conditions from Figures 5.6(a-i). Figure 5.7 summarizes the maximum COP as a function of corresponding chiller capacities. If the two chillers operate along the curve in Figure 5.7, maximum COP can be achieved at certain supply water temperature or anticipated cooling load. This information can be utilized as a variable setpoint to the PI controller to regulate the system such that maximum COP of the overall system can be achieved.

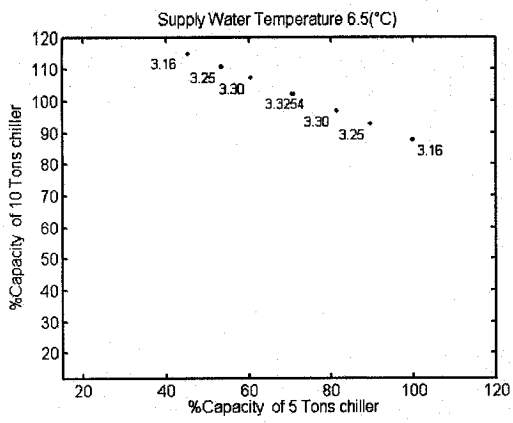
Supply Water Temperature 6.5(°C)
%Capacity of 10 Tons chiller
%Capacity of 5 Tons chiller
3.16
3.25
3.30
3.3254
3.30
3.25
3.16

(a)

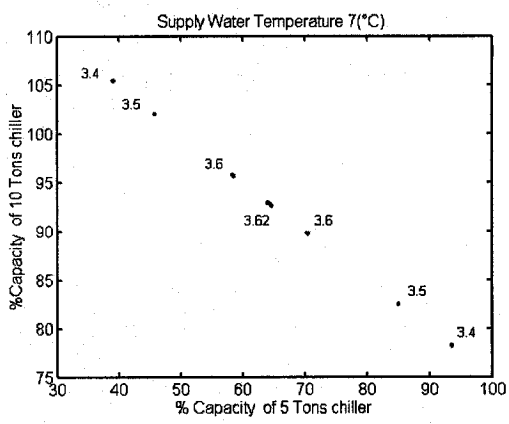
Supply Water Temperature 7(°C)
%Capacity of 10 Tons chiller
% Capacity of 5 Tons chiller
3.4
3.5
3.6
3.62
3.6
3.5
3.4

(b)

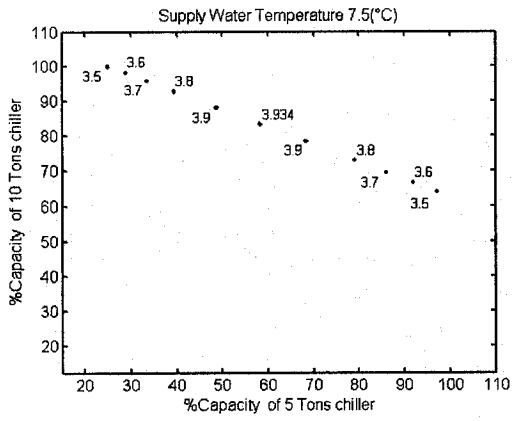
Supply Water Temperature 7.5(°C)
%Capacity of 10 Tons chiller
%Capacity of 5 Tons chiller
3.5
3.6
3.7
3.8
3.9
3.934
3.9
3.8
3.7
3.6
3.5

(c)

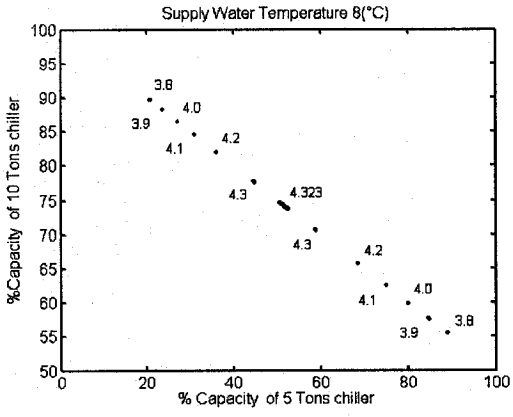
Supply Water Temperature 8(°C)
%Capacity of 10 Tons chiller
% Capacity of 5 Tons chiller
3.8
4.0
3.9
4.2
4.1
4.3
4.323
4.3
4.2
4.1
4.0
3.9
3.8

(d)

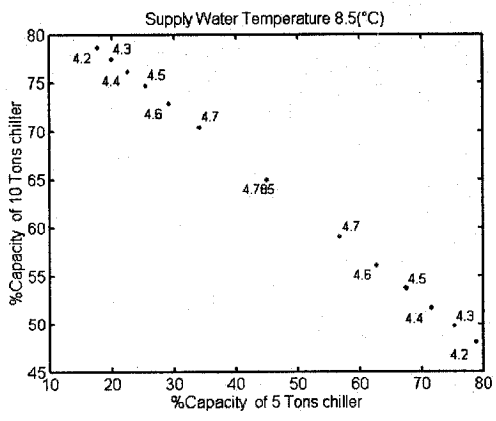
Supply Water Temperature 8.5(°C)
%Capacity of 10 Tons chiller
%Capacity of 5 Tons chiller
4.2
4.3
4.4
4.5
4.6
4.7
4.765
4.7
4.6
4.5
4.4
4.3
4.2

(e)

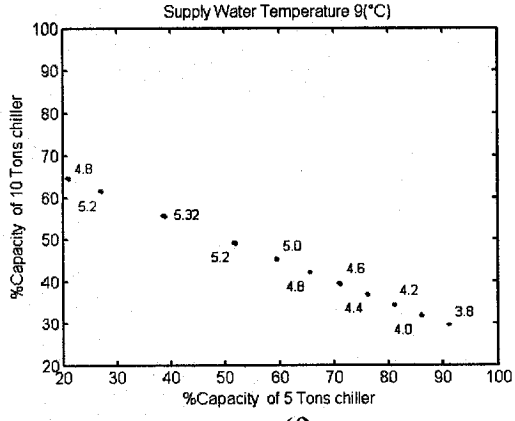
Supply Water Temperature 9(°C)
%Capacity of 10 Tons chiller
%Capacity of 5 Tons chiller
4.8
5.2
5.32
5.2
5.0
4.8
4.6
4.4
4.2
4.0
3.8

(f)

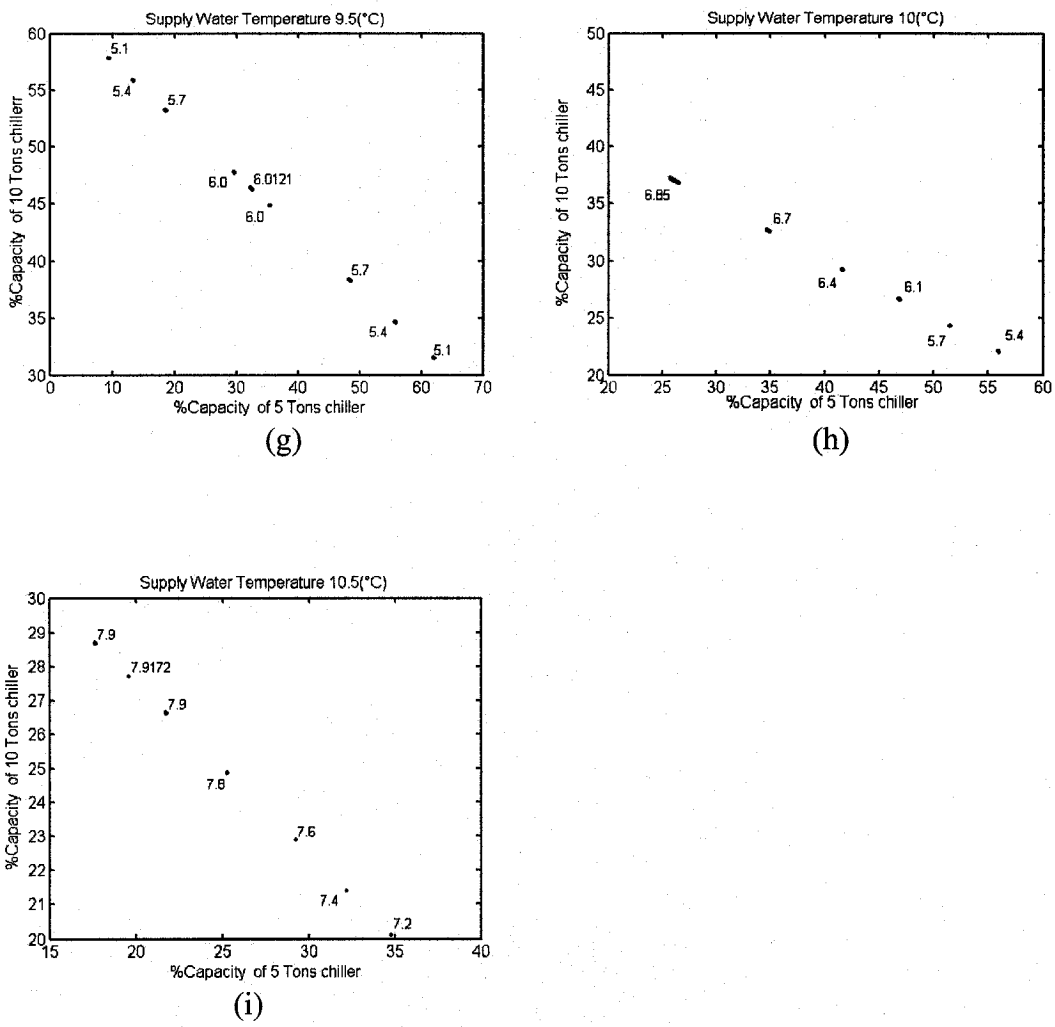

Figure 5.6 COP as a function of chiller capacity

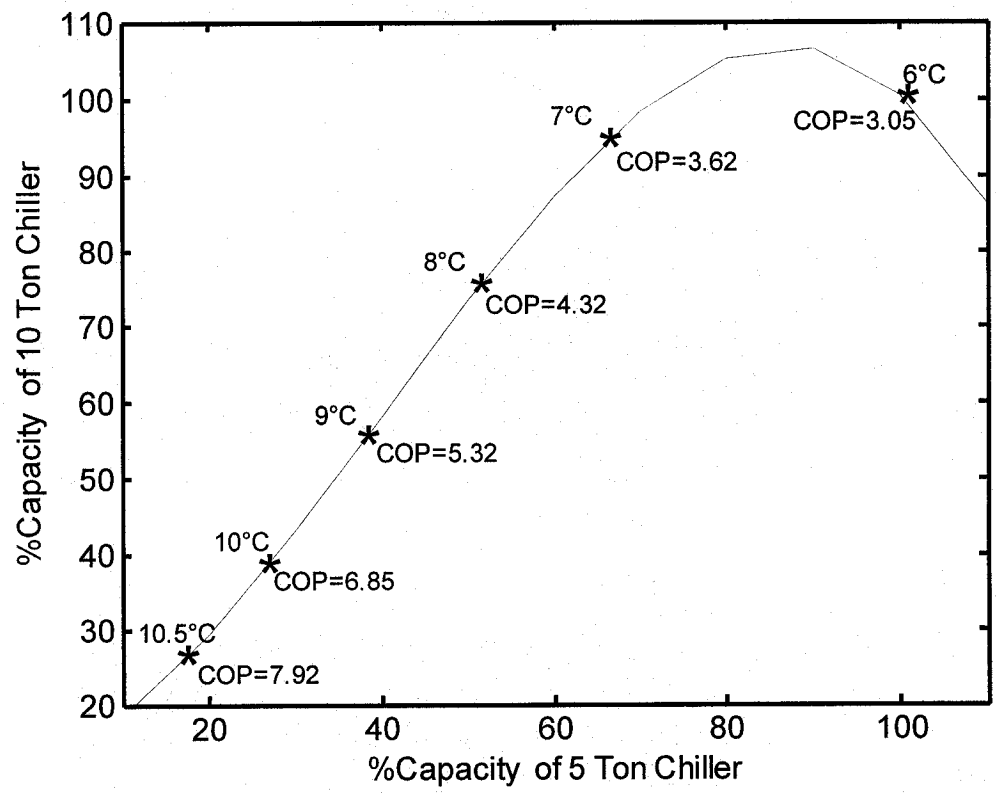

Figure 5.7 Maximum COP of multiple chiller system

5.5 Chiller control strategy analysis

As an example, consider three kinds of anticipated load scenarios. These are (1) the anticipated load is less than (or equal to) 5 Tons, (2) the anticipated load is less than (or equal to) 10 Tons and greater than 5 Tons, and (3) the anticipated load is less than (or equal to) 15 Tons and greater than 10 Tons. For matching the anticipated load, the 5 Ton or 10 Ton chiller can be run alone, or operated at the same time. The decision as to whether one chiller or two chillers should be run could be based on a criterion that would achieve maximum COP. In order to extract individual chiller capacities which yield maximum COP of the combined system, the following analysis are presented.

To this end, from the results presented in Figure 5.7, we can plot a relationship between maximum COP as a function of system supply water temperature. This is shown in Figure 5.8.

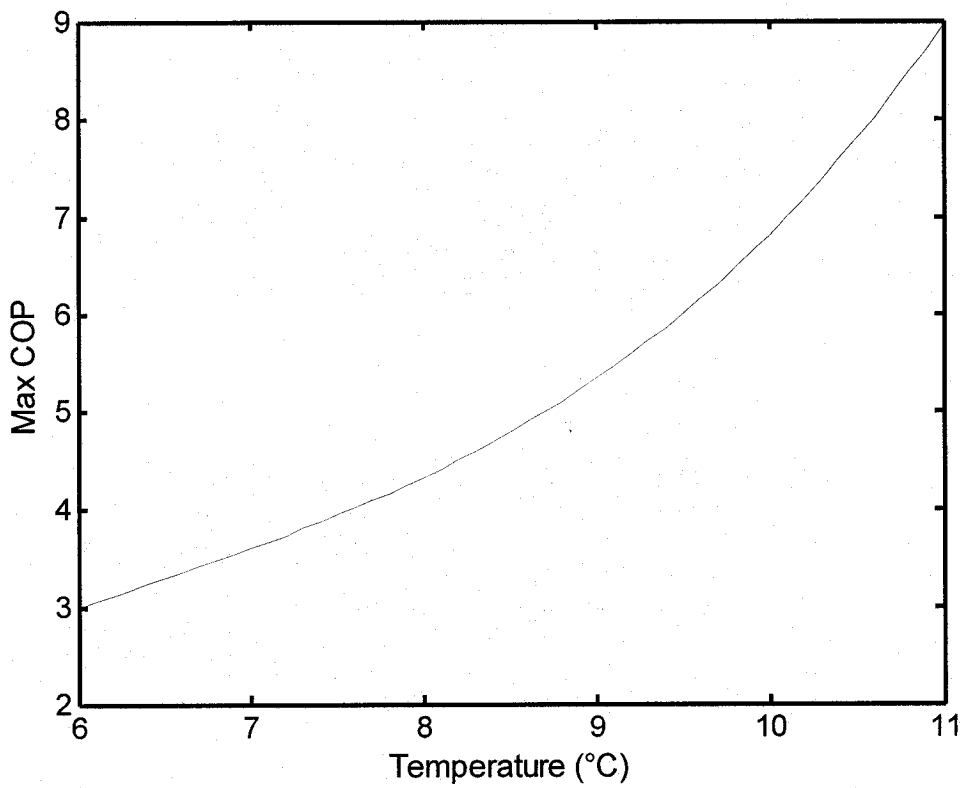

Figure 5.8 Maximum COP as a function of system supply water temperature

A third order polynomial was used to fit the simulation data. The polynomial function which describes this function is given by

$$COP_{max} = f(T_{sw})$$

$$COP_{max} = a_0 + a_1 T_{sw} + a_2 T_{sw}^2 + a_3 T_{sw}^3 \qquad (5.5.1)$$

where

a= [0.0307, 0.5914, 4.4124, -8.8136]

Similarly, from Figure 5.7, the corresponding chiller capacities can be determined. These are depicted in Figure 5.9.

The next step would be to determine the individual chiller supply water temperatures corresponding to the above max COP results. These are depicted in Figure 5.10. The functions describing these curves are shown below.

$$T_{sw1} = b_0+b_1r_5+b_2r_5^2+b_3r_5^3 \quad (5.5.2)$$

$$T_{sw2} = c_0+c_1r_{10}+c_2r_{10}^2+c_3r_{10}^3 \quad (5.5.3)$$

where

b= [0.5833, -11.8571, 59.1310, 41.4571]

c= [0.9167, -23.8571, 185.7976, -353.7429]

r is the percent capacity of the chiller.

By using the above functional relationships, the supply water temperatures of each chiller which result in maximum COP of the combined system can be determined. In the following section, the control implementation of this strategy is described.

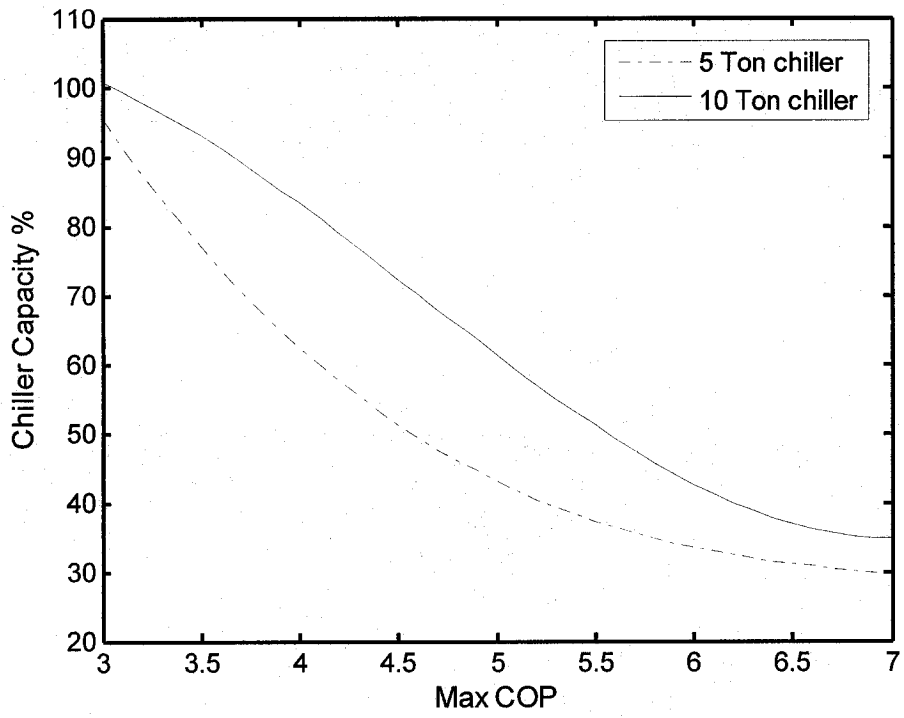

Figure 5.9 Chiller capacity as a function of maximum COP

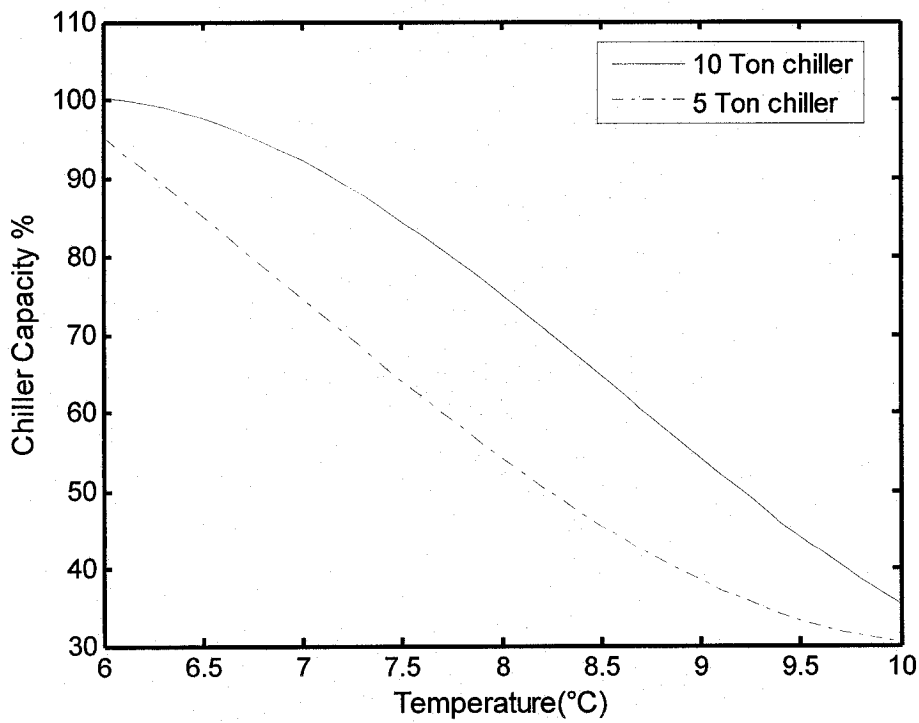

Figure 5.10 Chiller capacity as a function of supply water temperature

5.6 Closed loop system

In Figure 5.11 chiller capacity control scheme using PI controllers is depicted. The upper loop shows the 5 Ton chiller PI control, and the lower loop shows the 10 Ton chiller PI control block. The feedback signal from combined chilled supply water temperature (T_{swt}) is compared with anticipated load based set point temperature, and the respective errors are sent to the PI controllers to regulate each control loop. The implementation scheme shows the sequence of calculating the supply water temperature setpoint for each chiller. For example, when the operator chooses a system supply water temperature, then the corresponding max COP that can be achieved is determined by the first block. By using this information, the next two paralleled blocks compute the corresponding supply water temperature setpoint for each chiller. The closed loop PI control for each chiller takes over the function and regulates each loop to track the supplied setpoints. It should be noted that the analysis presented is based on steady state approach. However, such steady stste analysis are still useful in improving overall COP of multiple chiller systems compared to arbitrary setpoint normally used by the building operators.

Simulation runs were made to show the application of the maximum COP method discussed above. Two cases were considered. In the first case (case1) a step change in the cooling setpoint was considered and the resulting closed loop system outputs were recorded. In case 2, a typical daily performance of multiple chiller system using maximum COP analysis is presented.

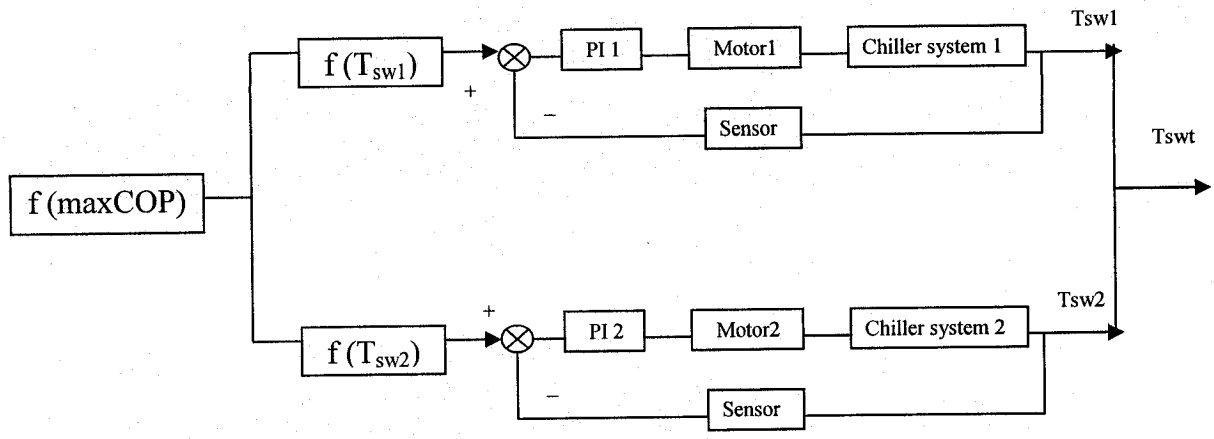

Figure 5.11 Two chillers capacity control system PI control block diagram

Case-1 simulation results

In case 1 two chiller system under a step change in cooling setpoint is simulated. Assuming a 8.0 °C setpoint for supply water temperature, the resulting closed loop output responses were recorded. These are depicted in Figures 5.12 through 5.16. Results show that following initial transient which lasted for about 0.2 hour, the system responses reach steady state. The supply water temperatures of 5 Ton and 10 Ton chillers under steady state were 8.8 °C and 7.4 °C respectively.

Figure 5.13 shows the two chiller system combined supply water temperature (T_{swt}) response as a function of time. The steady state value of T_{swt} is 8.0 °C, which is the designed set point temperature value.

In Figure 5.14 the two chiller capacities are depicted. The 10 Ton chiller attains a steady state capacity of about 7.4 USRt, while the 5 Ton chiller reaches steady state capacity of about 2.6 USRt. The combined capacity of the two chillers is the sum of the two capacities which is equal to 10 USRt.

In Figure 5.15 the variations in compressor motor speeds are depicted. The 10 Ton chiller steady state speed is about 860RPM, while the 5 Ton chiller steady state speed is about 605RPM.

In Figure 5.16 the corresponding COP of the combined system is depicted. The steady state COP value of chiller system is 4.3, which matches with the result in Figure 5.7. So when the chiller setpoint to an anticipated load is appropriately selected, the chiller control system can regulate the system to obtain the maximum COP value.

Case 2 simulation results

In case 2, the two chillers control system will be operated over a period of 24 hours. For this simulation a predicted daily load profile as shown in Figure 5.17 was assumed. The peak cooling load is from 12:00 to 16:00, which is about 12.5USRt, or 84% of full load. During unoccupied hours (after 21:00) minimum load of 25% was assumed.

Figure 5.18 shows refrigeration system's combined supply water temperature (T_{swt}) responses over a day, and the temperature setpoints are changed to match the variable anticipated load several times in the day. The lowest chilled supply water temperature was about 7 °C during the period between 12:00 to 16:00 hrs, and the highest chilled supply water temperature was about 10.5 °C during nighttime operation. Figures 5.19, 5.20, 5.21 respectively show the responses of system COP, the 5 Ton chiller motor speed, the 10 Ton chiller motor speed over one day. From these results, it is noted that the minimum COP is about 3.5, while the 5 Ton and the 10 chiller speeds were 750RPM and 1100RPM respectively. When the chillers were operating at night, a higher COP 7.5 and lower motor speeds of 205 RPM and 370RPM were obtained. These results show that a

relatively stable variable speed controller can be used to regulate the multiple chillers to achieve maximum COP.

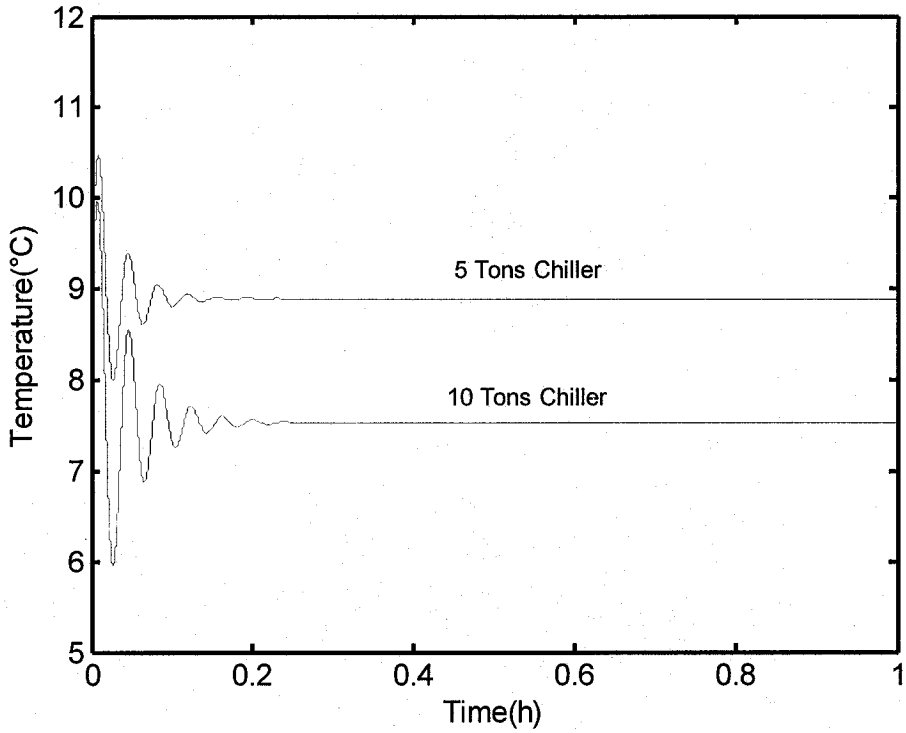

Figure 5.12 Supply water temperature responses to step change in T_{ws} setpoint

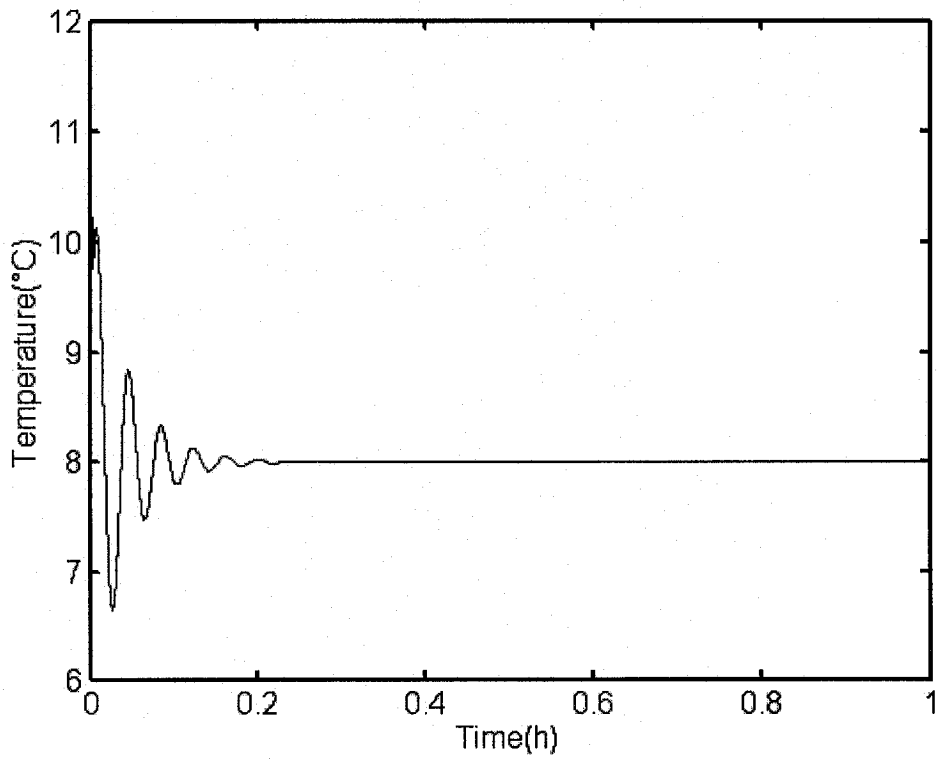

Figure 5.13 System supply water temperature response subject to step change in T_{ws} setpoint

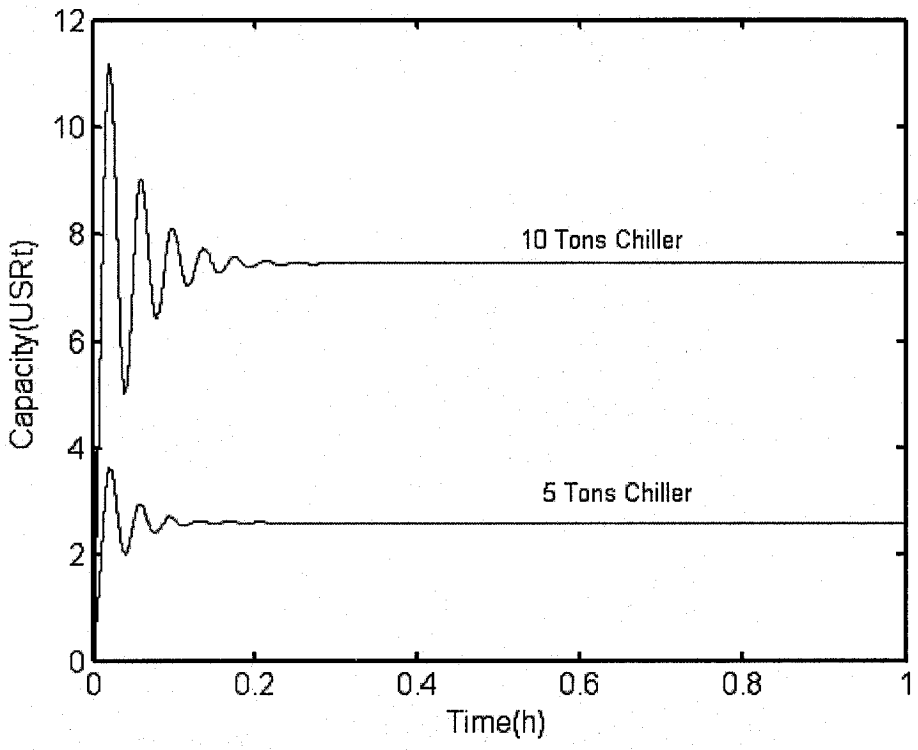

Figure 5.14 Chiller capacity responses

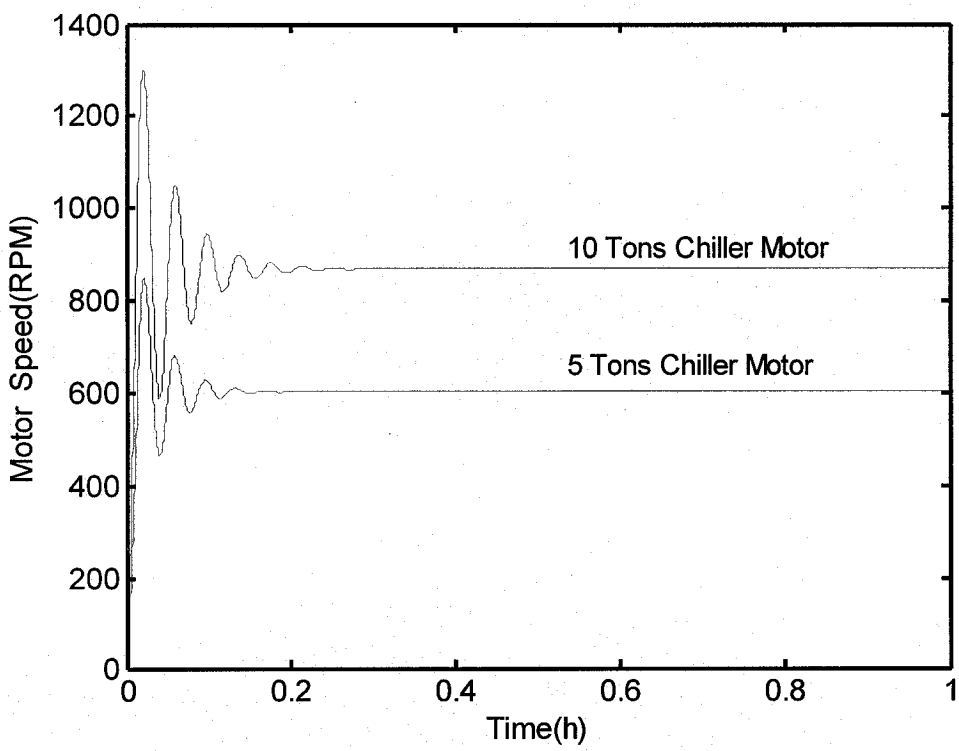

Figure 5.15 Motor speed responses

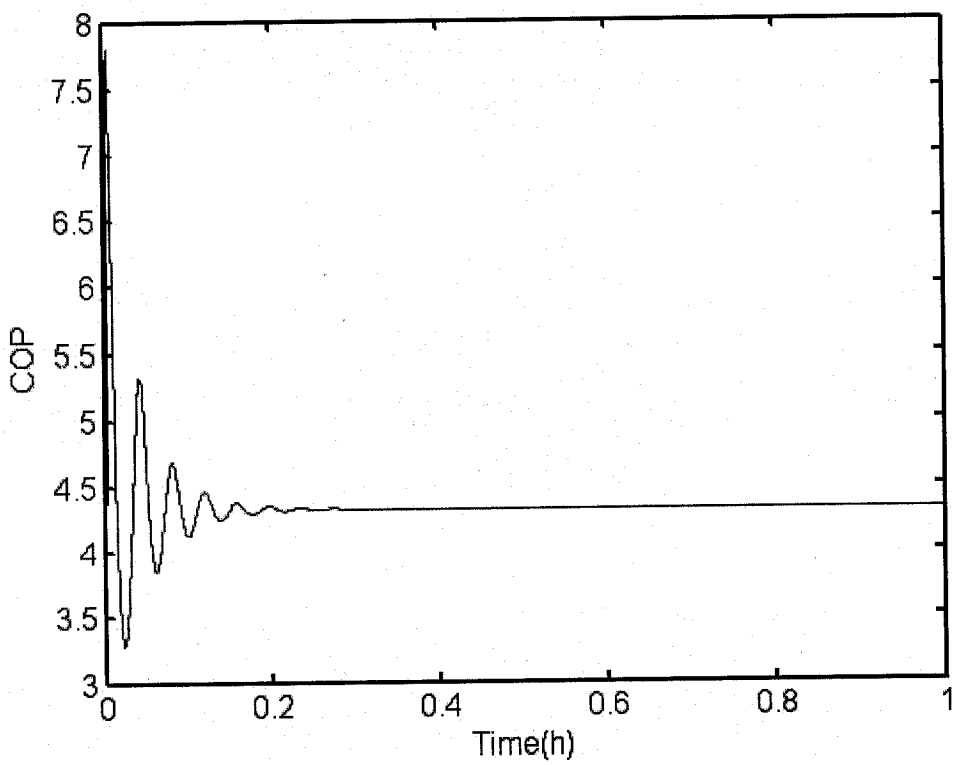

Figure 5.16 COP response to step change in T_{ws} setpoint

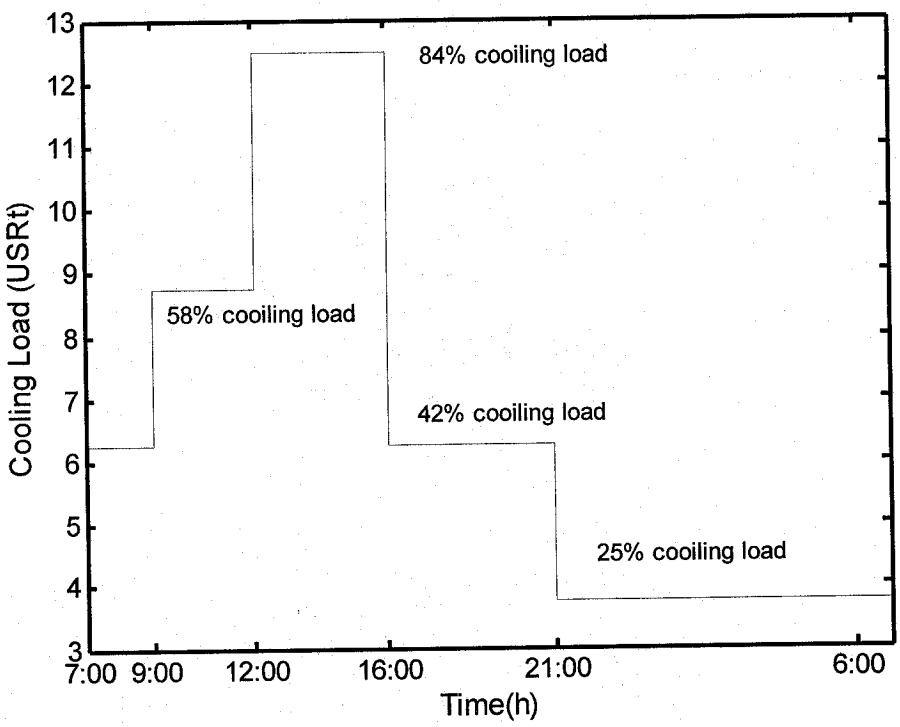

Figure 5.17 Cooling load over a day

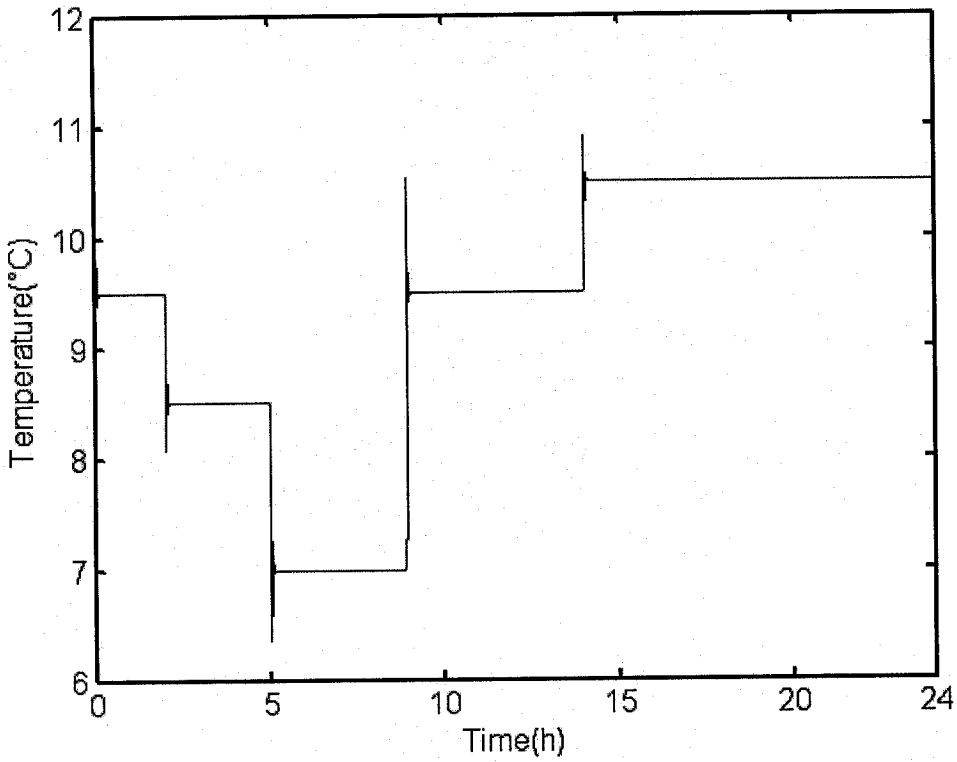

Figure 5.18 Supply water temperature responses over a day

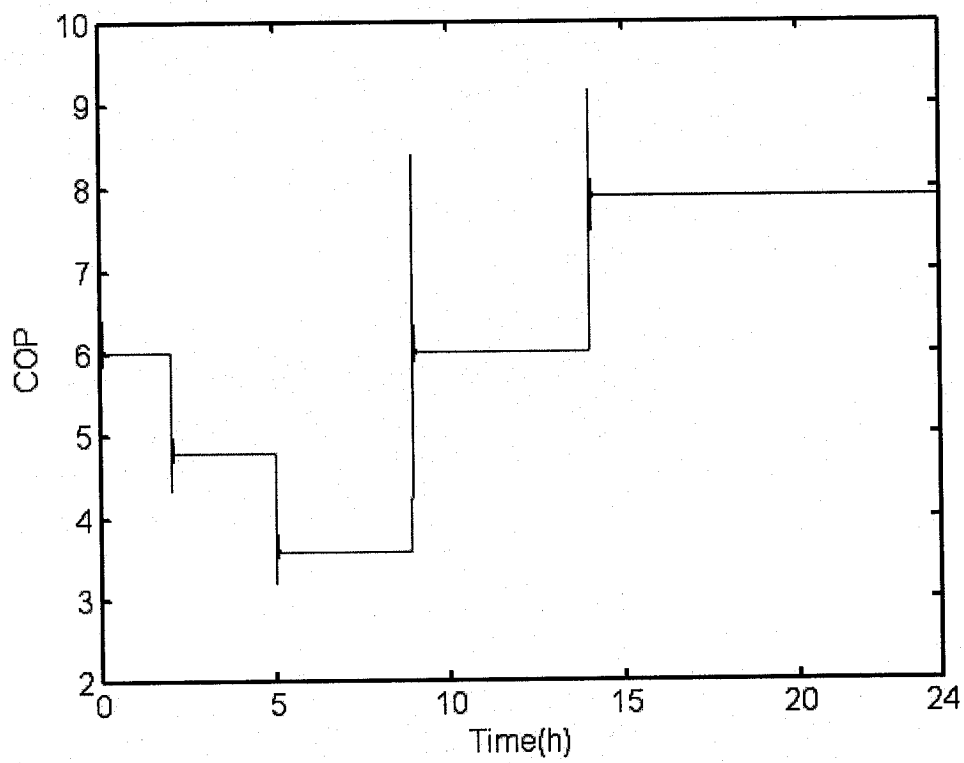

Figure 5.19 COP responses over a day

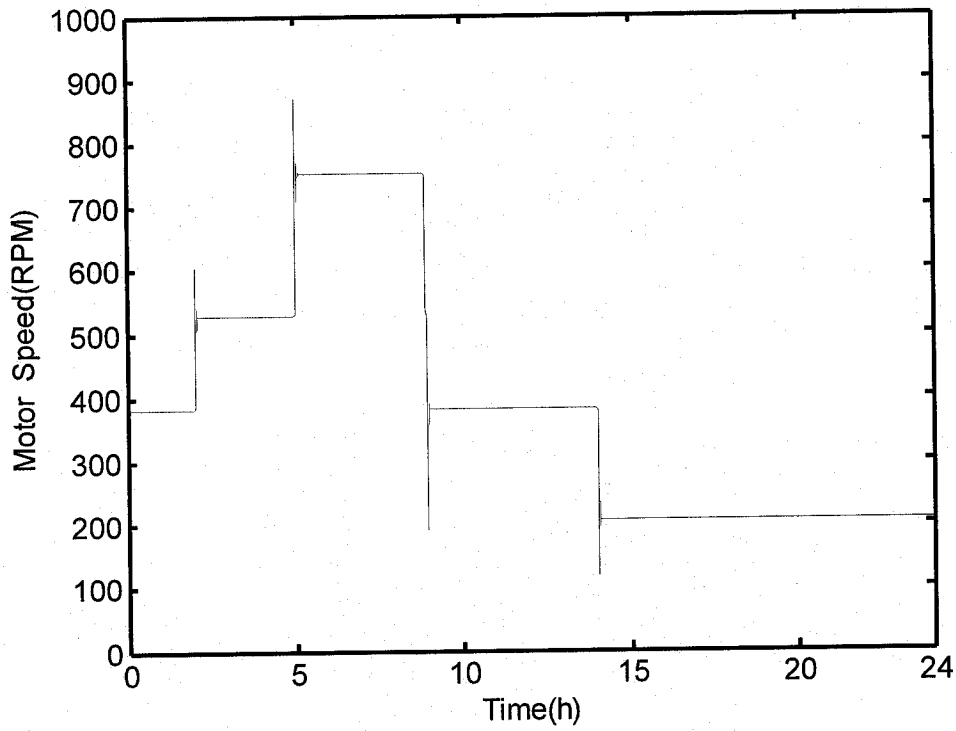

Figure 5.20 5 Ton chiller motor speed responses over a day

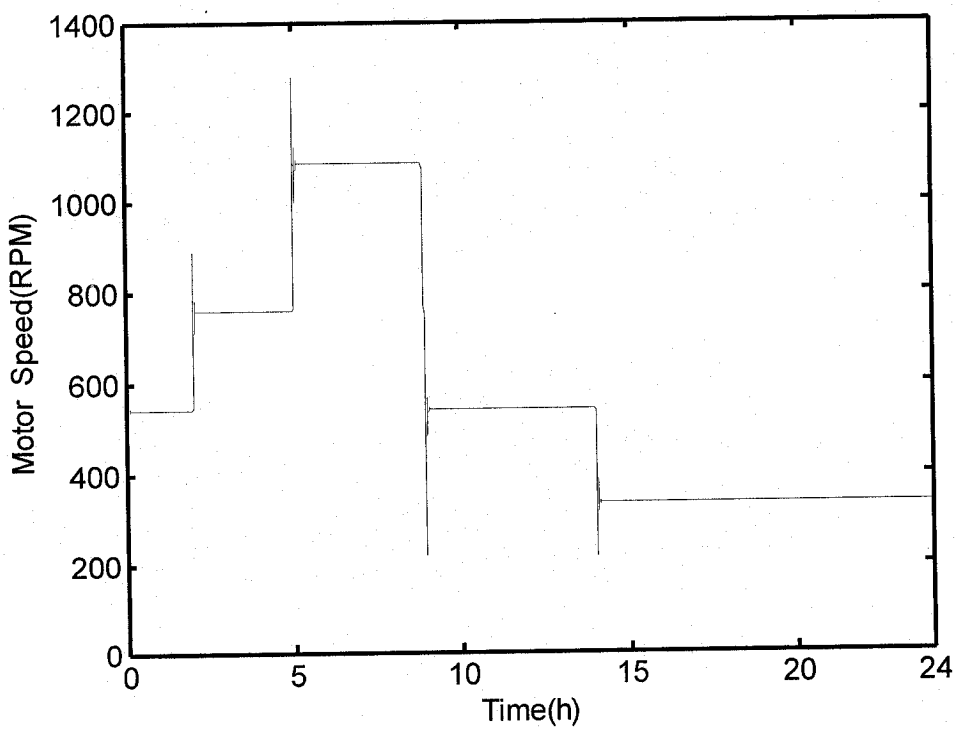

Figure 5.21 10 Ton chiller motor speed responses over a day

CHAPTER 6

CONTRIBUTIONS, CONCLUSIONS AND RECOMMENDATIONS

6.1 Summary

A dynamic model has been developed to better understand heat transfer phenomena inside each component of a chiller system so that the model is useful for control analysis and design. A PI feedback controller for single chiller is designed and utilized to analyze transient response characteristics of outputs such as refrigerant mass flow rate, supply water temperature, and COP. A multiple chiller control strategy was developed for matching anticipated cooling load with maximum COP. This strategy is expected to give practical benefits to chiller operators to achieve better operating efficiency.

6.2 Conclusions

The conclusions of the research work are summarized as follows.

(i) By increasing the motor speed, the refrigerant mass flow rate can also be increased, and the supply water temperature is reduced and vice versa. Open loop simulation results show that the compressor speed, condenser, evaporator pressures and refrigerant mass flow rate responses are faster than chilled water temperature responses. Therefore, it is concluded that the refrigeration system exhibit a two-time scale property in which both fast and slow system dynamics interact with each other.

(ii) Simulation results show that motor voltage, current and flux are sensitive to motor design parameters such as stator and rotor resistances and inductances, and rotor moment of inertia.

(iii) A constant gain PI controller was found to give acceptable responses to changing loads. The steady state response time of chilled water supply temperature was between 0.2 to 0.25 hours.

(iv) In a single chiller system, when the anticipated load increases, the compressor power also increases, therefore more capacity could be obtained. However, the system COP decreases.

(v) By using optimal chilled water setpoints in a PI controller, higher COP of the system could be achieved. This method is superior to other trial and error methods of selecting supply water temperature setpoints.

(vi) In multiple chiller operation, running all chillers at the same time by tracking the maximum COP curve, it is feasible to get better COP value than by running any one chiller alone.

6.3 Contributions

The contributions of the research work in dynamic modeling, open loop simulation tests and closed loop control results are summarized in the following.

(i) A relatively accurate dynamic model of chiller which includes a condenser, TXV, evaporator and compressor has been developed.

(ii) An AC induction motor dynamic model, which is adapted from the literature, was used to study relationships among motor angular velocity, stator current, and stator voltage. The motor model can be utilized to analyze transient effects and for calculating the energy consumption.

(iii) A closed loop feedback PI control strategy for single chiller is designed. Simulation runs were made to study output responses of chilled water temperature as a function of compressor speed.

(iv) Steady state optimization method was used to determine optimal setpoints. The optimal setpoints were implemented using a PI control system.

(v) A methodology for operating multiple chiller system which results in maximum COP is proposed.

(vi) Simulation results are presented which show how maximum COP could be achieved during day operation of multiple chiller systems.

6.4 Recommendations

Research work of the study gives clear opportunities for future further developments in system model verification, control strategy study and optimal control.

(i) These simulation results are based on mathematical model and run in the MATLAB program, so the model should be tested in an actual chiller to verify the model accuracy.

(ii) It is advisable to use adaptive controllers to track the variable setpoint to improve control performance.

(iii) Based on the research of multiple chiller capacity control, it is recommended to study the condensing water mass flow rate variation with condenser pumps speed modulation, the chilled water mass flow rate

variation with evaporator pumps speed modulation, and chiller tower fan speed modulation all combined into a whole chiller plant control system. It is important to develop a multiple control loop strategy for optimal control the whole chiller plant.

REFERENCES

Allen, J.J., Hamilton, J.F., 1983, "Steady-state reciprocating water chiller models." ASHRAE Transactions Vol.89, Part 2A, pp.398-407.

ASHREA, 1997 "Fundamental Handbook" America Society of Heating, Refrigerating and Air-Conditioning Engineers.

Braun, J.E., Mitchell, J.W., Klien, S.A., and Beckman, W.A., 1987, "Performance and control characteristics of a large cooling system." ASHRAE Transactions Vol.93, Part 1, pp.1830-1852.

Braun, J.E., Klein, S.A., Beckman, W.A., and Mitchell, J.W., 1989, "Methodologies for optimal control chilled water systems without storage." ASHRAE Transactions Vol.95, Part 1, pp.652-662.

Cecchini, C., Marchal, D., 1991, "A simulation model of refrigerating and air-conditioning equipment based on experimental data." ASHRAE Transactions Vol.97, Part 2, pp.388-393.

Chi, J, 1979, "DEPAC-A computer model for design and performance analysis of central chillers." ASME paper No. 79 WA/HT-28.

Cho, S.H, Zaheer-uddin, M., 2002, "Predictive control of intermittently operated radiant floor heating systems." Energy Conversion and Management 44 pp. 1222-1342.

Cooper, W.D., 1974, "Refrigeration compressor performance as affected by suction vapor superheating." ASHRAE Transactions Vol.79, Part 1, pp.195-204.

Crawford, R.R., Shirey, D.B., 1987, "Dynamic modeling of a residential heat pumps from actual system performance data." ASHRAE Transactions Vol.93, Part 2, pp.1179-1190.

Dabiri, A.E., Rice, C.K., 1981, "A compressor simulation model with corrections for the level of suction gas superheat." ASHRAE Transactions Vol.87, Part 2, pp.771-782.

Dhar, M., 1978, "Transient analysis of refrigerant system." Ph.D. Thesis, Purdue University.

Finney, D., 1988, "Variable frequency AC motor drive systems." Peregrinus Press, London.

Fischer, S.K., Rice, C.K., 1980, "A steady-state computer design model for air-to-air heat pumps." Oak Ridge National Laboratory ORNL/CON-80.

Garland, M.W., 1980, "Compressor capacity control for air-conditioning system partial load operation." ASHRAE Transactions Vol.86, Part 1, pp.477-484.

Gokdere, L.U., 1999, "Three-Phase Induction Motor VTB Model" University of South Carolina VTB publications.

Hackner, R.J., Mitchell, J.W., and Beckman, W.A., 1985, "HVAC system dynamics and energy use in buildings—Part II." ASHRAE Transactions Vol.91, Part 1B, pp.781-795.

Hamilton, J.F., Miller, J.L., 1990, "A simulation program for modeling an air-conditioning system." ASHRAE Transactions Vol.96, Part 1, pp.213-221.

He, X.D., Liu, S., Asada, H.H., Itoh, H., 1998, "Multivariable control of vapor compressor systems." Heating Ventilation Air-conditioning and Refrigeration Research July, Vol. 4, No. 3, pp.205-230.

Hussein, A 1996, "Interface Issues in Induction Motor Drives." Master's thesis Department of Electrical and Computer Engineering, Concordia University.

Jin, H., Spitler, J.D., 2002, "A parameter estimation based model of water-to-water heat pumps for use in energy calculation programs." ASHRAE Transactions Vol.108, Part 1, pp.3-17.

Johnson, G.A., 1985, "Optimization techniques for a centrifugal chiller plant using a programmable controller." ASHRAE Transactions Vol.91, Part 2B, pp.835-847.

Kim, M.H., Bullard, C.W., 2001, "A simple approach to thermal performance analysis of small hermetic reciprocating compressors." ASHRAE Transactions Vol.107, Part 1, pp.109-119.

Krakow, K.I., Lin, S., 1983, "A computer model for the simulation of multiple source heat pump performance." ASHRAE Transactions Vol.89, Part 2A, pp.590-616.

Krakow, K.I., Lin, S., 1987, "A numerical model of heat pumps having various means of refrigerant flow control and capacity control." ASHRAE Transactions Vol.93, Part 2, pp.491-510.

Lau, A.S., Beckman, W.A., and Mitchell, J.W., 1985, "Development of computerized control strategies for a large chilled water plant." ASHRAE Transactions Vol.91, Part 1B, pp.766-780.

Liaw, J.S., Liu, M.S., Wei, C.Z., Yang, B.C., and Wang, C.C., 2002, "Computer modeling for small air-conditioning systems capable of handling complex circuitry." ASHRAE Transactions Vol.108, Part 2, pp.613-626.

Lundberg, A., 1980, "Capacity control for partial load operation of screw compressor units." ASHRAE Transactions Vol.86, Part 1, pp.485-492.

Macarthur, J.W., 1984, "Transient heat pump behavior: a theoretical investigation." International Journal of Refrigeration Vol. 7, No. 2, March, pp. 123-132.

Popovic, P., Shapiro, H.N., 1995, "A semi-empirical method for modeling a reciprocating compressor in refrigeration systems." ASHRAE Transactions Vol.101, Part 2, pp.367-382.

Sami, S.M., Duong, T.N., Mercadier, Y., and Gaianis, N., 1987, "Prediction of the transient response of heat pumps." ASHRAE Transactions Vol.93, Part 2, pp.471-490.

Shah, R., Alleyne, A.G., and Bullard, C.W., 2004, "Dynamic modeling and control of multi-evaporator air-conditioning systems." ASHRAE Transactions Vol.110, Part 1, pp.109-119.

Spethmann, D.H., 1985, "Optimized control of multiple chillers." ASHRAE Transactions Vol.91, Part 2B, pp.848-862.

Smith, J.R., 1990, "Response analysis of A.C. electrical machines: computer models and simulation." Research Studies Press, New York.

Williams, V.A., 1985, "Optimization of chiller plant's energy consumption utilizing a central EMCS and DDC." ASHRAE Transactions Vol.91, Part 2B, pp.857-861.

Yasuda, H., Touber, S., and Machielsen, C.H.M., 1983, "Simulation model of a vapor compression refrigeration system." ASHRAE Transactions Vol.89, Part 2A, pp.408-425.

APPENDIX

These parameters used in 10 Ton chiller are listed in Table A.1, Table A.2, Table A.3, Table A.4, and Table A.5.

Table A.1 15Kw AC induction motor parameters

Symbol	Magnitude	Units
R_s	0.3	Ohm
R_r	0.15	Ohm
L_s	$15.5/(2\pi \cdot Fre)$	H
L_r	$15.2/(2\pi \cdot Fre)$	H
M	$15.0/(2\pi \cdot Fre)$	H
f	0.001	N·m /Rad·S
J	3.89	Kg·m·m

Table A.2 10 Ton chiller expansion valve parameters

Symbol	Magnitude	Units
C_v	0.75	dimensionless
A_v	0.001141	m^2

Table A.3 10 Ton chiller evaporator parameters

Symbol	Magnitude	Units
A_{ei}	0.2026	m^2
A_{eo}	0.6472	m^2
L_e	24.0	m
l_e	21	m
C_p	0.6	KJ/kg K

Table A.4 10 Ton chiller condenser parameters

Symbol	Magnitude	Units
A_{ci}	0.831	m^2
A_{co}	1.962	m^2

Table A.5 10 Ton chiller compressor parameters

Symbol	Magnitude	Units
V_{cl}	0.0007	m^3
V_d	0.014	m^3
N	20	RPS
n	1.3	dimensionless